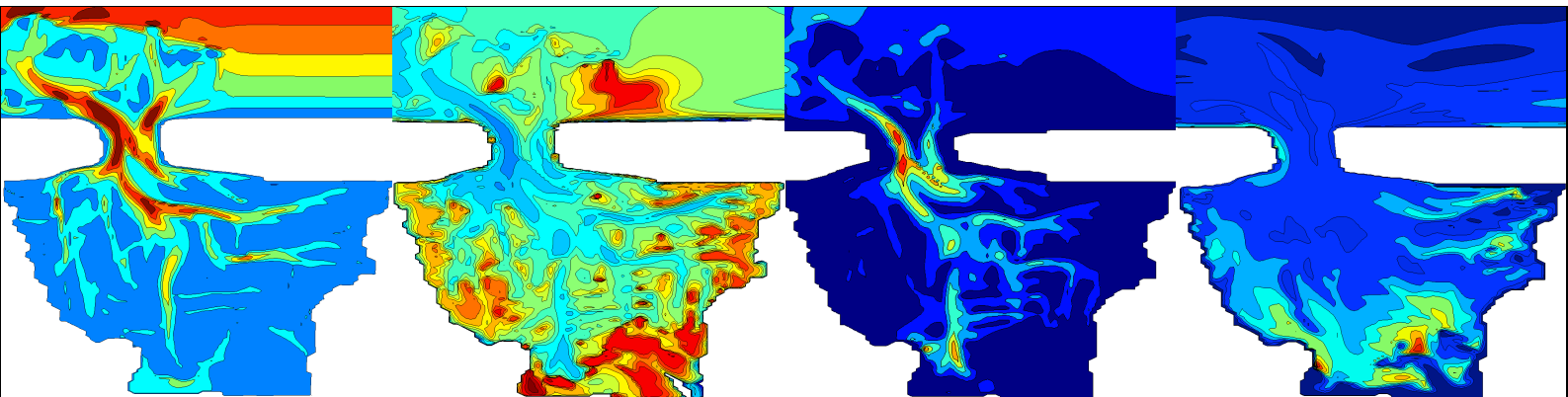# Simulating and classifying large-scale spatial sand-mud segregation using a process-based model for a tidal inlet system

A process-based assessment on the relation between different forcing conditions and large-scale spatial sand-mud segregation

MASTER'S THESIS

Freek Scheel 2012

Faculty of Civil Engineering
Delft University of Technology

TUDelft
Delft
University of
Technology

Challenge the future

Simulating and classifying large-scale spatial sand-mud segregation using a process-based model for a tidal inlet system

SIMULATING AND CLASSIFYING LARGE-SCALE SPATIAL SAND-MUD
SEGREGATION USING A PROCESS-BASED MODEL FOR A TIDAL INLET SYSTEM

MASTER'S THESIS

For obtaining the international degree 'Master of Science' (M.Sc.) and national degree 'ingenieur' (ir.)

at

DELFT UNIVERSITY OF TECHNOLOGY

by

Freek SCHEEL

Hydraulic- & Coastal Engineer

(BBE)

born in Woerden, The Netherlands

Composition of graduation committee

Prof. dr. ir. M.J.F. Stive	Delft University of Technology
Prof. dr. ir. Z.B. Wang	Deltares & Delft University of Technology
Prof. dr. ir. J.C. Winterwerp	Deltares & Delft University of Technology
Dr. ir. M. van Ledden	Royal Haskoning & Delft University of Technology
Dr. ir. B.C. van Prooijen	Delft University of Technology

In collaboration with

TUDelft Delft University of Technology

ROYAL HASKONING Enhancing Society

Deltares Enabling Delta Life

Cover images (from left to right):

(1) Initial model bathymetry given by bottom depth [m], obtained from 50 years of tidally induced forcing on a sand only model, initiated with a flat bed and linearly plotted from 0 to 21 meters depth;

(2) Instantaneous mud content in fluff layer [kg/m^2], after 3 months of simulating process-based sand-mud segregation under normal conditions, plotted using a logarithmic scale from 0 to 100 kg/m^2;

(3) Instantaneous bed shear stresses [N/m^2], after 3 months of simulating process-based sand-mud segregation under normal conditions, plotted using a linear scale from 0 to 3,5 N/m^2;

(4) Instantaneous amount of mud in suspension [g/m^3 or mg/l], after 3 months of simulating process-based sand-mud segregation under normal conditions and linearly plotted from 0 to 250 g/m^3 (or mg/l).

If I have seen further,

it is by standing on the shoulders of giants

Isaac Newton

Preface & Acknowledgements

Deze thesis markeert, naast het einde van mijn studie Civiele Techniek aan de Technische Universiteit te Delft (TU Delft), tevens het einde van mijn gehele studieloopbaan. Eén waarin ik met bescheiden trots én succes reeds gedurende mijn bachelor studie te Utrecht parallel de stap richting een universitaire master heb gezet. Na de specialisatie in waterbouwkunde (te Utrecht) ben ik mij bij de TU Delft verder gaan specialiseren in de kustwaterbouwkunde, met een nadruk op morfodynamische processen.

Ondanks dat een individuele studie het niet suggereert, heb ik deze studie verre van alleen afgerond. Met de termen ondersteunen, meeleven en samenwerken zijn een hoop personen gemoeid, die allen in zekere mate hebben bijgedragen aan de afronding van mijn studieloopbaan. Daar wil ik graag even stil bij staan.

Allereerst gaat mijn dank naar de medestudenten waarmee ik veel tijd heb doorgebracht, opdrachten & projecten mee heb uitgevoerd en in afwachting van tentamenresultaten colleges mee heb gevolgd. Doordat we voorheen allemaal een HBO-bachelor hebben afgerond vormde we al snel een hecht groepje. In het bijzonder wil ik Pim en Bas bedanken, voor de samenwerking binnen enkele projecten, maar ook de vriendschap die daarbij is opgebouwd. Verder gaat mijn dank binnen de TU uit naar alle inspirerende docenten, in het bijzonder Marcel Stive, als professor & docent in de sectie kustwaterbouw én adviseur voor de deltacommissie heeft hij me al enkele jaren kunnen boeien. Om uiteindelijk onder zijn toezicht te mogen afstuderen heb ik dan ook als een eer ervaren. Daarnaast wil ik graag de overige commissieleden vanuit de TU bedanken, Bram van Prooijen, Han Winterwerp en Zheng Bing Wang, voor de tijd en inzet die ze op diverse manieren in mijn afstuderen en begeleiding hebben gestoken.

Om de commissie volledig te benoemen, wil ik tevens Mathijs van Ledden binnen Royal Haskoning bedanken. Zijn idee, visie, voorgaand onderzoek en formuleringen m.b.t. het modelleren van zand-slib segregatie zijn essentieel om dit onderzoek überhaupt mogelijk te maken. Daarnaast waren zijn betrokkenheid, kritische blik en adviezen minstens zo belangrijk. Onder andere het advies om te participeren aan het symposium van het Nederlands Centrum voor Kustonderzoek (de NCK-dagen 2012), samen met Mathijs van Ledden, Bram van Prooijen & Marcel Stive, geeft die betrokkenheid goed weer. Deze participatie was zeer leerzaam en heeft uiteindelijk geresulteerd in mijn eerste wetenschappelijke publicatie, iets waar ik ook veel van heb geleerd. Verder heeft zijn kritische commentaar een zeer belangrijke bijdrage geleverd aan de leesbaarheid van dit eindverslag, iets waar ook Bram van Prooijen een belangrijke bijdrage aan heeft geleverd. Ik wil verder Royal Haskoning en hierbinnen alle collega's bedanken voor hun interesse, de werkplek en de mogelijkheid om hier af te mogen studeren. In het bijzonder Thomas Vijverberg, voor de nodige begeleiding en adviezen. Verder wil ik Deltares bedanken voor de samenwerking die met Royal Haskoning is aangegaan t.b.v. deze studie, hierdoor heb ik toegang gekregen tot een nieuwe versie van Delft3D, die nog niet publiekelijk beschikbaar is, maar wel essentieel was voor dit onderzoek. Binnen Deltares gaat mijn dank in het bijzonder uit naar Bert Jagers, Thijs van Kessel en Luca Sittoni (*grazie!*).

Verder wil ik vrienden en familie bedanken, in het bijzonder mijn ouders, omdat ze mij oneindig veel mogelijkheden hebben gegeven, waaronder studeren, iets waar ik ze altijd oneindig dankbaar voor zal zijn.

Als laatst wil ik Carline bedanken, gewoon voor alles.

Freek Scheel

April 2012

i

Abstract

The total sediment distribution in tidal basins (estuaries, tidal lagoons and -bays), rivers and shallow seas is often a combination of sand, silt and clay particles (sand and mud). Under the influence of dynamic forcing (like short waves and tidal currents), particles can get transported through these systems. Therefore, these dynamic forces induce changes in morphology (bathymetry). This process is referred to by morphodynamics. To assess and predict any (upcoming) changes in morphology, numerical process-based models have been developed. These models are often based on schematizations, assumptions and simplifications, like the usage of a single particle diameter. This model parameter is often used to calibrate a model by combining it with field measurements.

Sand and mud particles respond different to identical forcing from waves and currents, for instance due to the differences in critical bed shear stress, fall velocity and transportation mode. Furthermore, mud particles are cohesive, and therefore accumulate other mud particles, forming larger aggregates (this process is called flocculation). Finally, sand-mud mixtures are harder to erode, as the combination of sand and mud particles enhances the soil. It is because of these physical differences that sand and mud particles can get transported to distinct areas, even under the influence of identical forcing conditions. This process, in which sand and mud get transported to different areas, is called sand-mud segregation.

While the previously mentioned process-based models are capable of simulating morphological evolution, they will not reproduce sand-mud segregation. Though, this process might significantly influence the morphology in distinct areas. Apart from the influence on local morphology, the ratio of sand and mud is an indicator for the survival of specific flora and fauna. Furthermore, due to the cohesive properties of mud, pollutants tend to accumulate to mud particles. Therefore, the mud content is an important indicator for potential pollution.

To successfully assess the above mud-related topics, mud particles (and their characteristics) must be adopted into a process-based model, but also the enhancement of the soil, due to sand-mud mixtures, must be taken into account. In recent research, propositions have been made on how to implement mud particles (and their influences) in process-based models. During this period, some attempts to assess practical applications have been made. These practical applications have shown the potential of sand-mud segregation modelling, but also showed how difficult it is to successfully quantify the relevant processes. Furthermore, when looking at these models more qualitatively, some discrepancies with observed macro patterns are also found.

These previous model applications indicate the complexity of complete 3-dimensional sand-mud segregation modelling for a practical case. It suggests a 'step back', to look at sand-mud segregation from a broader perspective, which became the aim of this thesis. Therefore, in this thesis, the interest shifted to an (qualitative) assessment of large-scale sand-mud segregation patterns and the associated spatial distribution, rather than an accurate (qualitative) reproduction of a practical case. This approach makes it possible to assess the influence of tidal current- and short wave dominance on the characteristics of the large-scale sand-mud segregation as well, since the forcing can easily be varied with. The schematized approach makes the indication of changes in large-scale sand-mud segregation, due to these changes in forcing, possible.

To successfully assess these large-scale sand-mud segregation patterns and spatial distribution, a simplified (schematized) scenario is needed. Furthermore, a large-scale description of sand-mud segregation (valid for a specific system) is needed, as qualitative comparison is then possible. A schematized model of the Amelander tidal inlet system, which features one of the tidal lagoons in the Dutch Wadden Sea, is used for this purpose. The Dutch Wadden Sea is an interesting area for sand-mud segregation research, as the entire area

is protected because of its natural value. The above mud-related topics are also related to natural value, indicating the need for sand-mud segregation modelling in the Dutch Wadden Sea.

The associated general description of large-scale sand-mud segregation in these Dutch Wadden Sea systems is found in various observations, measurements and (mainly) previous research. When combined, the overall patterns in the Dutch Wadden Sea indicate how mud is found in shallow- and less hydrodynamic active areas, like tidal flats, near tidal divides and near land boundaries. While little mud is found in deeper and hydrodynamic active areas, like tidal channels and –inlet. Furthermore, a hypothesis is set-up, relating the (relative) dominance of short waves or tide to the spatial distribution of sand and mud. Tide-dominated systems can be described like the ones in the Dutch Wadden Sea (see above), while short wave-dominated systems feature mud inside the basin/lagoon, rather than near the margins.

The Amelander tidal inlet system model is combined with a Delft3D version that supports sand-mud mixtures. This process-based Delft3D model is currently under development and extends the regular Delft3D version with soil enhancement due to mud, a stratified- and mixing bed and a fluff layer (which makes the quickly changing mud concentrations near the bed, during small hydrodynamic activity, and representation of consolidation lag, possible).

After verifying the Delft3D model, the Amelander inlet system model is executed using a reference scenario (which features realistic tidal forcing conditions, as observed in the field). From the results, realistic large-scale sand-mud segregation patterns are observed, with mud deposition on tidal flats. The observations and further analysis are in line with the above description and hypothesis. The reference scenario is even capable of representing some general quantitative information, even though the model is schematized.

By changing the forcing conditions (short waves and tide), the relative influence of tidal currents and short waves can be changed. These small changes appear very helpful, as the above hypothesis is also related to this relative dominance. Some additional scenarios were therefore set up, all representing different relative forcing dominance, related to tidal currents and short waves. The results from these different scenarios are again in line with the hypothesis. Settling of mud is highly related to the influence of hydrodynamic activity. While tidal currents are mainly found in deep tidal channels, mud is found in tidal flats for tidal dominance, whereas short waves dissipate their energy in the shallows, and mud is thus found in deeper areas with short wave-dominance.

By combining all these conclusions, observations, analysis and theory, a general classification for large-scale sand-mud segregation patterns, related to relative dominance of short waves or tide, is constructed. This classification can be considered as the final conclusion of this thesis (apart from successfully representing the large-scale sand-mud segregation patterns in the reference scenario), and is found in figure 4.18. This conclusion could not have been made when a non-schematized approach was chosen. It indicates the importance of schematized models (next to fully 3-dimensional models, representing a practical case) by giving another example of their strength: further insight in the overall processes and characteristics of a system.

Samenvatting

De totale distributie van sediment in getijdebekkens (estuaria, getijdelagunes en -baaien), rivieren en ondiepe zeeën bestaat vaak uit een combinatie van zand-, silt- en kleideeltjes (samen zand en slib). Onder dynamische invloeden (zoals korte golven en getijdenstroming) kunnen deze deeltjes door bovengenoemde systemen getransporteerd worden. De dynamische forceringen zijn daarom verantwoordelijk voor veranderingen in morfologie (bathymetrie). Dit proces wordt aangeduid met morfodynamica. Om veranderingen in morfologie te voorspellen en te beoordelen zijn numerieke fysische modellen ontwikkeld. Deze modellen zijn vaak gebaseerd op schematisaties, aannames en simplificaties, zoals het gebruik van een representatieve diameter voor sedimentdeeltjes. Als modelparameter wordt deze diameter vaak gebruikt voor modelkalibratie met hulp van veldmetingen.

Zand- en slibdeeltjes reageren verschillend op gelijke forcering van golven en getij, bijvoorbeeld door het verschil in kritische schuifspanning, valsnelheid en type transport. Verder zijn slibdeeltjes cohesief, waardoor ze andere slibdeeltjes kunnen accumuleren en er grotere deeltjes ontstaan (bestaande uit meerdere slibdeeltjes), dit proces heet flocculatie. Bovendien eroderen zand-slib mengsels moeilijker, aangezien de combinatie van zand- en slibdeeltjes de bodem versterkt. Door al deze verschillen in fysische eigenschappen kunnen zand- en slibdeeltjes naar specifieke locaties in een systeem getransporteerd worden, zelfs wanneer de forceringen op beide deeltjes identiek zijn. Dit proces, waarin zand en slib naar verschillende locaties wordt getransporteerd, heet zand-slib segregatie.

Hoewel (de hierboven beschreven) fysische modellen in staat zijn de morfologische evolutie te simuleren, zijn ze niet in staat de zand-slib segregatie te reproduceren. Ondanks dat dit proces de morfologie op specifieke locaties significant kan beïnvloeden. Naast deze lokale invloeden is de verhouding van zand en slib in de bodem van grote invloed op het overleven van specifieke flora en fauna. Verder trekken slibdeeltjes tevens verontreinigde stoffen aan, door de cohesieve eigenschappen (van slib). Daardoor geeft het slibgehalte een belangrijk signaal af betreffende potentiële verontreiniging.

Om de bovenstaande slib-gerelateerde onderwerpen succesvol te kunnen beoordelen en te voorspellen zullen slibdeeltjes (en de bijbehorende eigenschappen) in een fysisch model geïmplementeerd moeten worden. Daarbij moet ook rekening worden gehouden met het versterken van de bodem door zand-slib mengsels. In recent onderzoek zijn voorstellen gedaan voor de implementatie van slibdeeltjes (en hun invloeden) in fysische modellen. Gedurende deze periode zijn pogingen ondernomen richting praktische toepassingen van dergelijke modellen. De potentie van zand-slib modellering is bij deze toepassingen duidelijk naar voren gekomen. Echter, de kwantificering van de processen blijkt een groot probleem, daarnaast zijn discrepanties bij een kwalitatieve kijk naar zand-slib segregatie patronen (op macro schaal) geen uitzondering.

Deze modellen (voorafgaand aan dit onderzoek uitgevoerd), laten de complexiteit van 3-dimensionale zand-slib segregatie modellering voor praktische gevallen duidelijk zien. Ze suggereren een 'stap terug', om de zand-slib segregatie vanuit een breder perspectief te bekijken. Dit is te definiëren als het hoofddoel van dit onderzoek. Daarom is in deze thesis de interesse verschoven van een precieze (kwantitatieve) representatie van een werkelijk geval naar een (kwalitatieve) beoordeling van grootschalige zand-slib segregatie patronen en bijbehorende ruimtelijke verdeling. Deze aanpak maakt het tevens mogelijk om de invloed van relatieve getij- en golfdominantie op de eigenschappen van de grootschalige zand-slib segregatie te onderzoeken, aangezien de forcering gemakkelijk gevarieerd kan worden en een geschematiseerde aanpak de detectie van veranderingen in grootschalige zand-slib segregatie patronen, door de veranderingen in forcering, mogelijk maakt.

Een vereenvoudigd (geschematiseerd) model is nodig om een succesvolle beoordeling van grootschalige zand-slib segregatie patronen en ruimtelijke verdeling te kunnen verwezenlijken. Verder is een beschrijving van grootschalige zand-slib segregatie patronen (geldig voor het specifieke geval) benodigd, dit maakt een kwalitatieve vergelijking mogelijk. Een geschematiseerd model van het Amelander zeegat en getijdenlagune (één van de getijdenlagunes in het Nederlandse gedeelte van de Waddenzee) is gekozen vanwege deze mogelijkheden. Het Nederlandse gedeelte van de Waddenzee is een interessant gebied voor onderzoek naar zand-slib segregatie, aangezien het gehele gebied benoemd is tot beschermd natuurgebied. De bovenstaande slib-gerelateerde onderwerpen zijn ook gerelateerd aan natuurlijke aspecten (zoals flora en fauna), wat het belang van zand-slib segregatie (modellering) in het Nederlandse gedeelte van de Waddenzee versterkt.

De beschrijving van de grootschalige zand-slib segregatie patronen in de systemen in het Nederlandse gedeelte van de Waddenzee is gebaseerd op diverse observaties, metingen en (voornamelijk) voorgaande onderzoeken. Wanneer dit alles wordt gecombineerd laten de grootschalige patronen in het Nederlandse gedeelte van de Waddenzee zien hoe slib zich verplaatst naar ondiepere gedeeltes én minder hydrodynamisch actieve gebieden, zoals platen, slikken, wantij locaties en zelfs kwelders. Terwijl slib amper gevonden wordt in diepere én hydrodynamisch actieve gebieden, zoals de getijgeulen en zeegat. Verder beschrijft een hypothese hoe de relatieve dominantie van korte golven óf getij van invloed kan zijn op de ruimtelijke verdeling van zand en slib. Getij-gedomineerde systemen kunnen worden beschreven als degene in het Nederlandse gedeelte van de Waddenzee (zie hierboven), terwijl korte golf-dominantie slib naar diepere gedeeltes (het midden) van een systeem verplaatst, tegenover de (ondiepe en zandige) randen van een systeem.

Het model van het Amelander zeegat en getijlagune is gecombineerd met een Delft3D versie welke zand-slib mengsels ondersteund. Dit fysische model is momenteel in ontwikkeling en breidt de reguliere Delft3D versie uit met bodemversterking door slib, een gestratificeerde- & mengende bodem en een fluff laag (maakt snelle reacties van hoge slibconcentraties nabij de bodem, tijdens lage hydrodynamische activiteit, én representatie van vertraging in consolidatie mogelijk).

Na verificatie van het Delft3D model is het Amelander zeegat- en getijlagune model uitgevoerd voor een referentiescenario (gebaseerd op realistische getijforcering, zoals waargenomen in veldmetingen). In deze resultaten worden realistische grootschalige zand-slib segregatie patronen gevonden, met slib depositie in ondiepe gedeelten. De observaties en verdere analyse zijn tevens in lijn met bovenstaande beschrijving en hypothese. Het referentiescenario blijkt bovendien in staat om algemene kwantitatieve informatie te representeren, ondanks dat het model geschematiseerd is.

Door het variëren van de forcering (korte golven en getij) kan de simulatie van relatieve dominantie van getijdestroming en korte golven worden veranderd. Aangezien de hypothese gerelateerd is aan relatieve dominantie blijken deze kleine veranderingen erg behulpzaam voor het onderzoek. Daarom zijn enkele scenario's toegevoegd waarin gevarieerd is met dominantie van korte golven of getijdestroming. De resultaten van deze scenario's zijn wederom in lijn met de gerelateerde hypothese. De depositie van slib is in grote mate afhankelijk van de hydrodynamische activiteit. Aangezien getijdestromingen voornamelijk in diepere getijdegeulen te vinden is, wordt slib gevonden in ondiepe gebieden voor getijdominantie, terwijl de energie uit korte golven gedissipeerd wordt in ondiepe gebieden, slib wordt dus gevonden in diepere gebieden voor een systeem met korte golf-dominantie.

Door alle conclusies, observaties, analyses en theorie te combineren kan een algemene classificatie voor grootschalige zand-slib segregatie patronen, gerelateerd aan relatieve dominantie van korte golven of getij, worden opgesteld. Deze classificatie kan worden beschouwd als de algehele conclusie van deze thesis (naast het succesvol reproduceren van grootschalige zand-slib segregatie patronen voor het referentiescenario) en kan gevonden worden in figuur 4.18. Deze conclusie had niet geproduceerd kunnen worden wanneer was gekozen voor een niet-geschematiseerde aanpak. Het geeft duidelijk het belang van geschematiseerde modellen weer (naast de kracht van een volledig 3-dimensionaal model, welke een praktisch geval representeert), door wederom als voorbeeld van hun kracht te dienen: verder inzicht in de globale (fysische) processen en eigenschappen van een systeem.
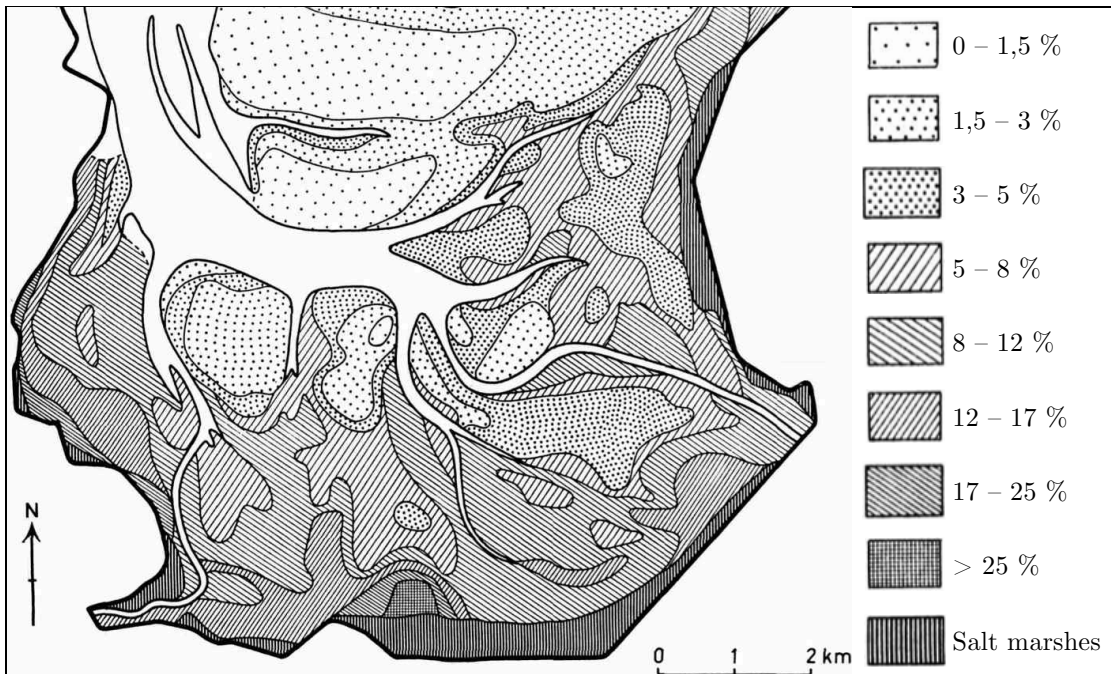
Contents

Chapter 1

Introduction

1.1 Sand-mud segregation

Silt and clay particles are present in many rivers, shallow seas and tidal basins (tidal lagoons, estuaries & tidal bays (Carter, 1988)). Together with sand, these mud particles (the combination of silt and clay) often form the total sediment distribution in the sediment bed of these systems. Sand and mud particles feature different physical properties, like different fall velocities and cohesiveness (for mud particles).

The different physical properties of mud and sand imply a different response to (identical) forcing, like waves and currents. As a result, spatial sand-mud segregation occurs. This process has been described by, amongst others, Van Straaten & Kuenen (1957), Postma (1954; 1961), De Glopper (1967), Carter (1988), Oost (1995), Venema *et al.* (1999) and Van Ledden (2003). Figure 1.1 below is reprinted from the first of this enumeration and shows the observations of spatial variation in clay content through the former Lauwerszee.

Figure 1.1: Clay content distribution ($d < 2~\mu$m) in the former Lauwerszee, near the Dutch Wadden Sea (Van Straaten and Kuenen, 1957)

The presence or absence of mud particles in the (spatial) sediment distribution can have significant consequences for certain mud-related management topics, which are listed below:

- Mud can get transported to distinct areas, as introduced in figure 1.1, where it can have a significant contribution on the morphological evolution. Furthermore, mud is capable of enhancing the soil structure (Mitchener & Torfs, 1996), making it more difficult to erode at these locations. This also has its local contribution on the evolution of the morphology (morphodynamics). Less uncertain results in this respect are always preferred, as it results in better knowledge on the bathymetry, and thus (amongst others) on navigation depth, the possible need for dredging and safety;
- The flora and fauna in tidal basins is highly correlated to the spatial sand-mud distribution, as various species require a certain sand- or mud content to grow/live. It therefore influences the distribution of flora and fauna throughout, for instance, a tidal lagoon or estuary (Reid & Wood, 1976). The flora and fauna also tends to influence bed properties, like erodibility and consolidation (Montserrat *et al.*, 2009 and Jacobs, 2011);
- Due to the cohesive properties of mud, as previously introduced, pollutants tend to adhere to mud particles (Förstner & Wittman, 1979 and George *et al.*, 2007). The spatial distribution of mud therefore indicates the (potential) degree of pollution for an area, given the mud content present.

Understanding sand-mud segregation is therefore important.

1.2 Modelling sand-mud segregation

Assessment of the above mud-related topics requires a description of the spatial sand-mud distribution. This description can be obtained by measurements in the field (like figure 1.1). Though, for future prospects, predictions of the spatial sand-mud distribution are required. Predicting the spatial sand-mud distribution requires, for instance, morphodynamic modelling. Morphodynamic modelling (process-based) involves the prediction of adjustments in the morphology[1] over time, due to dynamic forcing, like currents and waves. Although some morphodynamic models can be of an analytical nature, the majority of morphodynamic models are numerical (discretised), especially when more than one spatial dimension is considered

Every model is, by definition, a simplified representation of reality. A morphodynamic model stresses this fact, as schematizations, simplifications and assumptions are made, for instance because of computational (efficiency) reasons. One important simplification, which is often used in morphodynamic modelling, is the usage of a single value for the grain size, often chosen somewhere near d_{50} (this diameter represents the sediment particle in a sediment distribution of which 50% of all the sediment particles are smaller/larger). This variable is commonly used as a parameter for model calibration.

Although mud is often abundant in the (spatial) sediment distribution of many tidal basins, rivers and shallow seas, almost every morphodynamic model of these areas of interest is modelled using the previously introduced 'd_{50}-assumption'. This assumption often results in a model that only takes sand particles into account, and is thus neglecting the different physical properties of the finer mud particles. While the morphological changes can be calibrated to reality (field measurements) to great extent, the spatial sand-mud segregation remains unknown when the 'd_{50}-assumption' is applied. Therefore, the above mud-related topics cannot be assessed, and conclusions related to these topics cannot be drawn from these models. Therefore, a morphodynamic model, which predicts spatial sand-mud segregation, requires (at least) multiple sizes of sediment (both sand and mud), along with the influence by sediment mixtures (as suggested by Mitchener & Torfs (1996)).

Concepts for modelling sand-mud segregation exist since the early 1970's. These concepts have been further analysed and were first applied to river engineering problems in the late 1980's. Since the focus of this thesis is on tidal basins, relevant and practical research regarding these systems is provided in this section.

---

[1] In civil engineering and science, the underwater topography, commonly consisting of (fluvial) sediment, is called morphology.

Chesher & Ockenden (1997) applied sand-mud segregation in a simplified channel model (1DH) and a 2DH estuary model (Mersey estuary, England). Although this initiated the first application of a sand-mud segregation model in a coastal system, the sand and mud computations were based on separate modules, combined with a new sand-mud interaction module to obtain the final results. Chesher & Ockenden (1997) highlight the importance of a fully interactive sand-mud model (as opposed to their separate sand-mud interaction module), since the sand-mud interactions appeared significant for the final results. Furthermore, it is stressed that the gathering of field and laboratory data is very important to assess the uncertainty in the models properly. The influence of mud content in a sand-mud mixture on the critical shear stress for erosion is also considered as an important aspect. De Bake (2000) also stresses both of these statements (the importance of a fully interactive sand-mud model and laboratory/field data).

Erosion formulations for sand-mud mixtures were first proposed and applied by Van Ledden (2003), partly as a response to recommendations from Van Ledden (1998). These formulations are based on the mud content (p_m) and are divided in two regimes, either cohesive or non-cohesive. Apart from the erosion formulations, Van Ledden (2003) assumes that layer mixing within the bed is described by an advection-diffusion equation. He applied his formulation on idealised situations (1DH) and in a 3D application for the Frisian Inlet system in the Dutch Wadden Sea (near the former Lauwerszee, figure 1.1), also found in Van Ledden *et al.* (2006).

As stressed in the conclusions from the aforementioned 3D model of the Frisian tidal inlet system by Van Ledden *et al.* (2006), the long-term morphological computations show both similarities and discrepancies in bed level and -composition, when compared to actual measurements. Although some explanations are suggested for the discrepancies, they indicate the uncertain results from these complex models. But also the need for (long-term) measurements of both sand and mud is indicated within this conclusion, as these are important for correct calibration (though, these relevant (long-term) measurements are not always available).

Furthermore, in one of the recommendations from Van Ledden (2003), a suggestion is made to analyse idealised situations with the proposed process-based model, as it increases the understanding in large-scale sand-mud segregation patterns in tidal basins. Good examples, related to the value of an idealized case, are for instance the research by Hibma (2004), but also the 1DH models by Van Ledden (2003). The idealized approach results in a broad understanding of (physical) processes that occur. Also, research from e.g. Dongeren & De Vriend (1993) and Marciano *et al.* (2005) show interesting results from schematized models, the results are both consistent and insightful. Furthermore, it is advised (Van Ledden, 2003) to further elaborate on the idealized case using different geometries and/or processes (forcing), as it increases the understanding in different conditions and their contributions.

The recommendation by Van Ledden (2003) indicates a lack of physical understanding in the advanced 3D model of the Frisian tidal inlet system (Van Ledden *et al.*, 2006), as many non-linear processes simultaneously take place in a complex bathymetry and -model. Furthermore, assessing the influence from different forcing conditions allows for a general classification. This problem and recommendation can be linked to insightful simplified cases (like the previously mentioned Hibma, 2004 or Marciano *et al.*, 2005).

Waeles *et al.* (2007) developed a 3D model in which the same erosion regimes from Van Ledden (2003) were used. In addition, the bottom module accounted for different deposits of sediments, dependent on the mud-content. The model was applied for the mouth of the Seine River estuary. Consolidation was later introduced in sand-mud segregation modelling by introducing an empirical relation (Waeles *et al.*, 2008).

As stated in the conclusions from Waeles *et al.* (2007), the applied model for the Seine River estuary produces qualitative information (which can be observed in the field) rather than quantitative. The model simulates a total period of one year and is therefore unable to be compared to bathymetry data over time, as this data gets collected over longer periods (e.g. once per year). It is partly because of this reason that the model cannot be regarded as quantitative.

Continuing on the principals from Chesher and Ockenden (1997), Sanford (2008) introduced 1DH models using separate eroding modules for sand and mud (so no distinction between cohesive and non-cohesive mixtures is made), though consolidation and bioturbation was taken into account.

Recently, Le Hir *et al.* (2011) continued with the principles from Waeles *et al.* (2007, 2008) and further elaborated this 3D model. In addition, the model uses multi-layered, mixed (sand-mud) sediment and respects concentrations for both sorted and mixed sediments. Unfortunately, the proposed model from Le Hir *et al.* (2011) is not used for modelling a practical (3D) situation, but only laboratory tests and small-scale measurements have been used and verified. Previous research (Le Hir *et al.*, 2008) is also mainly aimed at theory and laboratory tests. Furthermore, Le Hir *et al.* (2011) also provides an overview of sand-mud mixture related research, of which an overview is provided in this section as well.

Van Duren *et al.* (2011) advice process reduction in sand-mud models, as many processes determine transport of fine sediment. Identification of dominant processes is important to reduce (unnecessary) long computation times and difficult models (regarding physical understanding). By analysing a schematized model, influence from processes can be identified as dominant or of minor influence. But also the differences in results for a schematized model and a very accurate model can be assessed within further research.

1.3 Objectives and research questions

From the previous section, it becomes evident that a limited number of applications on sand-mud segregation in morphological process-based models (for tidal basins) have been executed. Especially when looking at sand-mud segregation in morphodynamic 2DH or 3D models of tidal basins (models that represent the morphology of a tidal basin, with a certain bathymetry, over time), the number of practical applications is very limited. The several numerical methods, which have been developed and adopted in computational software programs, made the modelling of these (few) practical applications possible. Although great for research purposes, it appears that a risk in the elaboration of these problems is losing the physical understanding behind it, as many processes/contributions simultaneously take place. Therefore, a 'step back' is suggested, and the assessment of a schematized case is preferred/advised. This way, a further understanding of the physical processes, which are responsible for certain characteristics of large-scale sand-mud segregation patterns, can be achieved.

To make this assessment possible, a general description of the physical processes behind the large-scale sand-mud segregation is indispensible. This description can be based on measurements, observations and literature, but also (proposed) hypotheses and assumptions (which can be reviewed using this model).

The main contributors to the sand-mud segregation patterns and spatial distribution are, amongst others, the forcing on- and the geometry of the considered basin. Within this thesis, the focus is laid upon the different forces that are mainly responsible for sand-mud segregation, being short waves and tidal currents. By combining the proposed schematized reference model with different forcing conditions (as recommended by Van Ledden (2003) and Van Duren *et al.* (2011)), the relative influence of the forcing conditions on large-scale spatial sand-mud segregation patterns, can be assessed. Different cases with various combinations (and magnitudes) of forces should thus be considered.

The results from these different scenarios can also be used to construct a general classification, regarding the influence of short wave- and tidal current dominance on the large-scale spatial sand-mud segregation patterns. This classification should be in line with the general description of the physical processes behind the large-scale sand-mud segregation. Therefore, a hypothesis (which is based on this description), relating relative dominance of short waves or tidal currents to the large-scale spatial sand-mud segregation patterns, should be set up. This hypothesis can thus be verified using the results from the various scenarios, in which tidal current- and short wave dominance is varied with.

Finally, when using this schematized approach for a practical case, the availability of relevant measurements appears important. Furthermore, as mud-related topics are environmentally related (section 1.1), considering an environmentally valuable area increases the relevance of the research. Therefore, a tidal basin in the Dutch Wadden Sea is considered as the area of interest (as it satisfies both statements).

By combining all of the above objectives, the main research question can be defined as:

> " *What are the relative influences of tide and (short) waves on the large-scale sand-mud segregation patterns and spatial sand-mud distribution in a tidal inlet system?* "

To successfully assess the main research question, some sub-questions are listed:

- How can the large-scale sand-mud segregation patterns and spatial distribution in a tidal inlet system (like one in the Dutch Wadden Sea) generally be described?
- What are (presently) the governing equations regarding the erosional behaviour of sand-mud mixtures (which are used in the chosen model)?
- To what extend do the results from a schematized model (dis)agree with the general description of large-scale sand-mud segregation patterns and spatial distribution, as described with the assessment of sub-question one?
- How are sand-mud segregation patterns responding to different forcing, using different combinations of waves and currents in a number of model cases? Can these responses be explained qualitatively, using physical properties, -processes and –mechanisms?
- Is it possible to develop a general classification related to relative dominance of different forcing (like short waves or tide), regarding the results from sub-question four?

As previously stated, for the assessment of this thesis, a tidal basin in the Dutch Wadden Sea is used as a case scenario. To be precise, the Amelander tidal inlet system (the combination of the Amelander inlet and associated tidal lagoon) is considered as the spatial domain for this thesis. The study will therefore be limited to sand and mud particles (as gravel is hardly present in this system).

Investigating spatial sand-mud segregation in the Dutch Wadden Sea is very relevant. This becomes evident when relating the properties of the Dutch Wadden Sea to the previous sections. First, many (relevant) measurements are available in the Dutch Wadden Sea. Secondly, when looking at the mud-related topics in section 1.1, any of these topics can be identified as environmentally related. The tendency to assess environmental consequences from any interference by a project in, for example, an environmental impact assessment (EIA), also highlights the need for knowledge in sand-mud segregation for this location, as the area is environmentally valuable (see section 2.1.1). Finally, the area is a typical location for spatial sand-mud segregation, as figure 1.2 (and section 2.1.4) suggests.

Considering all these statements, one gets familiar with the importance in knowledge on sand-mud segregation in the Dutch Wadden Sea. Combining this with the insightful idealized research by e.g. Hibma (2004) and recommendations from Van Ledden (2003) to analyse idealised tidal basins (to further understand the physical processes behind sand-mud segregation patterns) and the relative influence from different forcing conditions, a final aim for the execution of the thesis can be stated: the elaboration of a sand-mud segregation model in an idealised tidal basin in the Dutch Wadden Sea, using different forcing conditions. By doing so, a general classification can be constructed as well, relating relative dominating forcing conditions to the overall characteristics of large-scale sand-mud segregation patterns.
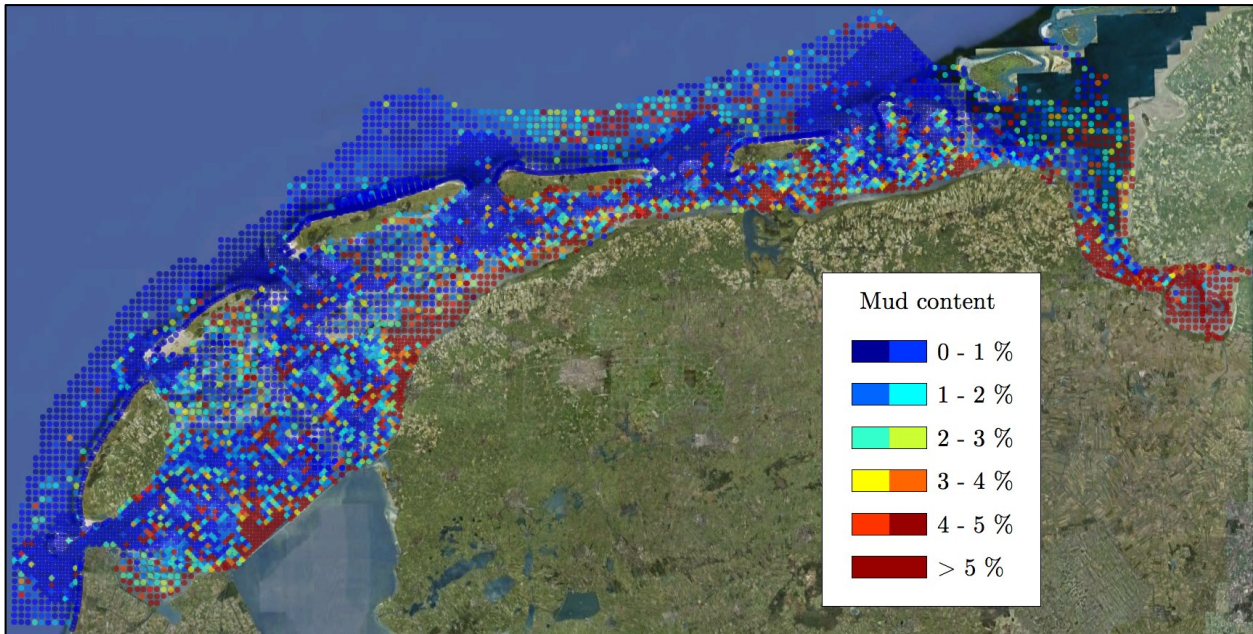
Figure 1.2: Spatial mud content distribution in the Dutch Wadden Sea, based on 7502 measurements starting in 1989 ('Sedimentatlas' of the Dutch Wadden Sea, RIKZ, 1998)

1.4 Outline

The focus of chapter 2 is on observations and theory, starting with a general description of the Wadden Sea and its features, before providing more specific information on the Amelander tidal inlet system itself. After this, observations, descriptions and theory regarding large-scale sand-mud segregation are addressed. Furthermore, a description of the forcing on these systems is provided, as it is very important for the (morphological) development and sand-mud segregation. Section 2.3 provides relevant theory behind sediment transport. Divided in sand, mud and sand-mud mixtures, subject to the previously described forcing. The chapter ends with a sand-mud segregation classification hypothesis, which combines all theory and observations from the previous sections with an existing classification (and thus proposes an extension).

All the aspects of the tidal inlet system model are considered in chapter 3. This chapter starts with an introduction to the schematized Amelander tidal inlet system model by Dissanayake (2011). The theoretical background behind the Delft3D model is addressed after, focussing, respectively, on Delft3D in general and on the sand-mud mixture version. Furthermore, important model assumptions are elaborated and the sand-mud mixture version of Delft3D is verified using a (previously developed) 1D model (based on Van Ledden *et al.*, 2004b).

Chapter 4 starts with an introduction into the different scenarios and an assessment of the time aspect of the model. Sections 4.2-4.4 present the model results. Starting with the reference situation, divided in observations and further analysis. Continuing this course, the different scenarios are addressed after and further analysis is elaborated. Using these results, the proposed classification is verified, which is based on the hypothesis from section 2.4 (also using observations from section 2.1.4). The chapter ends with a discussion related to the entire thesis, (model) approach and final classification.

Finally, conclusions and recommendations from the thesis are provided in chapter 5, answering the research questions and relating model results to hypotheses, physical background and observations in the field, while also stating some advice for future research.

Note that, although the specification of most variables is introduced within the text, some variables are (for the sake of brevity) only denoted in the list of symbols (which is provided at the end of this thesis).

Chapter 2

Observations, Theory & Classification Hypothesis

One important objective within this thesis is setting up a hypothesis that relates relative dominance of short waves or tidal currents to the large-scale spatial sand-mud segregation patterns, which can be verified using the proposed schematized model. The setup of this hypothesis can be regarded as the overlapping aim of this chapter. It starts with a general description of the Dutch Wadden Sea (and Amelander tidal inlet system) and its relevant features before providing observations and assumptions related to large-scale sand-mud segregation patterns. Furthermore, relevant theory behind forcing and sediment transport is provided. By combining all this information, the hypothesis is setup at the end of this chapter.

2.1 The Dutch Wadden Sea

2.1.1 Areal description

The Wadden Sea, stretching nearly 500 kilometres from the northwest of the Netherlands to the southwest of Denmark, is a shallow sea, which is separated from the North Sea by several barrier islands (called the Frisian Islands in the Dutch part of the Wadden Sea). The many features, for instance the intertidal areas (sand- and mudflats), wetlands (salt marshes), tidal lagoons, estuaries and channels make it a diverse and rich area in both flora and fauna, but also in natural, touristic and aesthetic value.
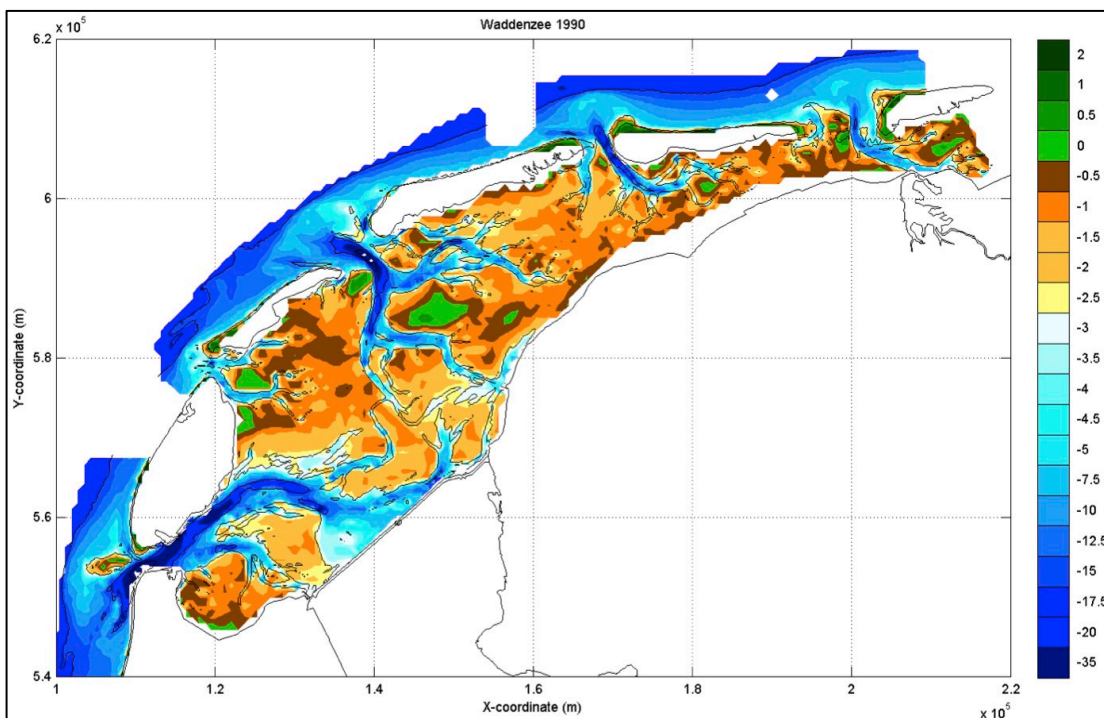

Figure 2.1: Bathymetry of the Dutch Wadden Sea, measured in 1990 (Elias *et al.*, 2007)

The Dutch part of the Wadden Sea consists of tidal basins, which can be classified as tidal lagoons (Carter, 1988). These tidal lagoons are defined as partly enclosed bodies of water, which are connected to the adjoining North Sea through a tidal inlet and are enclosed by barrier islands, the mainland and tidal divides. Intertidal zones (e.g. mudflats) are, also by definition, present in tidal lagoons, due to the tidal influence. This tidal influence also creates channel structures within the tidal lagoons. When looking at the bathymetry of the Dutch Wadden Sea (figure 2.1), these channels and intertidal zones can easily be identified. A typical cross section in the Dutch Wadden Sea combined with sea levels (after Flemming & Bartholomä, 1997) also clearly indicates the bathymetry and its features, like intertidal zones and tidal channels (figure 2.2).
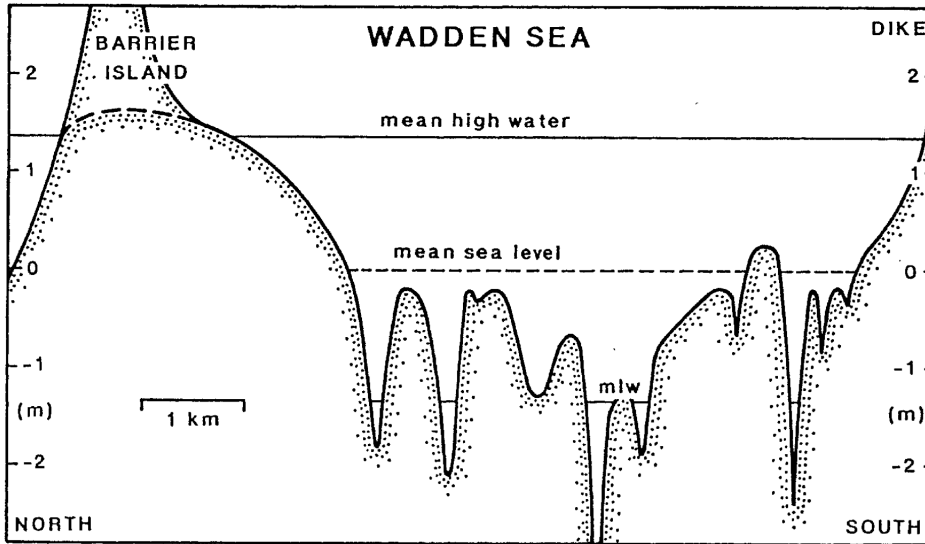
Figure 2.2: Typical topography cross-section in the Dutch Wadden Sea (Flemming & Bartholomä, 1997)

Each tidal lagoon in the Dutch Wadden Sea features an associated tidal inlet, together called a tidal inlet system. Each tidal inlet system has distinct properties, like the (intertidal) area and tidal prism. The distinction between different tidal basins in the Dutch Wadden Sea is generally made using the location of the tidal divide (also watershed/wantide). The tidal divide (Vroom, 2011) is defined as the border where tidal currents meet. This definition implies no transport of water and sediments on this border[2]. Note that a vertical tide is still present at the tidal divide locations, whereas the horizontal tide (by definition) cancels out against the several tidal components (commonly two, or three at some locations)

The different tidal lagoons and associated tidal inlets (tidal inlet systems) in the Dutch Wadden Sea have different characteristics and properties. The basin size, the area of the tidal flats and the tidal prism are, for example, some important properties of the tidal inlet systems. The different tidal inlet systems in the Dutch Wadden Sea are geographically introduced in figure 2.3, in which dashed lines indicate the tidal divides of the different tidal lagoons. Some associated properties, as mentioned above, are listed in table 2.1.

Inlet	Average tidal prism [10^6 m^3]	Area during mean high water [km^2]	Tidal flat area [km^2]
Texel Inlet	1054	712	121
Eierlandse Gat Inlet	207	153	106
Vlie Inlet	1078	668	323
Ameland Inlet	478	309	165
Frisian Inlet (+ Pinkegat)	300	195	124
Eems-Dollard Inlet	1000	520	214

Table 2.1: Properties of tidal inlet systems in the Dutch Wadden Sea (Louters & Gerritsen, 1994)

---

[2] This definition is based on tidal currents, though short (wind) waves can transport water and sediment through these tidal divides
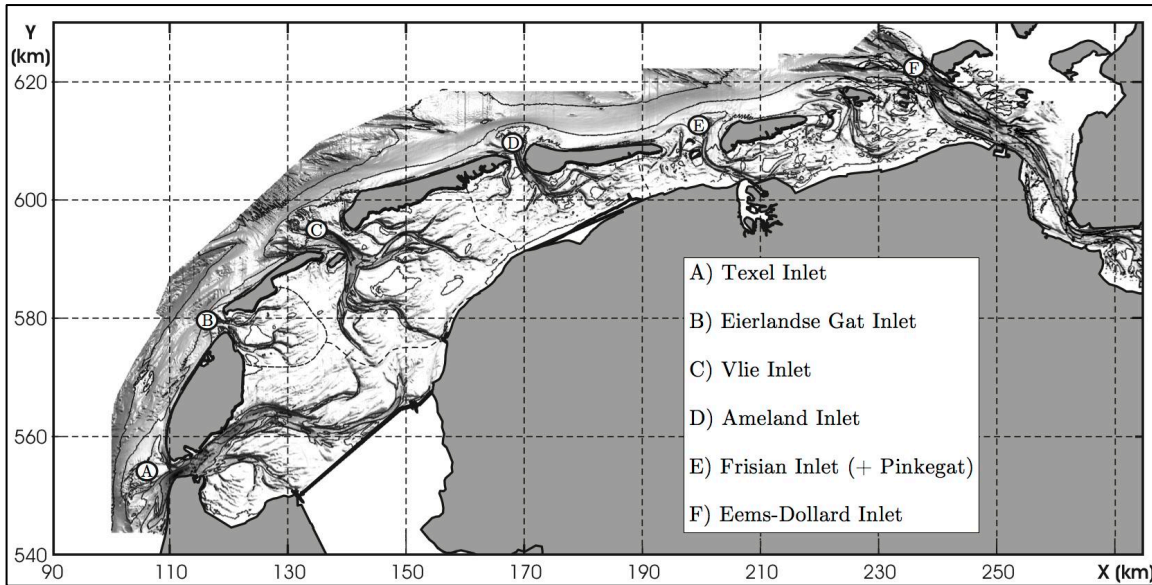
Figure 2.3: Tidal inlet systems in the Dutch Wadden Sea (modified after Elias, 2006, based on '*Vaklodingen*' 1997-1999)

The tidal basins in the Dutch Wadden Sea are valuable systems, for both man (e.g. recreation, navigation and nearby settlement) and nature (e.g. growing, feeding and breeding). The granting of 272.449 hectares in the Dutch Wadden Sea with the Natura 2000 status and inscription in the UNESCO world heritage list, both in 2009, clearly stresses this statement, as it protects the natural value of almost the entire Dutch Wadden Sea area (figure 2.4). Again relating this to the mud-related topics from section 1.1, an important reason for modelling sand-mud segregation in the Dutch Wadden Sea (related to the environmental value) is evident.

Figure 2.4: Natura 2000 area (in yellow) of the Dutch Wadden Sea (Website of Dutch ministry of economic affairs, agriculture and innovation, 2009)

2.1.2 Morphological features

The different morphological features, present in the tidal inlet systems in the Dutch Wadden Sea, are strongly determined by the tide and associated currents, but also waves play a significant role at certain parts of the system. A tidal inlet system can either be flood-dominated, ebb-dominated or have a mixed tidal dominance, as indicated in figure 2.5 (the tidal inlet systems in the Dutch Wadden Sea typically have a mixed tidal dominance, and thus, approximately equal in- and outflow of water). The different morphological features, like salt marshes, priels (gullies) and locations for sediment deposition are also indicated within this

figure. Note that the locations of the tidal divides (wantide/watershed) highly determine the locations for mud settling (based on tidal forcing only), since currents (and thus bed shear stress) are practically zero at these locations (as introduced in section 2.1.1), it is commonly here, that mudflats are found (although mudflats are also often found near the inner land boundaries, the local situation (e.g. non linearity in tides) is of great influence on these characteristics).
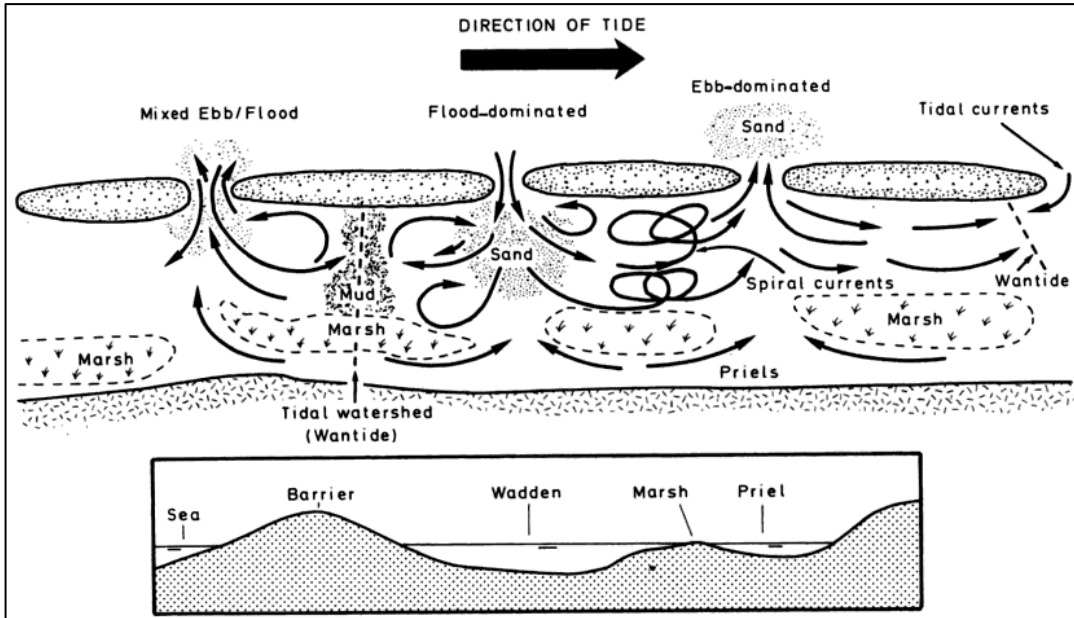
Figure 2.5: Tidal induced morphodynamic aspects in the Dutch Wadden Sea with types of passes, currents and features (Carter, 1988)

The tidal inlet systems in the Dutch Wadden Sea can be divided in 3 parts, the (inner) flood-tidal delta, the tidal inlet (between the barrier islands) and the (outer) ebb-tidal delta. All of these segments are tide dominated, but waves also play a significant role in the morphology of the ebb-tidal delta and the outer part of the barrier islands (short waves are also responsible for the generation of barrier-islands, according to Davis & Hayes, 1984). Global patterns of tidal inlet systems in the Dutch Wadden Sea were provided by Van Veen (1950) and are reprinted in figure 2.6 below. The different parts of the tidal inlet systems in the Dutch Wadden Sea are further elaborated in the following sections.
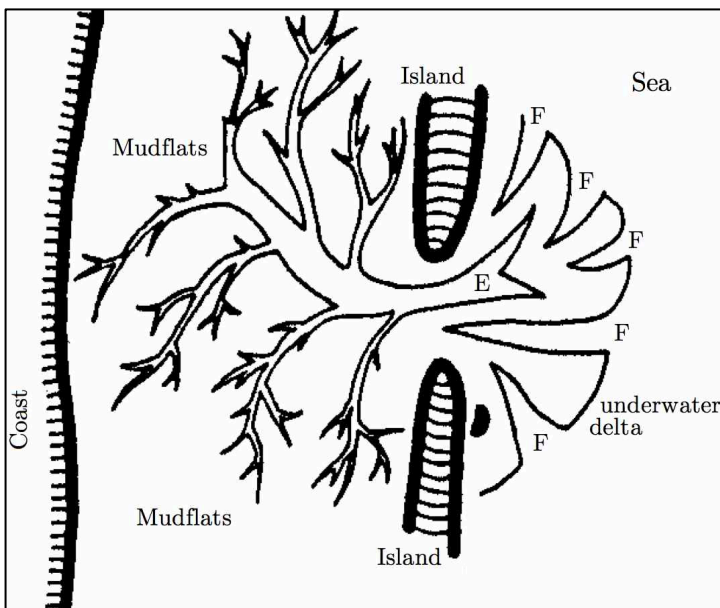
Figure 2.6: Overview of tidal inlet systems in the Dutch Wadden Sea, indicated with F and E for relative flood and ebb dominance (modified after Van Veen, 1950)
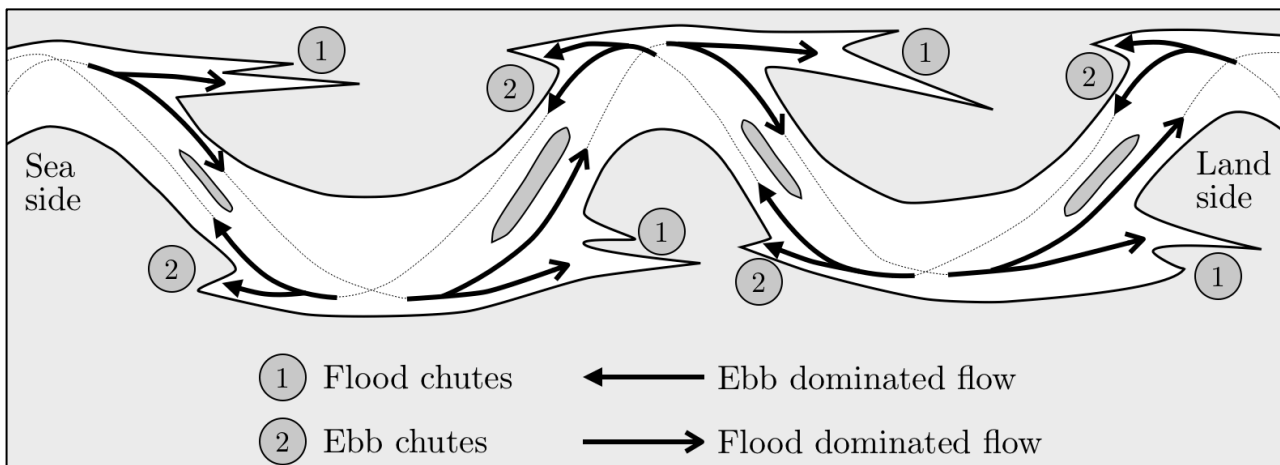
Flood-tidal delta

The (inner) flood-tidal deltas in the Dutch Wadden Sea consist of complex channel systems (Cleveringa & Oost, 1999) and intertidal areas, as indicated in figure 2.1 and 2.6. The channel systems are formed due to the strong tide, in which distinct channels can be identified with a relation to either ebb or flood dominated currents. Residual circulations in the flow conditions explain the phenomenon of distinct ebb and flood channels, but are also created due the continuously changing morphology (and thus hydrodynamics). Secondary flows are dwarfed by tidal flows, but play a significant role in the morphodynamic behaviour and evolution of the meandering channels. Contributors to the secondary flow are, among others, curvature, inertia and the Coriolis effect.

The secondary flow is responsible for a net sediment transport towards the inner side of a channel bend, which accretes, while eroding the outer side of the bend. This means that channel bends experience positive feedback, i.e. they enhance their characteristics over time. Since positive feedback applies for channel bends, straight channels are by definition unstable, and a small eccentricity results in an ever-growing channel bend[3]. This behaviour explains why channels in a tidal basin are commonly meandering through the system.

The Coriolis effect is responsible for splitting up tidal channels in distinct ebb and flood-dominated channels, as it acts perpendicular to the direction of the flow. Ebb and flood currents are generally in opposite (approximately 180°) direction, forcing the ebb and flood flow to opposite channel sides.

When enough accommodation space is available, the ebb and flood channels can develop independent/separately. The different flood and ebb channels feature different characteristics that can be related to physical processes. Flood channels are, for instance, shallower than ebb channels and tend to diverge into intertidal areas, while ebb channels are often more deep and continuously shaped.

When channel bends are present (and growing due to the processes explained above), the inertia of the tidal prism can result in overshoot, the flow will then take a wider bend. The ebb and flood currents can create an ebb and flood chute. The flood chutes lead to the adjacent intertidal areas, and are, because of the higher water levels, better developed compared to ebb chutes, since the ebb tidal current mainly follows the main channels (and are therefore deeper, as indicated above). Van Veen (1950) described ebb- and flood chutes for various cases, figure 2.7 visually describes this behaviour.

Figure 2.7: Meandering channel with distinct (less developed) ebb- and (well developed) flood chutes

For more info on flood tidal deltas, one is referred to Hayes (1980) and Bosboom & Stive (2011).

---

[3] Physical limits, related to, for instance Coriolis and inertia (spill-over), prevent channel bends from increasing 'to infinity' in reality. An oxbow lake is a very interesting and practical example for this in the field of river engineering.

Tidal inlet

The tidal prism enters the (inner) flood-tidal delta through the tidal inlet. The behaviour and stability of the inlet is dependent on, amongst others, the tidal prism, tidal currents, waves, storms and littoral sediment transport. The stability of the cross-sectional area of a tidal inlet has been described within various researches, Escoffier (1940) being an important contributor to this list.

Since the tidal inlet itself is less relevant within this thesis, one is referred to a brief, but complete, overview of relevant researches and associated conclusions, found in Bosboom & Stive (2011).

Ebb-tidal delta

The (outer) ebb-tidal delta is an area that is subject to both waves and tidal currents. For the Dutch Wadden Sea, the tide propagates from west to east (section 2.2.1) and dominant waves come in from a NW-NNW direction (figure 2.8). While the ebb tidal current deposits sediment in the ebb-tidal delta, the waves shape, smoothen and transport it. But also the interaction between the (alongshore) tidal propagation, waves and tidal currents triggers residual transport. The wave- and tide-induced residual transport results in a drumstick shaped barrier-island on the eastern side. Figure 2.8 shows a schematized representation of all the residual transports, induced by waves and tide.
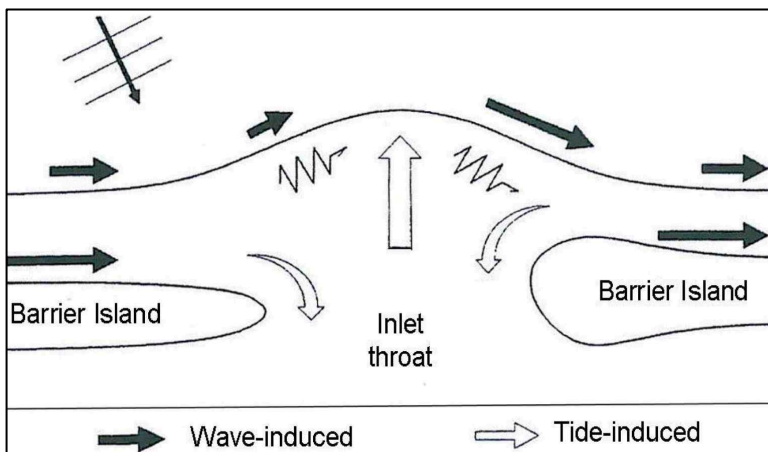

Figure 2.8: Residual transport due to waves and tides in the ebb-tidal delta, the main channel is ebb dominated, the tide propagates from west to east and waves come in from a NW-NNW direction (De Vriend *et al.*, 1994)

Since the ebb-tidal delta is, along with the tidal inlet, less relevant within this thesis, one is referred to a brief, but complete, overview of relevant researches and associated conclusions, found in Hayes (1980) and Bosboom & Stive (2011).

2.1.3 Amelander tidal inlet system

Between Terschelling and Ameland, the Amelander inlet is located, which, together with the inner flood-tidal basin (lagoon) and the outer ebb-tidal delta, is called the Amelander tidal inlet system. This is the area of interest (model domain) within this thesis. As indicated before, a tidal inlet system features channels and intertidal areas, which are labelled (by name), in figure 2.9 (where red stars indicate hydrodynamic measuring facilities).
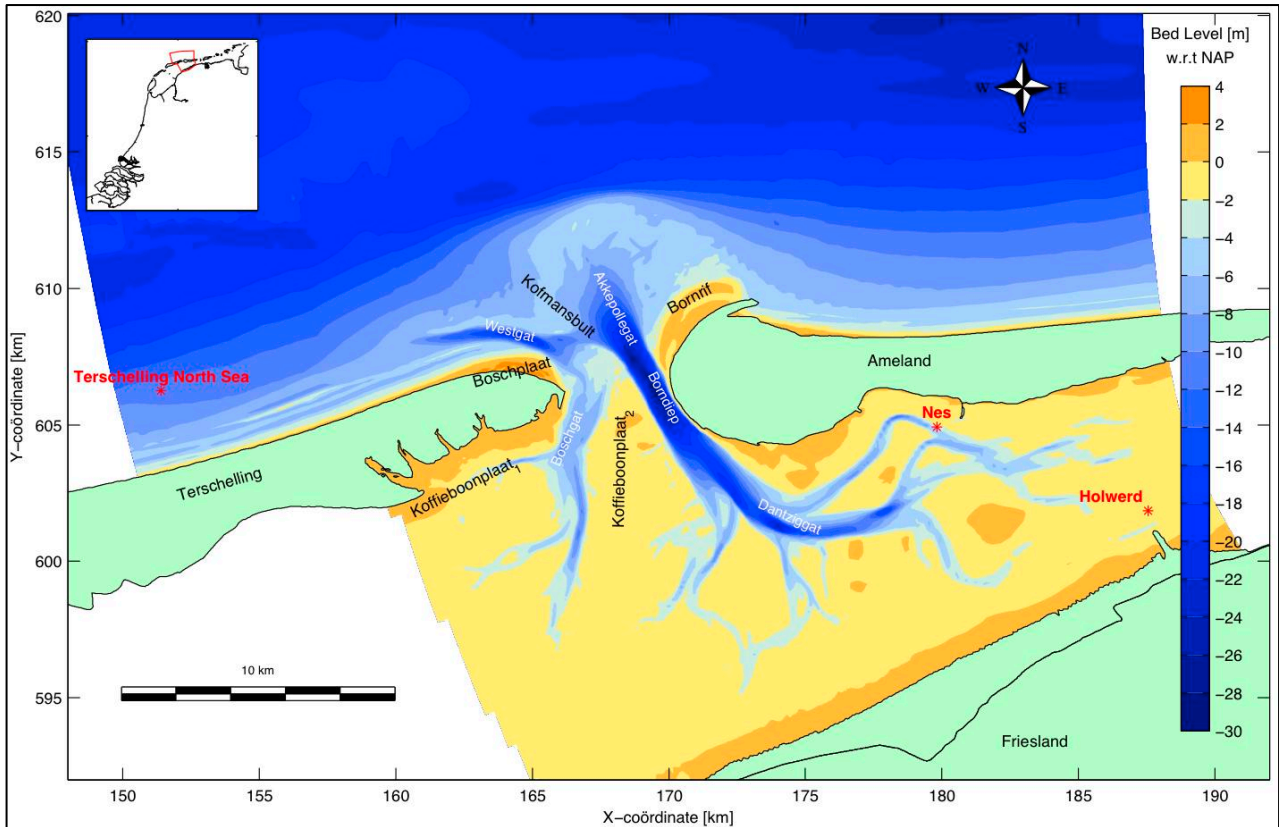
Figure 2.9: Amelander tidal inlet system and (in Dutch) associated channels and flats (Fockert, 2008, based on '*Vaklodingen*', 1989)

Some properties of the tidal inlet systems in the Dutch Wadden Sea were given in table 2.1. Table 2.2 extends this data specifically for the Amelander tidal inlet system.

The Amelander tidal inlet system	
Basin area (A_b)	269 km^2
Tidal flats area (A_f)	170 km^2
Length (L)	30 km
Tidal prism (Ω)	$275 \cdot 10^6$ m^3
Tidal range (H)	2,15 m
Tidal inlet width	2250 m
Mean inlet depth	14 m
Average sediment flux	$5,5 - 7,5 \cdot 10^6$ tons/year

Table 2.2: Properties of the Amelander tidal inlet system (Eysink, 1993)

According to Fockert (2008), the Amelander tidal inlet system accumulates sediment, though, due to the small amount, it can be (more or less) assumed that the Amelander inlet system is stable (and would accumulate sediment during relative sea level rise (see also, Dissanayake *et al.*, 2009a)).

Through the years, the Amelander inlet system has changed its appearance, mainly due to human interventions. Already since the year 1000, the Frisians slowly closed off the Middel Sea from the Wadden Sea over many centuries. The Middel Sea formerly adjoined the lagoon of the Amelander tidal inlet system and stored a significant part of the tidal prism during the tidal cycle. The Amelander inlet system has changed its characteristics and properties in accordance to the changes made by man. Tidal divides (both east and west) shifted eastward and channel patterns rotated from a north-south orientation to a more east-west orientation accordingly. Van Der Spek (1994) and Cleveringa *et al.* (2005) investigated these changes over time, a combination of their research is used to construct figure 2.10.
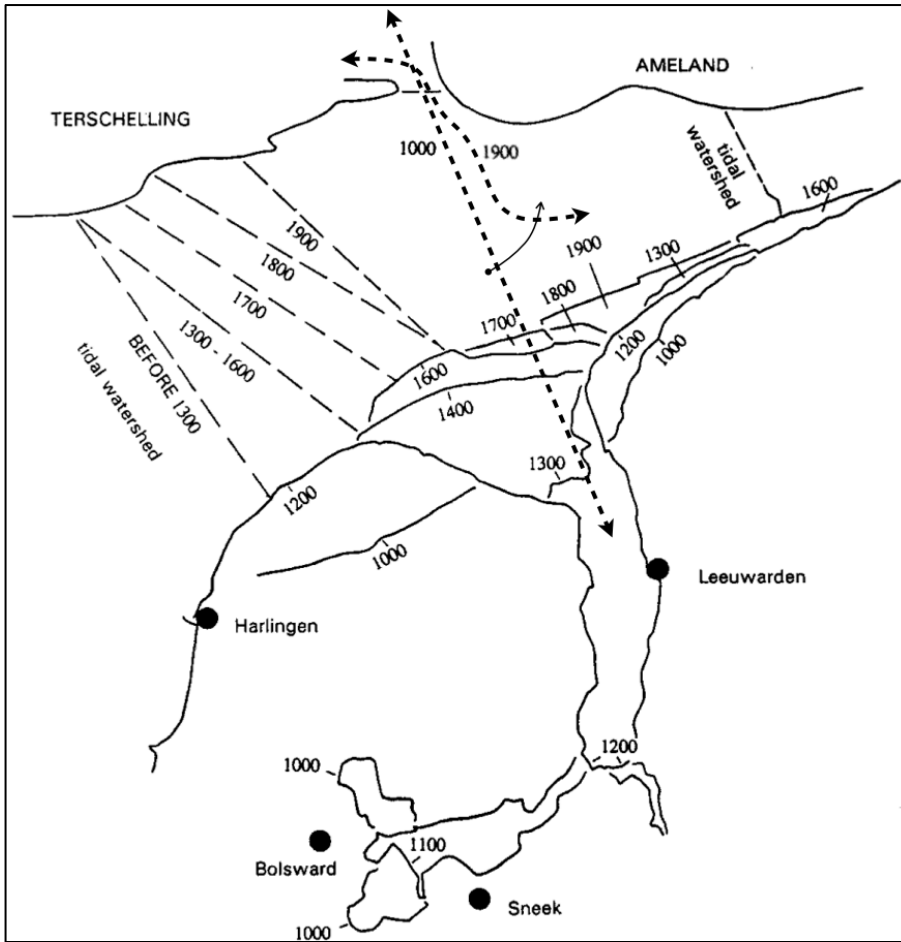
Figure 2.10: Damming of the Middel Sea in the past millennium and the influence on the tidal divides (watersheds) and main channel orientation (modified after Van der Spek, 1994 & Cleveringa *et al.*, 2005)

A more general description (as it is also valid for, for instance, the closure of the Lauwers Sea) is found in figure 2.11, which is inspired and modified after Van Veen (1950).
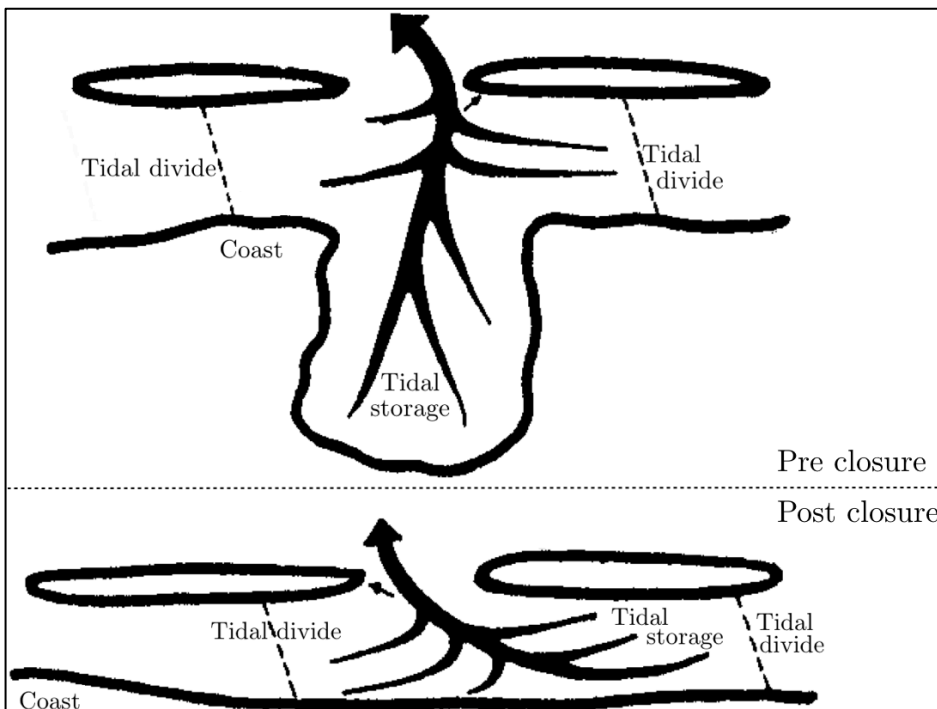
Figure 2.11: Changes in tidal divides and channel orientation (inspired and modified after Van Veen, 1950)

Though the influence of mankind over time is clearly shown in figure 2.10 and 2.11, the Amelander tidal inlet system is relatively stable, especially when compared to other tidal inlet systems in the Dutch Wadden Sea, where some huge changes in characteristics were made in a relatively short period of time (e.g. the completion of the Afsluitdijk (in 1932) and the closure of the Lauwers Sea (in 1969), which were abrupt compared to the slow closure of the Middel Sea).

For an overview of the history of the entire Dutch Wadden Sea (also on a much longer timescale) one is referred to Speelman *et al.* (2009), in particular section II (by A.P. Oost).

2.1.4 Large-scale sand-mud segregation patterns

Around the world, sand-mud segregation patterns can be recognized, as various tidal basins show comparable behaviour related to sand-mud segregation. The most obvious observation is the settlement of mud in less dynamic areas. This implies, in the tidal lagoons in the Dutch Wadden Sea, an accumulation of cohesive sediments near the inner (and shallower) land boundaries and near tidal divide areas (as previously described and introduced in figure 2.5).

Various descriptions, observations and measurements on sand-mud segregation have been made in the past. The measurements, for instance, (described by) Postma (1954), De Glopper (1967) and provided by Rijkswaterstaat (1997) in project Strobodi, by RIKZ (1998) in the *Sedimentatlas* (in Dutch) and by Zwarts *et al.* (2004), indicate the presence of high mud content in the Dollard, (former) Lauwerszee and near the coastlines of Groningen and Friesland. But also the tidal divide areas are characterized by higher mud contents. Postma (1954) executed a huge analysis on the Dutch Wadden Sea, addressing various topics, also related to the distribution of sediment properties throughout the Dutch Wadden Sea. Figure 2.12 indicates the mud content at various test locations, carried out with a Van Veen bottom sampler (grab). This figure is one of the first indications of sand-mud segregation, and, according to Postma (1954), it occurs due to a decrease in hydrodynamic activity further into the Wadden Sea.


Figure 2.12: Mud content in the south-western area of the Dutch Wadden Sea, measured with a Van Veen bottom sampler (grab), large circles indicate high mud contents (up to 50%) while points indicate no mud content at all (Postma, 1954)

Furthermore, figure 2.13 shows the mud content in the entire Wadden Sea (Zwarts *et al.*, 2004), while figure 2.14 indicates the mud content specific for the Amelander tidal inlet system. Figure 2.15 shows the median grain size distribution in this area. Although discrepancies between figure 1.2, 2.13 and 2.14 can be found (probably due to differences in measuring techniques and choices for representation (maximum value in the legend scaling)), the overall observations from these figures show an identical spatial distribution of mud content.
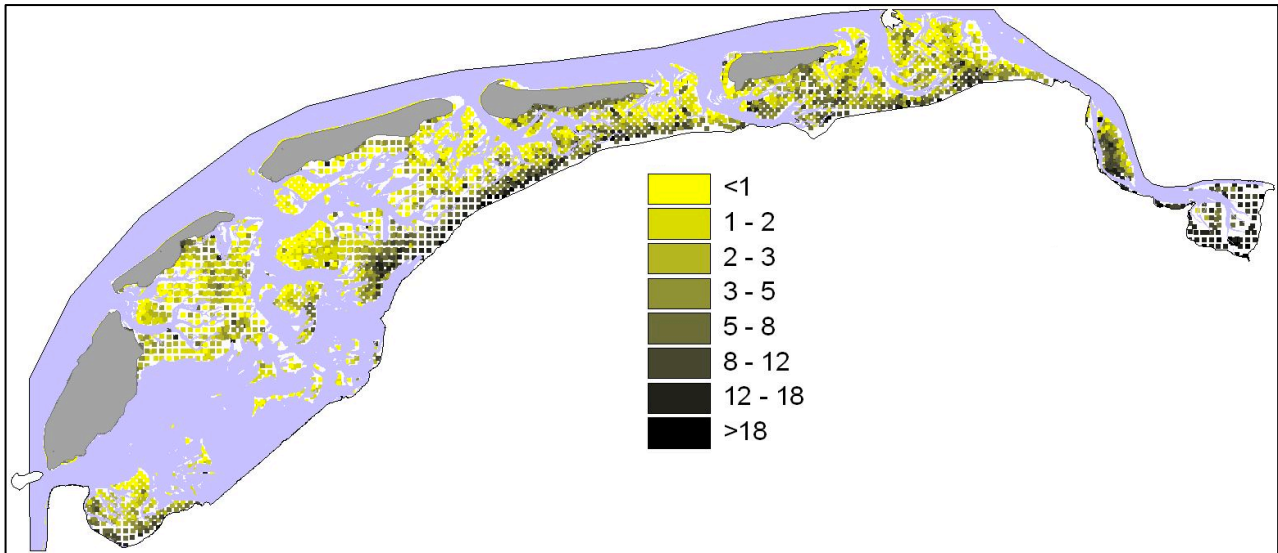
Figure 2.13: Mud content [%], combined from Malvern-, Coulter- and mud samples (Zwarts *et al.*, 2004)
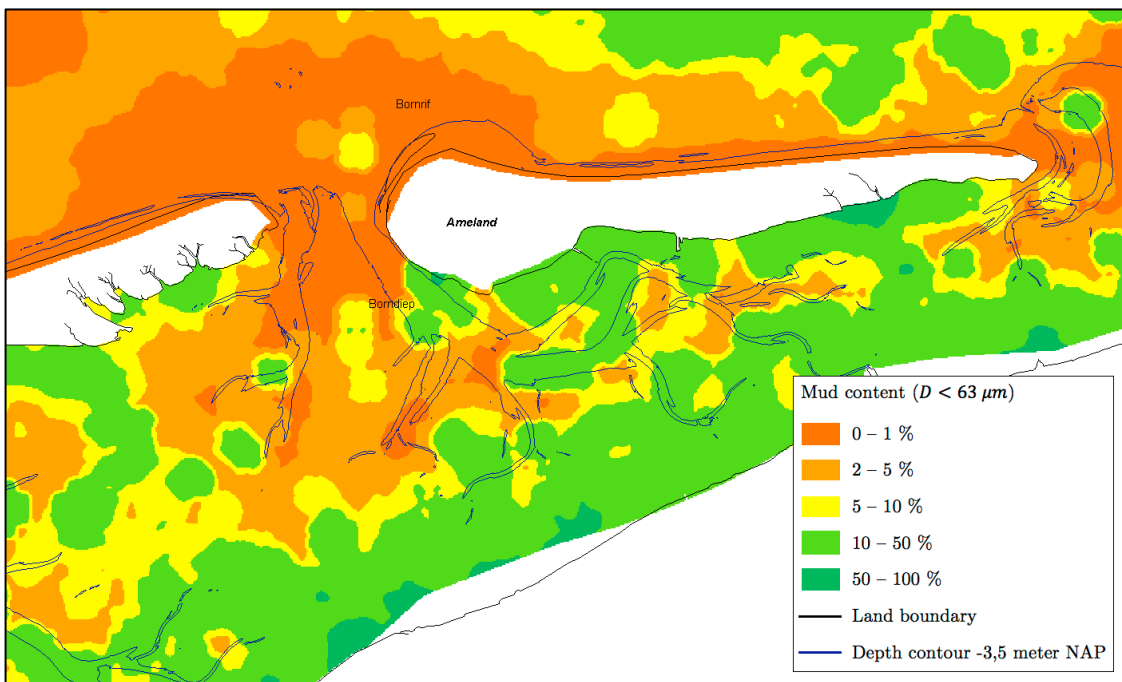
Figure 2.14: Distribution of mud content in the Amelander tidal inlet system (RIKZ, 1998)
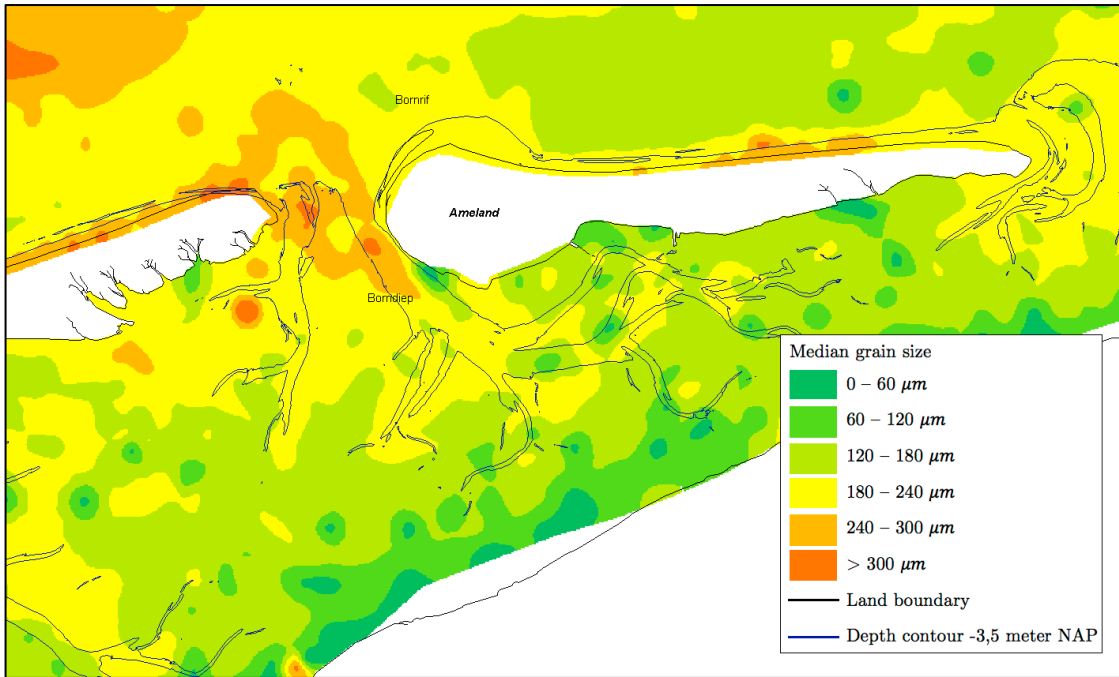
Figure 2.15: Median grain size distribution in the Amelander tidal inlet system (RIKZ, 1998)

Many (hypothetical) explanations for these observations have been given over time. Postma (1954), Van Straaten & Kuenen (1957) and De Glopper (1967) explained the increase of mud content over the basin length with the decrease of the energy gradient in this direction. Higher current velocities and waves (from sea) restrict mud particles from settling near dynamically active areas, like tidal channels and inlets. Whereas mud particles can settle in the less dynamic active areas like tidal divide locations and near the inner land boundaries, where mudflats are, indeed, commonly found. "The calmer the water, the higher the mud content" can be stated as a rule of thumb that is specifically related to this statement, though, it must be stressed that it is only valid if mud availability is large enough (Van Ledden, 2003). Former WL|Delft Hydraulics (1998) and De Bake (2000) visualized the correlation between mud content and bed shear stress by plotting measurements for, respectively, the Molenplaat and the Westerschelde, both located in the Netherlands. Both are plotted in figure 2.16 below, which is modified by Van Ledden (2003).
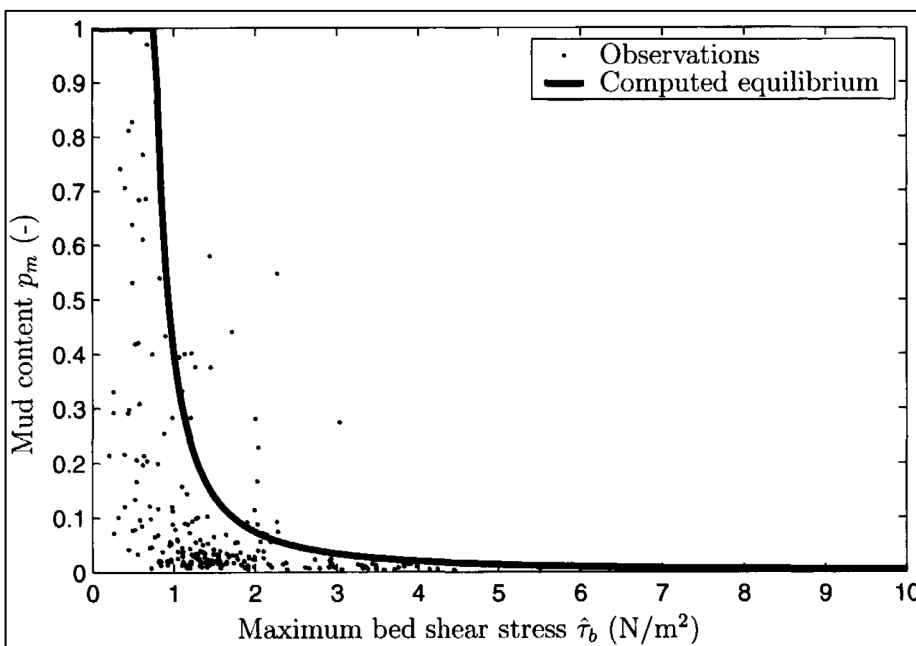
Figure 2.16: Correlation between observed mud content and maximum bed shear stress (Van Ledden, 2003, modified after WL|Delft Hydraulics, 1998 and De Bake, 2000)

Non-linear tidal asymmetry in shallow basins combined with lag effects (the mud particle transport during the (long) settling period after the critical shear stress is no longer exceeded, which is observed during the slack water period) implies inward transport of suspended sediment (section 2.2.1 and 2.3.1) with a small settling velocity w_m (Van Straaten & Kuenen, 1957; Postma, 1961; Groen, 1967; Oost, 1995; Wang *et al.*, 1999), which is typical for mud particles. This statement also explains the transport of mud particles, towards the end of channels (and towards the tidal divides and tidal lagoon boundaries).

Furthermore, a sharp transition between sandy- and muddy areas is both observed (e.g. Flemming & Ziegler, 1995 and Flemming & Bartholomä, 1997) and computed (Van Ledden, 2003; Van Ledden *et al.*, 2004b). These observations are shown in figure 2.17 and 2.18, while a 1DH computation is given in figure 2.19.
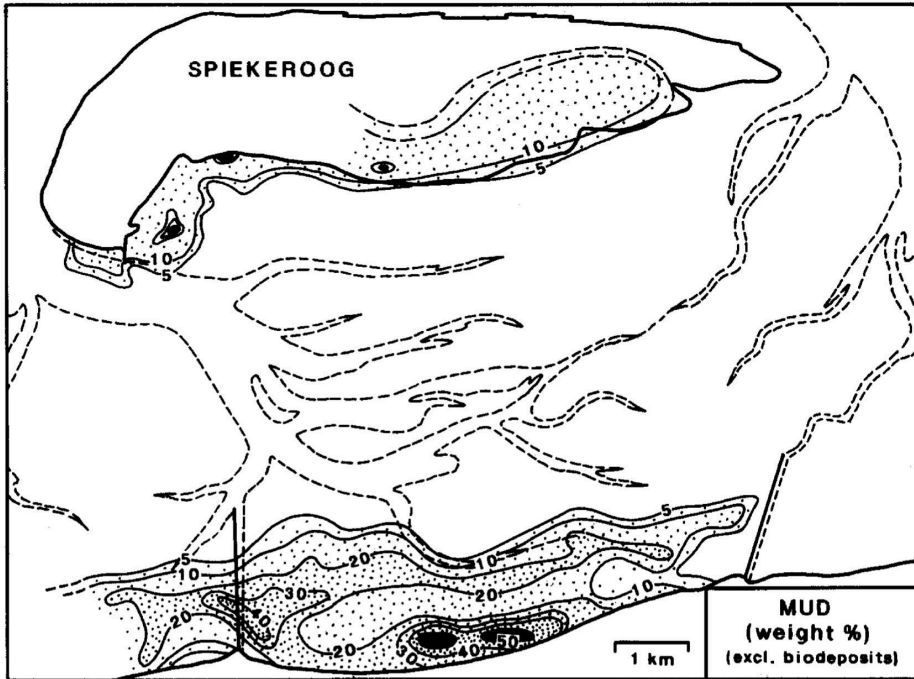
Figure 2.17: Mud content (% weight) in the tidal lagoon (indicated with contour lines) near Spiekeroog, Germany (Flemming & Ziegler, 1995)
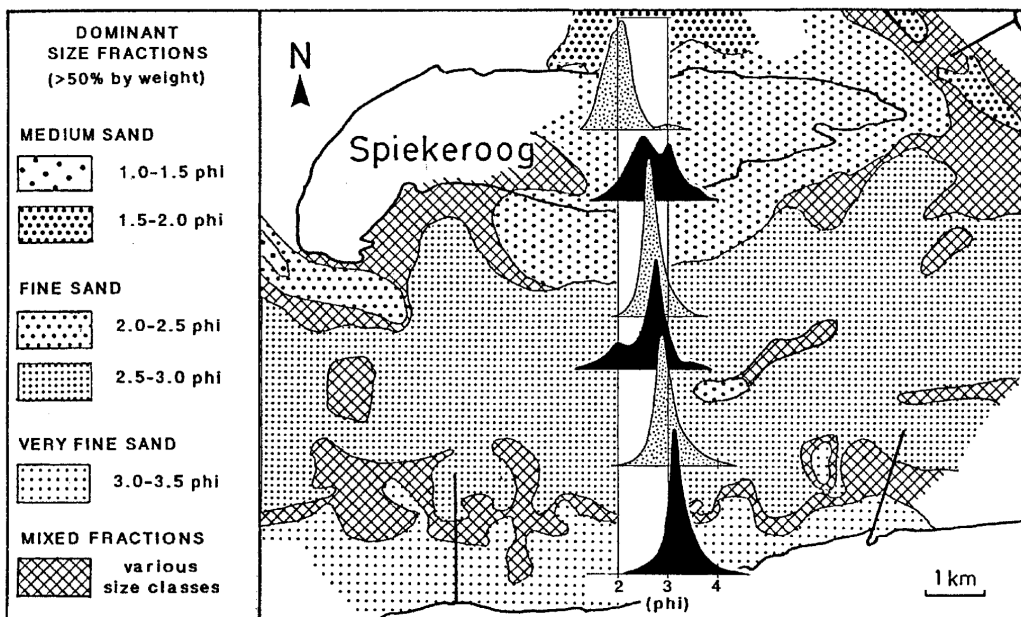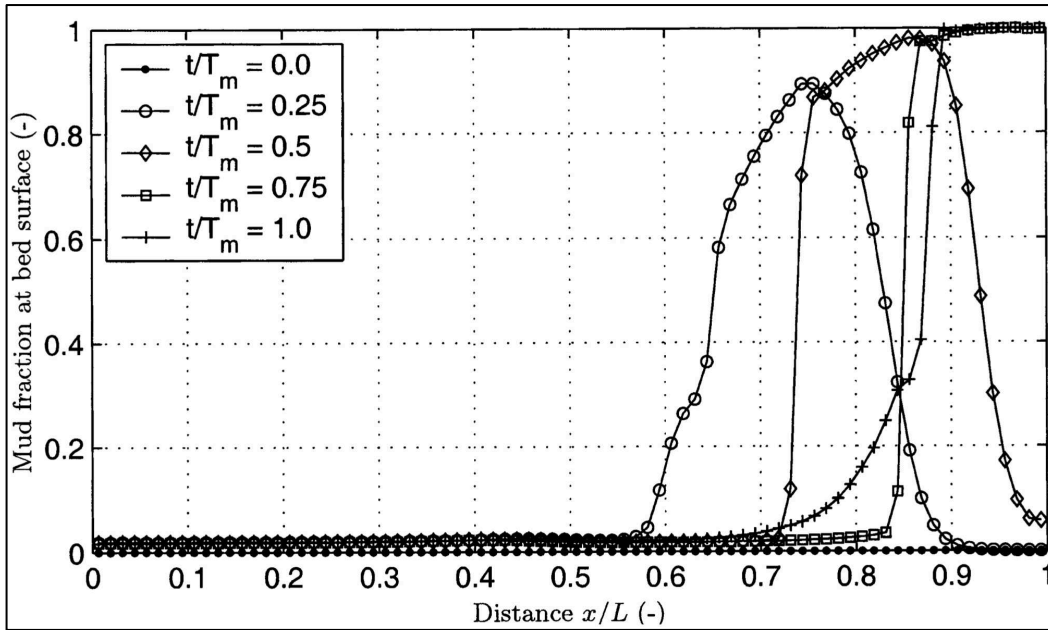

Figure 2.18: Dominant (>50% by weight) sediment sizes in the tidal lagoon near Spiekeroog, Germany. Expressed in phi, as indicated in the legend (Flemming & Bartholomä, 1997)

Figure 2.19: Computed mud fraction over morphological time ($T_m = 115$ yrs.) and plotted over basin length in a short (1D) tidal basin (Van Ledden *et al.*, 2004b)

Apart from the above, general patterns, small patches of higher mud content can be addressed by looking at the presence of (amongst others) mussel beds (introduced in section 1.1 as part of the flora and fauna). Mussels filter water and fine sediment, aggregating them into faeces, which are far more resistant to erosion (the erosion flux decreases due to a local increase in $\tau_{e,cr}$, while the deposition flux decreases at a more gentle rate, as it is dependent on both the erosion flux and the inflow of suspended sediment from other areas). Mussel beds are present in the Amelander tidal inlet system, as indicated in figure 2.20 below. They mainly appear in shallow areas, enhancing the above patterns. Though, they cannot be described as a general pattern, related to morphology and forcing, and will therefore not be taken into account during further analysis (though, again note the influence of flora and fauna on the mud content and the erosional behaviour of the bed as well, as introduced in section 1.1, and this represents only one (of many) species).
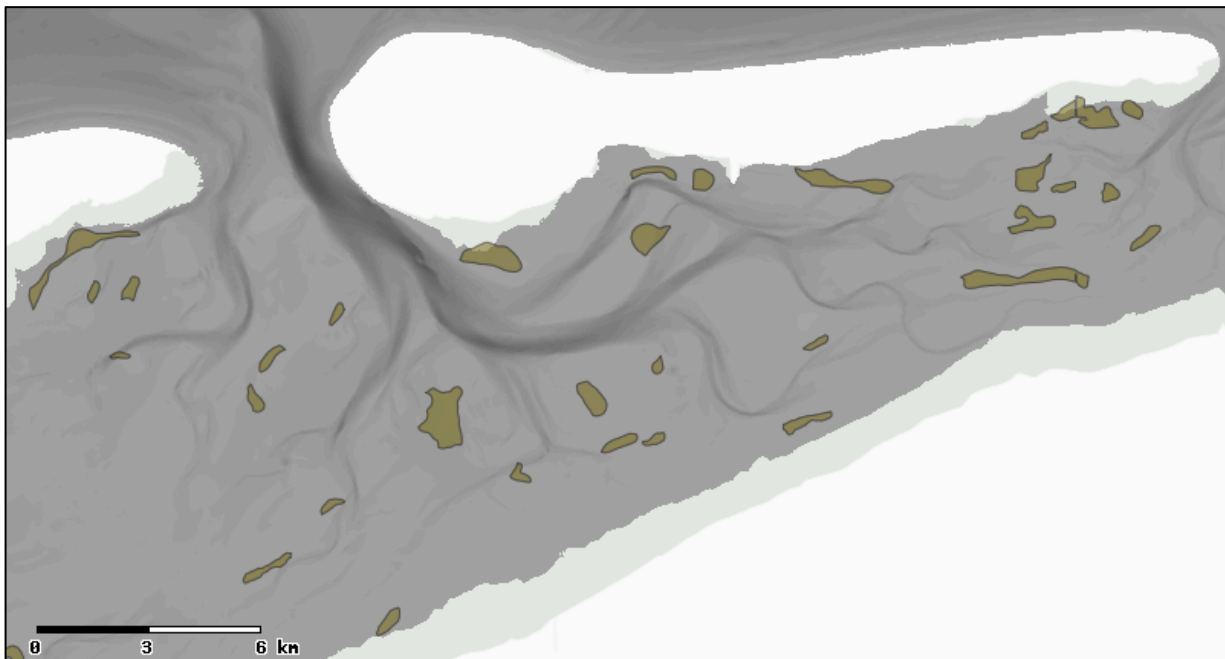
Figure 2.20: Locations of natural mussel beds in the Amelander tidal inlet system (Interwad, 2008)

2.2 Forcing

Tidal inlet systems (like the Amelander-) are subject to external forcing due to movements of water, the most significant movements herein being (short) waves and (tidal) currents (note that currents are also induced by waves, though, on a much larger (tidal) scale). Newton's physical laws of motion, dated 1687, explain the accelerations (movements) of objects (for instance water) with external forces. The external forces for short waves and tidal currents are, respectively, wind- and astronomically induced.

Although wind generates wind waves, it can also generate currents and water level set-up. Furthermore, gravity can induce currents due to water level gradients (for instance river runoff) and gradients in air pressure could produce seiches. These (and other processes) are not taken into account within this thesis, as waves and tidal currents dominate all other forcing processes in tidal inlet systems without river runoff.

2.2.1 Tidal currents

The tidal currents in the Dutch Wadden Sea are generated by the in- and outflow of the tidal prism (Ω). This flow is initiated by a combination of gravity and the water level differences between the Wadden Sea and the North Sea. Due to the M_2-tide, which is present in the North Sea, these water level differences occur. The M_2-tide is generated by the semi-diurnal astronomical tide, present in the North Atlantic Ocean, which finds its initiation within the centrifugal- and tractive forces, respectively between the Earth-Moon and Earth-Sun (systems). A description of the (generation of the) astronomical tide is found in, for instance, Steward (2008) and Bosboom & Stive (2011).

The propagation of the M_2-tide in the North Sea across the Wadden Sea barrier islands runs from the south-western Texel Inlet, past all other inlets, in the direction of the north-eastern Ems-Dollard Inlet and is a combination of two meeting amphidromic systems, as shown in figure 2.21.
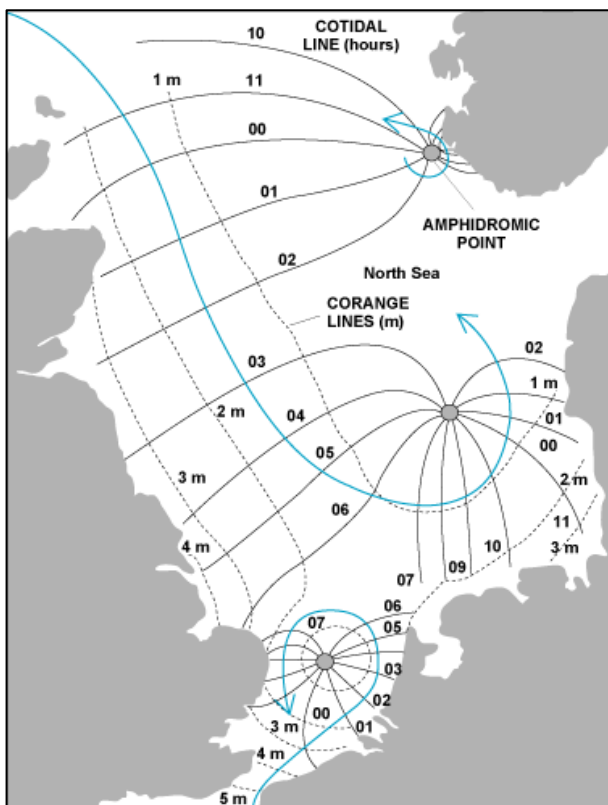

Figure 2.21: Tidal (amphidromic) systems in the North Sea (Kvale, 2008, modified from Dalrymple, 1992)

Due to the tidal phase difference between two successive inlets, the tidal divides are located at the east side of the barrier islands. Due to this property of the tide, the tidal channels are directed towards the east as well. This concept has been graphically introduced in some classic sketches by Van Veen (1950), of which one is reprinted in figure 2.22.
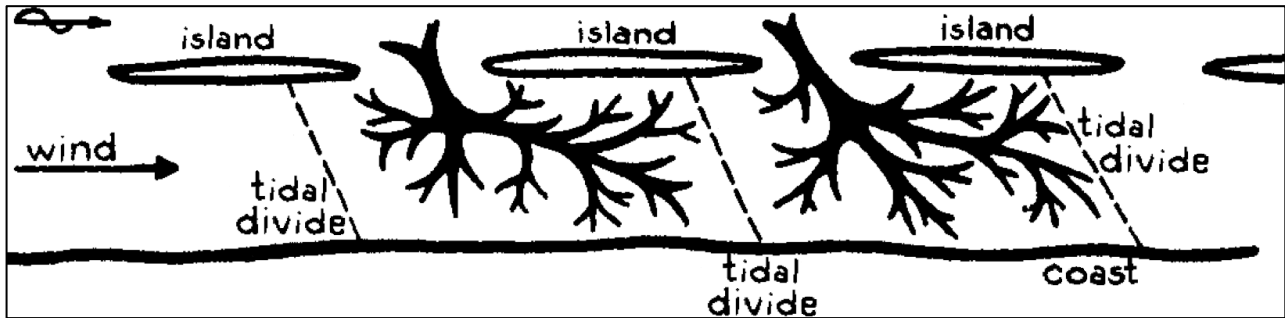
Figure 2.22: Graphical representation of tidal divides in the Dutch Wadden Sea (modified after Van Veen, 1950)

Tidal currents induce sediment transport due to bed shear stresses. Within the Dutch Wadden Sea, the tidal currents are the main contributor to sediment transport. To model this, it is of paramount importance to understand the behaviour of the tide.

Tidal asymmetry in a tidal basin

A propagating linear tide can lose its linear properties under the influence of non-linear interaction in shallow areas. Small depth, combined with continuity and/or bottom friction can create shallow-water tides, these tides feature higher harmonics (overtides). In the case of an M_2-tide, this can result in M_4 and M_6 tidal components, respectively originated from the continuity- and bottom friction principles[4].

The continuity principle can be reviewed by looking at the wave celerity in shallow water, which is given by the basic equation 2.1.

$$c_0 = \sqrt{gh} = \sqrt{g(h_0 + \eta)} \tag{2.1}$$

For shallow areas, the relative differences in instantaneous water depth result in different phase speeds during high and low tide. The differences in celerity, combined with continuity results in a saw-tooth-shaped tidal profile. This profile can be described mathematically by adding a tidal component with a double frequency (e.g. an M_4 in the case of an M_2-tide).

The proportionality of the bed shear stress due to tides ($\tau_b \propto \cos(\omega t)|\cos(\omega t)|$) is considered for the assessment of the bottom friction principle. A Fourier expansion of this term (Wang *et al.*, 1999) shows tidal constituents with tripled frequencies (e.g. an M_6 in the case of an M_2-tide).

2.2.2 Short waves

In the Wadden Sea, short waves are the second important mechanism (after tidal currents). Although short waves are larger in the North Sea (due to larger fetch and depths), the barrier-islands block almost all incoming short waves from the North Sea. Although some 'North Sea waves' penetrate the tidal lagoon from the tidal inlet, they are subject to heavy diffraction (due to the relative size of the tidal inlet versus the size of the tidal lagoon). Furthermore, the short waves from the North Sea enter the tidal lagoon through the deep tidal inlet into an area with (commonly) deep tidal channels, where short waves hardly contribute to

---

[4] These processes are (respectively) responsible for all tidal components featuring periods with doubled or tripled frequencies (e.g. from the astronomic M2 or S2 tide). Other tidal components (e.g. MS4) are generated by interactions between tidal components, these components are, along with the S-tide and third order M-components, not considered within this thesis.

sediment transport (and thus possible sand-mud segregation). Therefore, the influence from short waves from the North Sea is neglected in this thesis.

Apart of the incoming waves from the tidal inlet, local short waves are also generated within the tidal lagoon, due to wind forcing. These waves do contribute to sediment transport, mainly by stirring up sediments within the tidal lagoon. Short waves commonly dissipate their energy in the shallows (waves 'feel' the friction induced by the presence of the bottom in the shallows), which stirs up sediment. Relating this to tidal asymmetry, the short waves can be responsible for high mud concentrations near shallow system boundaries.

Short waves in oceanic and coastal waters are commonly described using the linear wave theory (Airy, 1845). Commonly, the harmonic (co)sine wave, travelling in the positive x-direction (equation 2.2) with a phase speed (celerity) c_0 [m/s] (as indicated in equation 2.3) is used to mathematically describe (short) waves.

$$\eta(x, t) = a \sin(\omega t - kx) = \frac{H}{2} \sin(\omega t - kx) \tag{2.2}$$

$$c_0 = \frac{\mathrm{d}x}{\mathrm{d}t} = \frac{\omega}{k} = \frac{2\pi/T}{2\pi/L} = \frac{L}{T} \tag{2.3}$$

Where

η	Instantaneous water level relative to water depth h_0 [m]
a	Amplitude of the oscillating wave ($a = \frac{1}{2}H$) [m]
H	Wave height [m]
ω	Absolute radian frequency ($\omega = \frac{2\pi}{T}$) [s^{-1}]
T	Wave period [s]
k	Wave number ($k = \frac{2\pi}{L}$) [m^{-1}]
L	Wave length [m]

Within this thesis, characteristics of waves are described using some of the above variables ($a = \frac{1}{2}H$, k, ω).

Waves are (after the tidal currents, as described in section 2.2.1) the second most important mechanism that is responsible for sediment transport. The presence of waves implies orbital movements within the water column (as found in the linear wave theory (Airy, 1845) as well). In intermediate and shallow water (as found within the Dutch Wadden Sea) these orbital movements result in a horizontal oscillating 'flow' near the bed. This moving water enhances bed shear stresses and therefore influences sediment transport. Figure 2.23 indicates these orbital movements (note the near-horizontal movements near the bed for intermediate- and shallow water, which is common for the Dutch Wadden Sea).
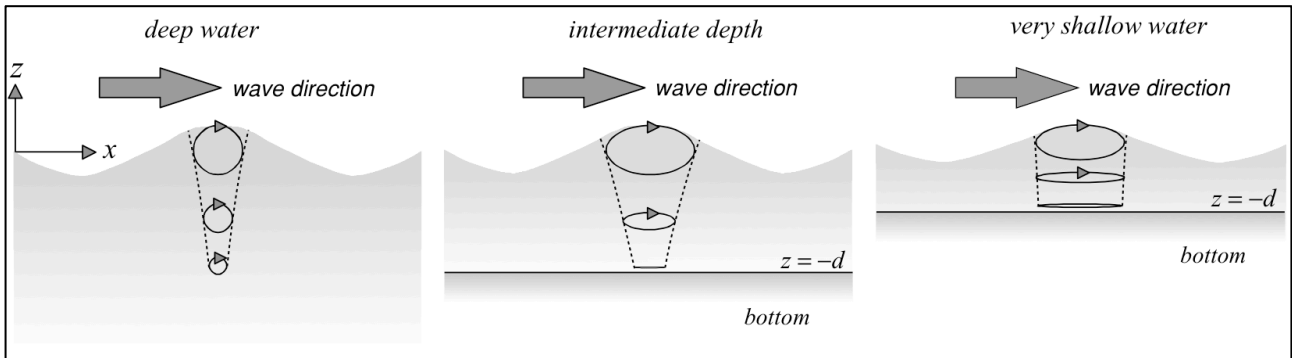
Figure 2.23: Orbital movement of water particles (according to the linear wave theory) for various depth conditions, indicating the different trajectories and their associating magnitudes (Holthuijsen, 2007)

Within tidal inlet systems (like the Amelander tidal inlet system), short waves commonly occur in an irregular wave field. Describing these irregular wave fields using a combination of wave components (based on equation 2.2) is possible, though, quickly becomes a daunting and pointless task. Therefore, it is common practice to describe wave fields using statistics, like the significant wave height (H_s) and (the continuous) variance density spectrum ($E(f)$). The variance density spectrum provides a complete statistical description of the surface elevation and is defined by equation 2.4 (1-dimensional) and 2.5 (2-dimensional)

$$E(f) = \lim_{\Delta f \to 0} \frac{1}{\Delta f} E\left\{\frac{1}{2}\underline{a}^2\right\} \tag{2.4}$$

$$E(f,\theta) = \lim_{\Delta f \to 0}\lim_{\Delta \theta \to 0} \frac{1}{\Delta f \Delta \theta} E\left\{\frac{1}{2}\underline{a}^2\right\} \tag{2.5}$$

These spectra are also used to model short waves in process-based (numerical) models. Section 3.2.2 describes the usage of the variance density spectrum (and the relation with the action density spectrum) for the application in these models.

A total description of the linear wave theory, the derivations, applications and further (statistical) expressions can be found in Holthuijsen (2007).

2.3 Sediment transport

Sediment transport can be defined as the movement of sediment particles over time. The transport is dependent on the interaction between the hydrodynamic conditions and the sediment, with its various properties, like the grain size and fall velocity. The non-linear interaction between these aspects results in almost all formulations for sediment transport being based on empiricism, and many expressions are often available.

The sediment distribution of the bed in the (Dutch) Wadden Sea consists of both sand and mud. Mud particles feature different physical properties when compared to sand particles. Apart from physical forces (e.g. buoyancy, inertia, drag, lift, friction), mud particles feature electrostatic forces, called cohesion. Due to cohesion, mud particles tend to accumulate in the water column. This process is referred to as flocculation, as it produces flocks (with different physical properties) from several aggregating mud particles. The small settling velocity (w_m), of an individual mud particle, is another important difference in physical properties as well, as it implies lag effects to occur (see section 2.2.1 and Nieuwenhuis, 2001).

The physical description of sediment transport is also separated, as non-cohesive (sand) and cohesive (mud) particles. The particles are transported under the influence of both waves and (tidal) currents. This section will describe some basics of sediment properties, related to sediment transport, and describe the transport of both non-cohesive sand and cohesive mud, under the influence of waves and currents. Finally, sand-mud mixtures are considered, these are the final expressions that are mainly used throughout this thesis.

2.3.1 General

Sediment properties

To make sediment related calculations, the sediment must be defined according to some specific properties/parameters. The most important parameters herein are grain size (commonly expressed in diameter d) and fall velocity, both assumed to be constant in space and time for a certain particle. The different types of sediment are classified according to their size (diameter) in the standard, ISO 14688, as follows (table 2.3).

2 mm <	Gravel	< 64 mm
0,063 mm <	Sand	< 2 mm
2 μm <	Silt	< 63 μm
	Clay	< 2 μm

Mud (fines)

Table 2.3: Standard sediment gradation according to sieve diameter d (ISO 14688)

The median particle diameter (d_{50}), as introduced in section 1.2, is generally used to express the grain size when dealing with a sediment distribution. But, since a sediment bed consists of many particles, all different in size, the grading (for instance d_{90}/d_{10}) is often used as well.

A sediment particle that gets released for 'free-fall' in a water column will eventually fall towards the bottom with a constant velocity (zero acceleration). At this point in time, all particle forces are in balance and it travels with a constant speed, the fall velocity (denoted by w_s for sand and w_m for mud particles). The force balance is an interaction between the downward linear gravitational force F_G (minus buoyancy) and the upward quadratic drag force F_D.

Obtaining the fall velocity can be done analytically, though this requires the sediment particles to be (perfect) spheres. In practical applications, such spheres are not present, and empirical relations become indispensible, for instance the expression (equation 2.6) by Van Rijn (1993), which is valid for non-cohesive sediment and is applied in the Delft3D-FLOW module (Deltares, 2011a) for particles with $d > 65 \, \mu$m.

$$w_s = \begin{cases} \dfrac{(s-1)gd^2}{18\nu} & 1\,\mu m < \ d \ \leq 100\,\mu m \\[2ex] \dfrac{10\nu}{d}\left(\sqrt{1+\dfrac{0{,}01(s-1)gd^3}{\nu^2}}-1\right) & 100\,\mu m < \ d \ \leq 1000\,\mu m \\[2ex] 1{,}1\sqrt{(s-1)gd} & 1000\,\mu m < \ d \end{cases} \qquad (2.6)$$

Where

s Specific gravity $(\frac{\rho_s}{\rho_w} = 2{,}65$ (common value))

ρ_s Sand density

ν Kinematic viscosity coefficient $(\nu = \frac{\mu}{\rho_w})$

μ Dynamic viscosity coefficient

It can be concluded from equation 2.6 and the use in Delft3D-FLOW, that, according to Deltares (2011a), particles with a diameter $d < 65\,\mu m$ are classified as cohesive (as the domain of this non-cohesive expression funs from $65\,\mu m$ to infinity[5]).

Furthermore, two distinct proportionalities can be found. For the larger (gravel) particles $w_s \propto \sqrt{d}$ holds, and for the smaller (silt, but also valid for clay) particles $w_s \propto d^2$ is found (consistently denoted as $w_m \propto d^2$). Sand particles are found within the transition zone between these two proportionalities, when looking at the classification in table 2.3 and equation 2.6.

As indicated before, flocculation of mud particles largely influences the settling velocity, as a flock settles (much) faster compared to an individual particle. The degree of flocculation is mainly dependent on the salinity (S) of the water and is therefore an important parameter in the expression for the settling velocity.

Bed shear stress

Water motions (mainly waves and currents, as introduced in previous sections) introduce forces on a bed consisting of particles. By using individual particle properties (e.g. d) or bed forms (e.g. ripples, dunes), these forces can be parameterized. This parameterization is found within the dimensionless friction coefficient, (for the sake of brevity, denoted here as) c_f. The bed shear stress is then specified by equation 2.7.

$$\tau_b = \rho_w c_f |\vec{U}|\vec{U} \qquad (2.7)$$

Where $\vec{U}$ is the total horizontal velocity vector (u and v combined). It must be noted that the bed shear stress $\tau_b \propto \vec{U}^2$ (is proportional to velocity squared) and is based on d_{50} within this thesis (found in c_f).

Initiation of motion

Sediment transport takes place when water movements exert a shear stress (τ_b) on particles that exceeds a certain critical shear stress $(\tau_{b,cr})$. This critical shear stress describes the point for initiation of movement for specific sediment. Exceeding $\tau_{b,cr}$, by definition, implies sediment particles to be transported.

When all forces on a single particle are looked at, the drag- and lift forces tend to move the particle from its position, while gravity forces it in its place. The drag- and lift forces are proportional to $\rho_w u^2 d^2$ while the gravitational force is proportional to $(\rho_s - \rho_w)gd^3$. Assuming equilibrium forces on a single grain and defining $\tau_{b,cr} = \rho_w u_{*,cr}{}^2$ (with $u_{*,cr}$ as the critical shear velocity) results in the proportionality given in equation 2.8.

$$(\rho_s - \rho_w)gd^3 \propto \rho_w u_{*,cr}{}^2 d^2 = \tau_{b,cr}d^2 \qquad (2.8)$$

---

[5] For as long as this is practically realistic and still considered to be hydrodynamically transportable sediment.

This proportionality can be rewritten to a critical constant parameter (C_S), as indicated in equation 2.9. This parameter is defined as the Shields parameter (Shields, 1936).

$$C_S = \frac{\tau_{b,cr}}{(\rho_s - \rho)gd} = \theta_{cr} \tag{2.9}$$

Shields (1936) found a constant value for a, smoothly placed, horizontal sand bed, being $C_S \approx 0,05$. Furthermore, Shields (1936) found that the 'constant' C_S was a weak function of the grain Reynolds number ($Re_* = \frac{u_* d}{\nu}$). This dependency can be visualized by plotting C_S (or θ_{cr}) against the grain Reynolds number, as is done in figure 2.24, which is the original figure by Shields (1936). The area indicated with lines represents initiation of motion (above/below this area particles are/aren't in motion). The indicated area is often represented as a line (or curve), which is called the Shields curve.
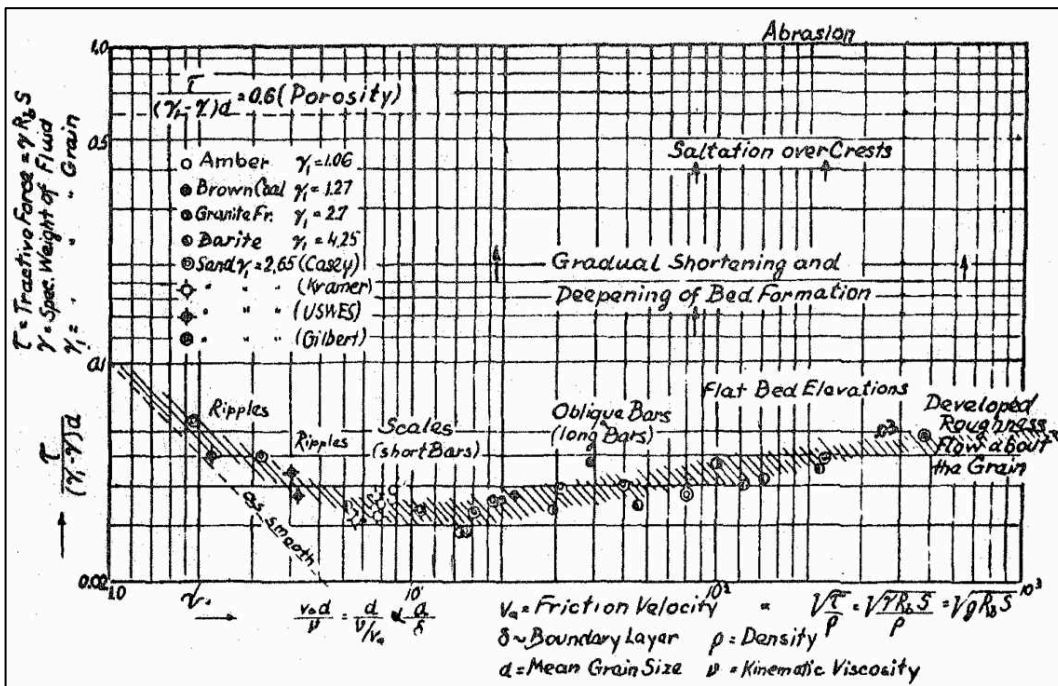
Figure 2.24: Introduction of the Shields curve, θ_{cr} plotted against Re_* (Shields, 1936)

Transport modes

Sediment transport takes place in 2 distinct modes, bed load transport (q_b, S_b) and suspended transport (q_s, S_s). Mud particles are only transported through suspension, making bed load transport a 'sand-only' process. While bed load transport completely occurs in the bed load layer, running from the bed level ($z = 0$) to the top of the bed load layer (commonly called Van Rijn's reference height and indicated with $z = a$), suspended transport occurs completely above the top of the bed load layer (from $z = a$ to $z = h_0 + \eta = h$). The total transport per unit width can be defined as $q_t = q_b + q_s$ (volume) or $S_t = S_b + S_s$ (mass). Equation 2.10 shows the relation between these two definitions, where ρ_{tm} is the density of the transported mixture.

$$S_t = q_t \rho_{tm} \tag{2.10}$$

Bed load transport can occur in two types, distinctly occurring during low and higher shear stresses, these are the regular bed load and sheet flow transport respectively[6].

- **Regular bed load** occurs near the exceedance of the critical shear stress (θ_{cr} somewhere near 0,03 and 0,1), the sediment particles roll, slide and make jumps (called saltations) in the direction of the

---

[6] Sheet flow is described here for completeness, although it is not expected to occur within the scenarios used within this thesis

flow. As long as sediment particles remain in contact with the bed (e.g. falling to the bed after making a small saltation), the transport mode is considered bed load transport.

- **Sheet flow transport** (form of bed load) occurs during higher shear stresses (θ_{cr} in the order of 0,8-1 or even higher), sediment particles tend to move in (multiple) layers over the bed, like sheets.
- **Suspended transport** occurs above the (before mentioned) bed load and sheet flow layer(s). The particles are not returning to the bed due to their settling velocity (w_s or w_m) because turbulent motions in the water column keep the particles in suspension.

The bed load transport is often expressed using an occurring bed shear stress and critical bed shear stress for erosion, while the suspended transport is often expressed using the product of the horizontal water velocities ($u(z,t)$) and $v(z,t)$) and sediment concentration ($c(z,t)$).

With these transport modes, the modelling of sediment transport is divided in both bed- and suspended load. But, as previously stated, the modelling of sand-mud segregation also requires the division of cohesive mud and non-cohesive sand calculations. Furthermore, the different forcing, introduced as (tidal) currents and (short) waves in section 2.2, should also be addressed separately, since they contribute to both stirring and transporting of sediments in various ways. This results in $2^3 = 8$ different states, of which an overview is given in table 2.4.

	Bed load transport		Suspended transport	
	Sand	Mud	Sand	Mud
(Tidal) Currents	S & T	X	S & T	S & T
(Short) Waves	S	X	S	S

Table 2.4: Overview of transport modes, (non-)cohesive sediments and different forcing (T = transport, S = Stirring, X = no contribution), note that stirred sediment get transported by currents.

To introduce expressions for sediment transport, a coordinate system is introduced in figure 2.25, in which the bed load- and suspended transport is schematically indicated, along with some sediment (transport) and wave characteristics. Note that this coordinate system is also consistent with previous statements and equations, like the sine wave from equation 2.2 (when taking h_0 as a reference height).
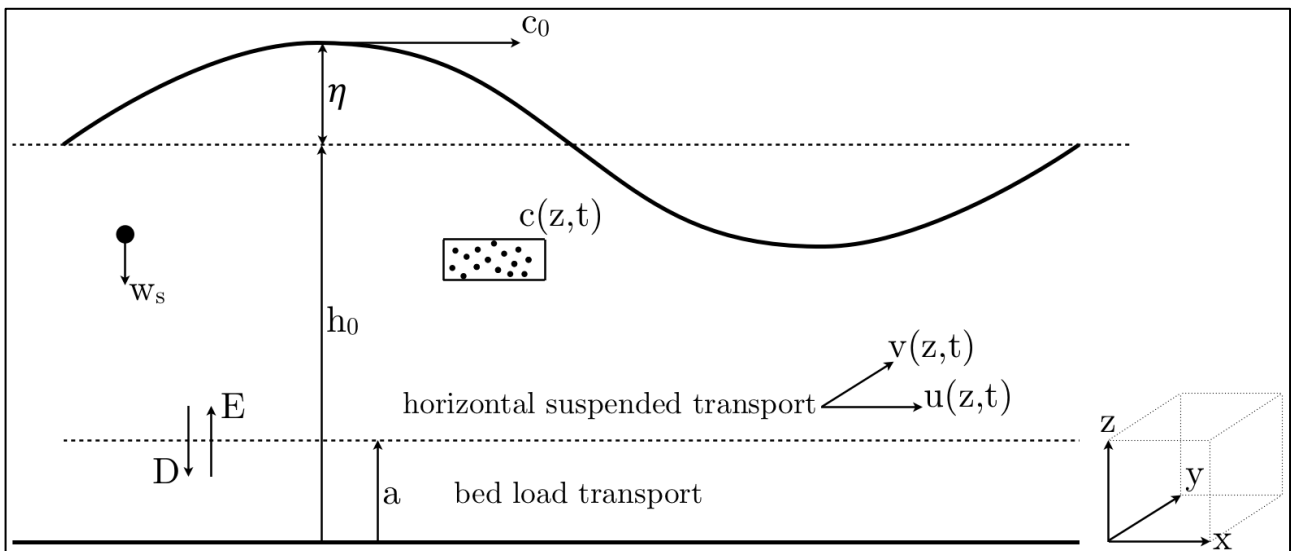
Figure 2.25: Coordinate system for sediment transport formulations

Horizontal transport

Although almost all transport of sediment is described using vertical (erosion/deposition) fluxes for suspended transport and empirical relations for bed load transport, some aspects for horizontal transport are important as well.

Wang *et al.* (1999) indicate the importance of tidal asymmetry for sediment transport, especially for fine sediment (mud), as lag effects/relaxation time results in significantly higher mud transport in the direction of the flood flow. Groen (1967) illustrated this effect using a model based on equation 2.11.

$$\frac{\partial c}{\partial t} = \frac{c_e - c}{T_a} \qquad\qquad\qquad (2.11)$$

Where

c	Depth averaged concentration
c_e	Equilibrium concentration
T_a	Adaptation time

By considering a saw-tooth-shaped velocity profile, which features overtides (u in figure 2.26), and assume that $c_e \propto u^3$, we end up with a concentration profile (over time) of c (in figure 2.26), when considering equation 2.11. The transport of suspended sediment can be calculated with the product of the concentration and the velocity (u times c, also see figure 2.27), indicated by uc in figure 2.26. Note that more suspended sediment is transported in the direction of the flood flow, since $\int_{t}^{t+T} uc\, dt$ is positive (where T is the tidal period).
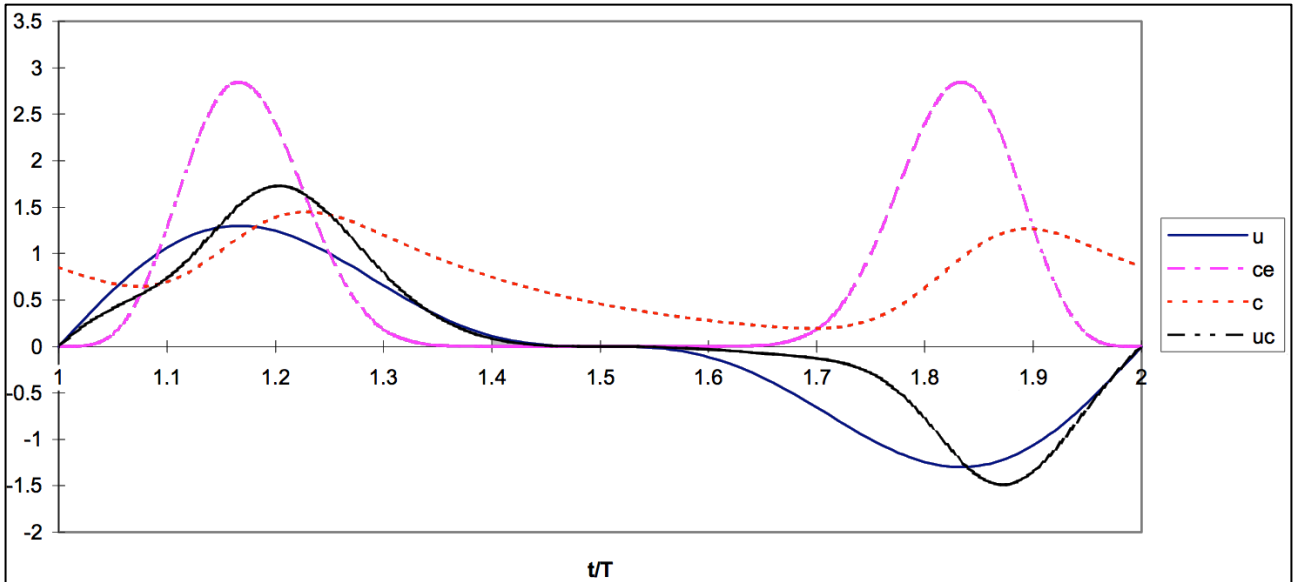
Figure 2.26: Transport of fine sediment (uc), based on velocity profile u, $c_e \propto u^3$ and equation 2.11

The small settling velocity of fine sediment is responsible for this lag effect (the difference between the observed concentration and the equilibrium concentration, which is based on hydrodynamic activity). This difference due to the lag effect implies (according to figure 2.26) inward transport of fine sediments.

Tidal asymmetry enhances the consequences of the lag effect. Though, without tidal asymmetry, a net flow of fine material is still expected in the direction of the tidal wave (since water levels differ for flood flow and ebb flow, transporting different amounts of dissolved matter over time.

2.3.2 Sand

Defined as $0,063 < d < 2$ mm, according to the ISO-14688 standard (table 2.3), sand is the main contributor to the sediment distribution and morphology in the Amelander tidal inlet system. Therefore, the initial computation, for obtaining the morphology of the schematized Amelander tidal inlet system model, is based on sand-only expressions. Separate relations for suspended- ($q_{s,s}$, $S_{s,s}$) and bed load transport ($q_{b,s}$, $S_{b,s}$) are commonly used to describe the erosional behaviour of pure sand beds, as introduced in the previous section.

The net sand flux (F_s), which is defined as the sand flux from the bed into the water column, is defined with equation 2.12.

$$F_s = \nabla q_b + w_s \frac{(c_a - c_s)}{\rho_s} = \frac{\partial q_b}{\partial x} + \frac{\partial q_b}{\partial y} + w_s \frac{(c_a - c_s)}{\rho_s} = \frac{\nabla S_b}{\rho_s} + w_s \frac{(c_a - c_s)}{\rho_s} \qquad (2.12)$$

Where

    c_s Suspended sand concentration

    c_a Sand concentration at the reference height $(z = a)$

Many researchers empirically describe the non-cohesive behaviour of sand transport in various ways. Van Rijn (1993, 2000) is used as the default expression within Delft3D models, and is also selected for this thesis. The distinction between bed load transport and suspended transport is also made within this expression.

An expression for the settling velocity, used in the transport formulations by Van Rijn (1993) was introduced in equation 2.6. The following sections on bed load- and suspended transport are mainly based on Van Rijn (1993, 2000).

Suspended sand transport

Suspended sediment is modelled in 3 dimensions, the vertical exchange of sediment between the bed and water column determines the concentration, while the horizontal velocities (consisting of component u and v, in x and y direction, respectively) transport these concentrations of sediment.

Vertical modelling of suspended sediment concentrations is done using deposition and erosion terms, between the bed and the flow (indicated in figure 2.25). These terms act near the bed, but entirely above Van Rijn's reference height. The upward sediment fluxes are due to bed shear stress and upward diffusion, while the downward sediment fluxes are due to the settling of sediment particles (the settling velocity w_s being a very important parameter herein).

Sediment concentrations are computed using the reference concentration, this concentration is located at $z = a$ and therefore denoted as c_a. According to Van Rijn (2000), the reference concentration is described by an empirical relation, which is found in expression 2.13.

$$c_a = 0{,}015\rho_s \frac{d_{50}(T_a)^{1,5}}{a(d_*)^{0,3}} \qquad (2.13)$$

Where

    T_a Non-dimensional bed-shear stress

    d_* Non-dimensional particle diameter

By means of expanding the reference concentration (at $z = a$) with (for instance) a Rouse distribution, the concentration of sediment in space and time can be determined.

The basic idea behind the horizontal transport of suspended matter is quite simple; it is assumed that the instantaneous current/velocity transports the instantaneous concentration. This can be expressed mathematically by expression 2.14 (in x-direction) and is indicated with figure 2.27.
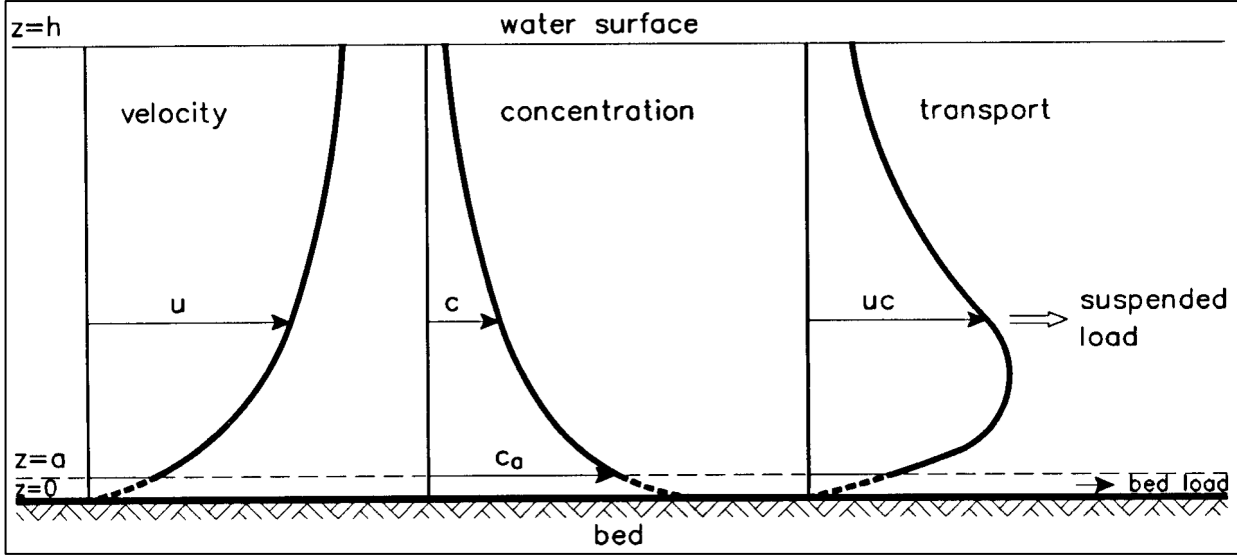
Figure 2.27: Visualization of the principles behind suspended transport (Van Rijn, 1993)

$$s_{s,s} = cu \tag{2.14}$$

By integrating over depth (from the reference height up to the instantaneous water level $(h = h_0 + \eta)$) we end up with the suspended sediment mass transport per unit width in direction of current u, indicated in equation 2.15.

$$S_{s,s} = \int_{z=a}^{h} s_s dz = \int_{z=a}^{h} cu dz \tag{2.15}$$

When dividing the concentration and velocity in a mean (current) and oscillating (wave) related part $(c = C + \tilde{c}$ and $u = U + \tilde{u})$ and average over time, we end up with equation 2.16.

$$\langle S_{s,s} \rangle = \underbrace{\int_{a}^{h} UC dz}_{current-related} + \underbrace{\int_{a}^{h} \overline{\overline{\tilde{u}\tilde{c}}} dz}_{wave-related} \cong \int_{a}^{h} UC dz = \langle S_{s,s,c} \rangle \tag{2.16}$$

Wave related suspended transport could occur due to short wave asymmetry, though, to compute the wave related intra-wave suspended transport; the intra-wave concentrations and velocities are needed. Apart from the (computer) time-consuming intra-wave computations, the knowledge on intra-wave concentration is limited (and would result in very uncertain results). Horizontal suspended sediment transport is therefore mainly modelled using the simplification as indicated on the right hand size in equation 2.16.

Bed load sand transport

Waves and currents induce bed load transport, as indicated in table 2.4. Within the applied expression for the bed load transport (Van Rijn *et al.*, 2003), a distinction is made between current- and wave related transport, this expression is given below (equation 2.17).

$$|S_b| = 0,006\rho_s w_s d_{50} M^{0,5} M_e^{0,7} \tag{2.17}$$

Where M is the dimensionless sediment mobility number due to waves and currents and M_e is the dimensionless excess sediment mobility number, as defined in the set of equations 2.18 to 2.20.

$$M = \frac{v_{eff}^2}{(s-1)gd_{50}} \tag{2.18}$$

$$M_e = \frac{(v_{eff} - v_{cr})^2}{(s-1)gd_{50}} \tag{2.19}$$

$$v_{eff} = \sqrt{v_R^2 + U_{on}^2} \tag{2.20}$$

In which v_{cr} [m/s] is the critical depth averaged velocity for initiation of motion, v_R [m/s] is the magnitude of an equivalent depth-averaged velocity, assuming a logarithmic velocity profile and U_{on} [m/s] is the near-bed peak orbital velocity in wave propagation direction (based on the significant wave height H_s).

Since the bed load transport consists of a wave and current related part, a bed load transport vector must be computed, consisting of the wave- ($|S_{b,w}|$) and current related part ($S_{b,c}$). These expressions are found in equations 2.21 and 2.22.

$$S_{b,c} = \frac{S_b}{\sqrt{1 + r^2 + 2|r|\cos\varphi}} \tag{2.21}$$

$$|S_{b,w}| = \frac{(|U_{on}| - v_{cr})^3}{(|v_R| - v_{cr})^3}|S_{b,c}| \tag{2.22}$$

Where φ is the angle between current and wave direction. The wave related part acts in the wave propagation direction and the current related part in the direction of the near-bed current.

Included in the 'bed load' expression is an approximation method for wave-related suspended transport, suggested by Van Rijn (2001). This expression is given in equation 2.23 and is not indicated in table 2.4.

$$S_{s,s,w} = f_{SUSW}\gamma U_A L_T \tag{2.23}$$

Where

f_{SUSW}	User defined tuning parameter
γ	Phase lag coefficient ($\gamma = 0.2$)
U_A	Velocity asymmetry value (Van Rijn, 2001 and Deltares, 2011a)
L_T	Suspended sediment load ($L_T = 0{,}007\rho_s d_{50}M_e$)

2.3.3 Mud

Transport behaviour of cohesive sediments (mud) is modelled using suspended load only, as indicated in table 2.4 and section 2.3.1. The general formulation for vertical movements (fluxes) is found in Van Ledden (2003), which is based on Partheniades-Krone formulations (see also e.g. Partheniades (1965) and Van Rijn (1993)). A basic mathematical description is used for horizontal movements (identical for the description of suspended transport of sand, horizontal movements transport the suspended sediments, which is represented in figure 2.27).

The expression for vertical fluxes is based on deposition and erosion formulations, as stated in equation 2.24.

$$F_m = E_m - D_m = M_m\left(\frac{\tau_b}{\tau_{e,m}} - 1\right)H\left(\frac{\tau_b}{\tau_{e,m}} - 1\right) - w_m c_m\left(1 - \frac{\tau_b}{\tau_{d,m}}\right)H\left(1 - \frac{\tau_b}{\tau_{d,m}}\right) \tag{2.24}$$

Where

F_m	Mud flux from the bed to the water column
E_m	Erosion flux of mud
D_m	Deposition flux of mud
M_m	Erosion coefficient for mud beds
D_m	Deposition flux of mud
$\tau_{e,m}$	Critical erosion shear stress for mud
$\tau_{d,m}$	Critical deposition shear stress for mud
H	Heaviside function, $H(f(x)) = 1$ if $f(x) \geq 0$, otherwise $H(f(x)) = 0$

Erosion and deposition of mud is dependent on flocculation, which is dependent on salinity (section 2.3.1), as indicated under sediment properties, this dependency is given in equation 2.25 (and 2.26).

$$w_{m,0} = \frac{w_{m,max}}{2}\left(1 - \cos\left(\frac{\pi S}{S_{max}}\right)\right) + \frac{w_{m,f}}{2}\left(1 + \cos\left(\frac{\pi S}{S_{max}}\right)\right) \qquad \text{When } S \leq S_{max} \tag{2.25}$$

$$w_{m,0} = w_{m,max} \qquad\qquad\qquad\qquad\qquad\qquad\qquad\qquad \text{When } S > S_{max} \tag{2.26}$$

The extra wave induced mixing of cohesive sediment is not taken into account in the current Delft3D model, which is a limitation. Though, it can be introduced by means of enhancement of the bed shear stress.

The principles of modelling horizontal transport of mud is the same as described under suspended sand transport, since, also here, it is assumed that the current/velocity transports the instantaneous mud concentration. Horizontal suspended mud transport is therefore again (see equation 2.20) modelled using the simplification as indicated in equation 2.27 (though, it runs from $z = 0$ to $z = h$, instead of starting at $z = a$). Note that C refers to the mud concentration in this expression.

$$\langle S_{s,m} \rangle \cong \int_0^h UCdz \tag{2.27}$$

2.3.4 Sand-mud mixtures

According to, for instance, Raudkivi (1990), the erosional behaviour of sand-mud mixtures behaves significantly different between two regimes: a non-cohesive and a cohesive one. While according to, for instance, Mitchener & Torfs (1996), the mud (or sand) content p_m (or p_s) is an important parameter for describing this behaviour. Later, Van Ledden (2003) showed that in fact rather the silt content is important for the erosional behaviour, though, the relation with mud content appeared approximately linear.

Van Ledden (2003) proposed a mathematical description for sand-mud mixtures, taking the division between the two regimes and the mud content into account. The separation of the regimes is defined by a critical mud content (by weight), $p_{m,cr}$, below this mud content, the mixture is assumed to be non-cohesive, where it is assumed as cohesive above this value. The value of $p_{m,cr}$ is user-defined, also making it a model parameter.

All of the following mathematical descriptions for (non-) cohesive sand-mud mixtures were proposed by Van Ledden (2003) and have been adopted into the Delft3D model during the 'Building with Nature' project by Deltares, which is used within this thesis and associated model. For further, in-depth, information and 'derivations' on these equations, apart from the ones presented here, one is referred to Van Ledden (2003).

Non-cohesive sand-mud mixtures

For non-cohesive sand-mud mixtures, mud is proportionally eroded with sand (Torfs, 1995). Therefore, the relation specified by equation 2.28 holds.

$$\frac{E_m}{E_S} = \frac{p_m}{p_s} \tag{2.28}$$

A specific critical shear stress was proposed by Van Ledden (2003) for non-cohesive sand-mud mixtures, being $\tau_{e,nc}$. This proposal was made as former propositions by Van Rijn (1993) and Whitehouse *et al.* (2000) resulted in large overestimations on the effect of mud content on the critical shear stress (for non-cohesive sand-mud mixtures) and is given in equation 2.29.

$$\frac{\tau_{e,nc}}{\tau_{cr}} = (1 + p_m)^\beta \Leftrightarrow \tau_{e,nc} = \tau_{cr}(1 + p_m)^\beta \tag{2.29}$$

With p_m the mud content (by weight) in the total considered sediment mixture (given $p_m < p_{m,cr}$) and $0{,}75 < \beta < 1{,}25$ for non-cohesive sand-mud mixtures (β is an empirical coefficient).

By introducing a transport parameter (T_{nc}) for non-cohesive mixtures, which is dependent on $\tau_{e,nc}$ (and thus p_m), any previously introduced, empirical, erosion formulation, can be made dependent on mud content. T_{nc} is specified by equation 2.30.

$$T_{nc} = \frac{\tau_b}{\tau_{e,nc}} - 1 = \frac{\tau_b}{\tau_{cr}(1 + p_m)^\beta} - 1 \tag{2.30}$$

The (pure) sand expressions for bed load transport, for instance by Van Rijn (1993), can be used for low mud contents as well (Torfs, 1995). Combined with the above T_{nc}, this results in equations 2.31.

$$q_b = \alpha_{b1}\Delta^{0,5}g^{0,5}d_{50}^{1,5}T_{nc}^{\alpha_{b2}}d_*^{-0,3} = \frac{S_b}{\rho_s}$$
$$c_a = 0,015\rho_s\frac{d_{50}}{a}\frac{T_{nc}^{1,5}}{d_*^{0,3}} \tag{2.31}$$

For non-cohesive sand-mud mixtures, observations show that mud particles are easily eroded, along with the sand particles. Therefore, the expression by Van Rijn (1993) for the erosion rate of mud (E_m) in non-cohesive sand-mud mixtures is suggested. This expression (for E_m) is given in equation 2.32 and can be substituted in equation 3.6. These equations are based on particle properties, rather than bed formations.

$$E_m = M_{nc}\frac{p_m}{1 - p_m}T_{nc}^{\alpha_{b2}-0,9} = \frac{\alpha_{b1}}{3}\frac{p_m}{1 - p_m}\frac{\sqrt{\Delta g d_{50}}}{d_*^{0,9}}T_{nc}^{\alpha_{b2}-0,9} \tag{2.32}$$

Cohesive sand-mud mixtures

From observations and experiments (e.g. Torfs, 1995), it has been shown that the erosive behaviour of cohesive sand-mud mixtures fully takes place as suspended transport, therefore, when $p_m > p_{m,cr}$, the bed load transport rate is assumed as $q_b = 0$. Furthermore, the erosion fluxes for both sand (E_s) and mud (E_m) can be combined to the total (vertical) erosion flux (E_t) and are substituted into a Partheniades-Krone comparable expression, like equation 2.24. Equation 2.33 shows the vertical erosion flux for cohesive sand-mud mixtures.

$$E_s = (1 - p_m)M_c\left(\frac{\tau_b}{\tau_{e,c}} - 1\right)H\left(\frac{\tau_b}{\tau_{e,c}} - 1\right)$$
$$E_m = p_mM_c\left(\frac{\tau_b}{\tau_{e,c}} - 1\right)H\left(\frac{\tau_b}{\tau_{e,c}} - 1\right) \tag{2.33}$$

Furthermore, the expression for the critical shear stress for cohesive sand-mud mixtures ($p_m > p_{m,cr}$) is given in equation 2.34, and is consistent with equation 2.29 for the transition between the two expressions (when $p_m = p_{m,cr}$), as it results in equal values.

$$\tau_{e,c} = \frac{\tau_{cr}\left(1 + p_{m,cr}\right)^\beta - \tau_e}{1 - p_{m,cr}}(1 - p_m) + \tau_{e,m} \tag{2.34}$$

Note that substituting $p_m = 1$ in equation 2.34 results in $\tau_{e,c} = \tau_{e,m}$, which is consistent with the definition of $p_m = 1$ ('mixture' consists of only mud).

Further theoretical development

Van Ledden *et al.* (2004a) describes a conceptual framework behind the erosional behaviour of sand-mud mixtures. Various bed types are considered and verified by a combination of laboratory tests and the conceptual framework, which appears valid. Furthermore, the application of the conceptual framework to natural sedimentary systems is assessed, from which constant clay/silt ratios appear important, as these ratios strongly determine what bed type (behaviour) occurs.

Ahmad *et al.* (2011) introduce new insights in mathematical descriptions for sand-mud mixtures. Initially based on Van Ledden (2003), the deletion of $p_{m,cr}$ is an important step, resulting in only one formulation for

critical shear stress, rather than two (equation 2.29 and 2.34). This method is yet to be generally accepted and is not implemented (as an option) in models like Delft3D (yet).

Van Prooijen & Winterwerp (2010) describe the erosion of cohesive sediments using stochastics.

Furthermore, interesting research by Jacobs (2011) and Jacobs *et al.* (2011) describes the erosion of sand-mud mixtures from a soil mechanical perspective. Different parameters to describe sand-mud mixtures are introduced, which are merely related to soil mechanics, like granular porosity and relative water content. Furthermore, a new erosion formula is introduced, based on this soil mechanical approach. The erosion threshold is based on the plasticity index (Jacobs, 2011), while the formula itself relates the surface erosion rate to the packing density, the undrained sediment strength and a coefficient for pore water pressure gradient dissipation.

Finally, Deltares is performing research, aimed at the implementation of cohesive and non-cohesive mixtures in the Delft3D-FLOW model (section 3.2), within the 'Building with Nature' project. Some additions and changes (section 3.3), compared to Van Ledden (2003), are made for successful implementation and representation of some physical processes that occur in reality (like consolidation lag).

2.4 Hypothesis for sand-mud segregation classification

When the observations and description of large-scale sand-mud segregation from section 2.1.4 is combined with forcing conditions (like short waves and tidal currents) and the associated theory (section 2.2 and 2.3), it becomes clear that tidal currents and short waves will individually result in significantly different large-scale sand-mud segregation patterns. The tidal currents result in mud deposition further in a system (where hydrodynamic activity, due to tidal currents, is smaller), while short waves result in mud deposition in deeper areas (where hydrodynamic activity, due to short waves, is smaller).

According to Nichols & Boon (1994), three types of basins can be classified, as indicated in figure 2.28, where the tidal lagoons of the Dutch Wadden Sea can be identified as type C. When looking at the characteristics of the basins, the distinction between type A and C is very interesting, as it can be related to physical characteristics of the basin, by respectively describing them as relatively wave- and tide dominated, as hypothesized above. In type A (Mobile Bay, AL, USA), locally generated short waves prevent mud from settling near the margins (a micro tide is found here), whereas tidal currents transport mud to the dynamically calmer intertidal mudflats within type C (Arcachon Bay, France), which features a macro tide.

These observations support the above classification hypothesis, in which relative tidal- or (short) wave dominance is responsible for the behaviour of sand-mud segregation patterns. Again, within this classification, the dominance of the tide is responsible for mud segregation towards shallow areas (like tidal flats and inner land boundaries), which are found further into a system, whereas short wave dominance is responsible for mud segregation towards deeper areas (like channels (if present) or deep basins), like observed in the cases of figure 2.28.
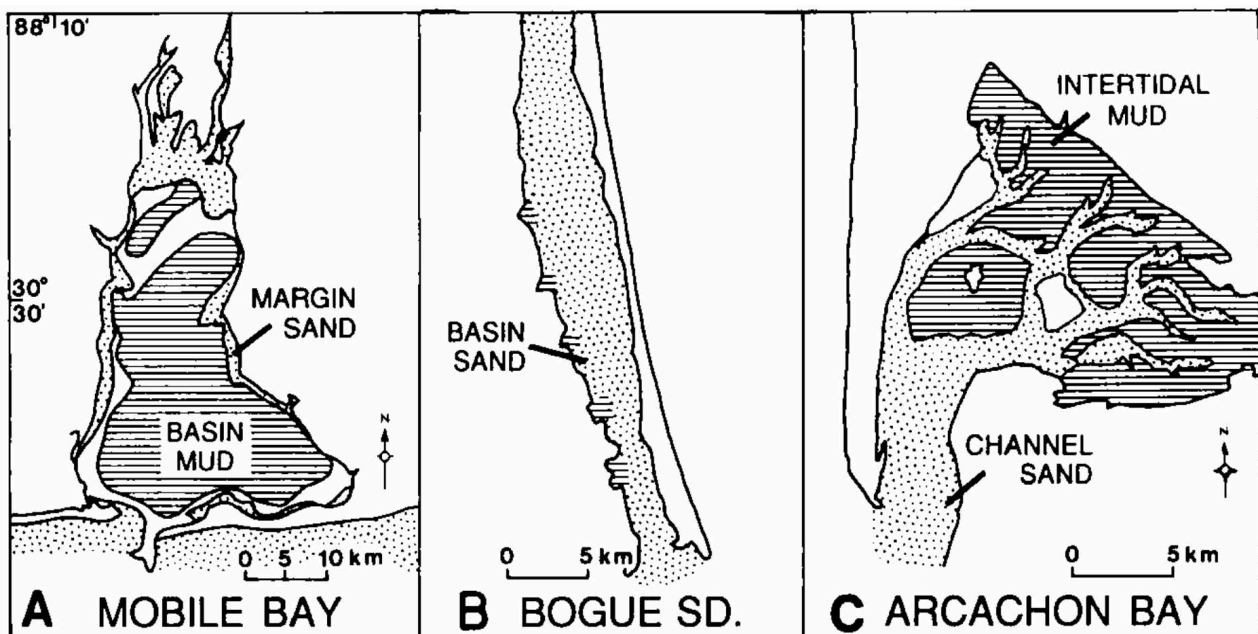
Figure 2.28: Types of textual patterns in lagoons: A. Mud basin and sand margins. B. Sand basin and mud margins. C. Sand channels and mud intertidal areas (Nichols & Boon, 1994)

According to this hypothesis, the relative dominance of tidal currents or short waves is related to the nature in which large-scale sand-mud segregation occurs. To classify this hypothesis, any considered system should be classified according to its tidal- or short wave-dominance. Figure 2.29 introduces such a classification (which is used by Davis & Hayes (1984) to assess which systems possibly feature wave-shaped barrier-islands). This classification will be used to support the above hypothesis and to construct an extended classification (regarding sand-mud segregation patterns and the original classification).
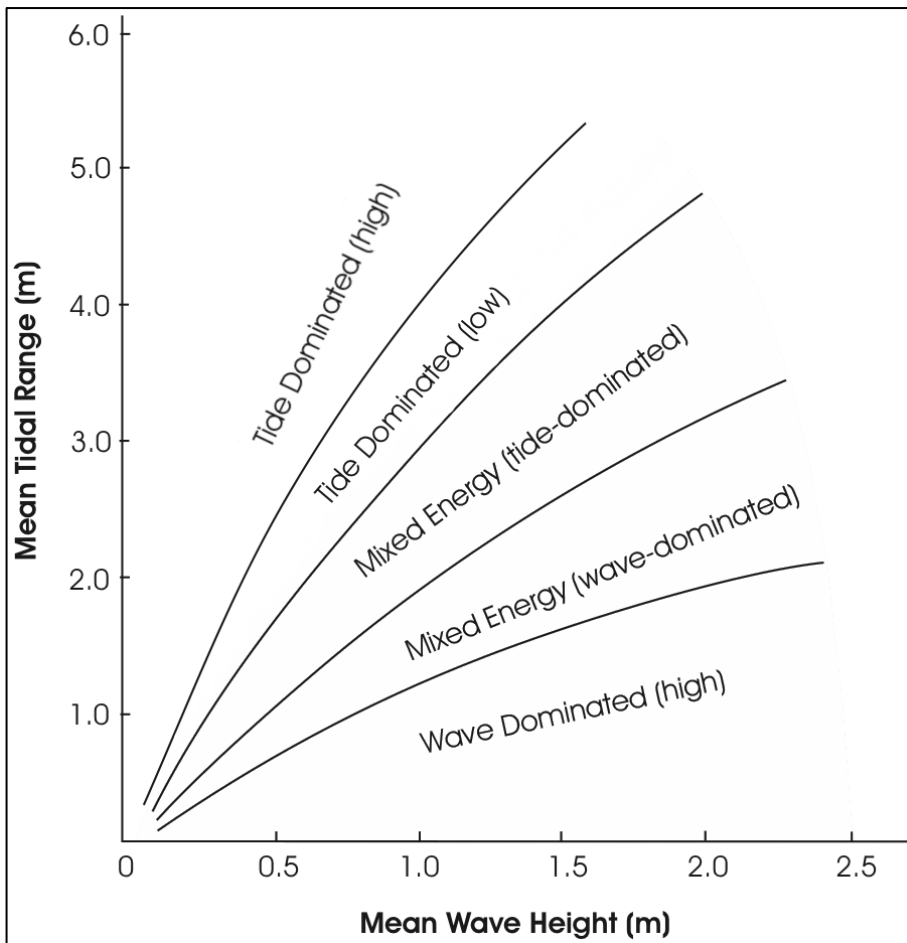
Figure 2.29: Classification of hydrodynamic systems according to forcing conditions of short waves and tidal range (Modified after Elias, 2006, after Davis & Hayes, 1984, modified from Hayes, 1975, 1979)

According to this classification, the Amelander tidal lagoon is tide dominated (like al other tidal inlet systems in the Dutch Wadden Sea). Furthermore, according to Davis & Hayes (1984), the tidal inlets are classified as mixed energy (with a tidal dominance), as waves are responsible for the formation of barrier islands (like the Frisian Islands).

In the objectives for this thesis, variation with waves and tides is suggested (see sub-question 4), to assess the influence of short waves and tidal currents on the large-scale sand-mud segregation patterns. This assessment can also be used to assess the above hypothesis. By doing so, the suggested classification can be verified and implemented in/added to the classification by Davis & Hayes (1984), to construct a new classification.

Chapter 3

Model Setup for a Schematized Tidal Inlet System

With the general description of large-scale sand-mud segregation patterns and associated hypothesis, which relates these patterns to relative forcing dominance, provided in chapter 2, a model is needed. This model will be used to reproduce the large-scale sand-mud segregation patterns in the Amelander inlet system, using a schematized approach. Furthermore, it will be used to assess the classification hypothesis. This chapter introduces the model itself, providing the theory and assumptions behind it, while also verifying it.

3.1 Introduction

As stated before, a schematized (Amelander tidal inlet system) model is needed to assess all research questions. For this, the model from Dissanayake *et al.* (2009a; 2009b) and Dissanayake (2011) is used as a starting point. Dissanayake *et al.* (2009b) modelled the development of channel patterns in a schematized Amelander tidal inlet system model, while Dissanayake *et al.* (2009a) focussed on the influence of relative sea level rise on the development of channel patterns. Dissanayake (2011) overlaps Dissanayake *et al.* (2009a; 2009b). The schematized Amelander tidal inlet system model, which is used within these researches, is introduced in figure 3.1, see also Dissanayake (2011).
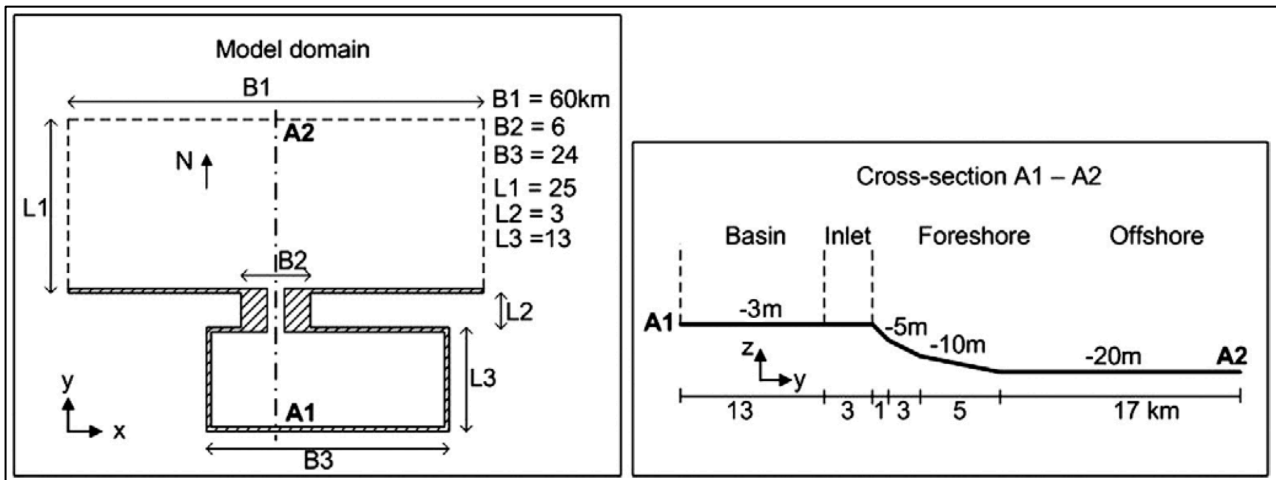
Figure 3.1: Schematized spatial model domain (Dissanayake *et al.* 2009a; 2009b and Dissanayake, 2011)

The model features an initially flat bed (-3 meters within the tidal lagoon), as observed in figure 3.1. To start the final sand-mud segregation computations, an initial bathymetry is needed. Within Dissanayake (2011), this bathymetry is generated using an equivalent of 50 years tidally induced hydrodynamic forcing (with tidal boundary conditions in the North Sea area). This computation is based on a model using only sand. Section 3.4.1 explains why sand-mud computations, initiated with a flat bed, require too much computational time to develop a stable bathymetry. To start the final computations, mud is added to this initial bathymetry (which is generated using only sand within the model). Adding mud to this bathymetry is an important assumption within this thesis.

After running the above morphodynamic model with an equivalent of 50 years, the generated bathymetry is considered as (more or less) stable[7]. The combination of this stable bathymetry (which is shown in figure 3.2) and the previously introduced model was kindly provided by Dissanayake and is used for the initial model conditions during the execution of this thesis[8].

Marciano *et al.* (2005) and Dastgheib *et al.* (2008) show how the Delft3D model is capable of representing tidal channels in the Dutch Wadden Sea and common branching[9] (Cleveringa & Oost, 1999). The approach by Dissanayake (2011) is comparable and therefore considered to be valid. The quantitative verification by Dissanayake (2011), related to the Amelander inlet system, also supports this statement.
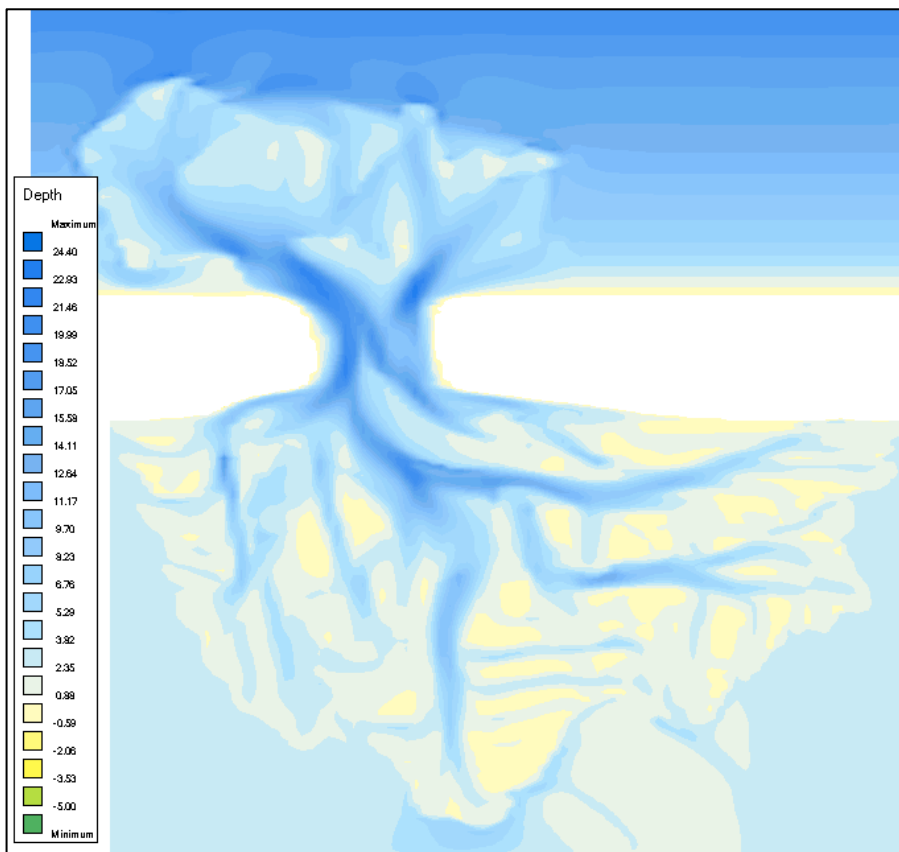
Figure 3.2: Initial bathymetry used within this thesis, based on 50 years of tidal induced morphodynamics in the Amelander tidal inlet system.

The basis behind the schematized Amelander tidal inlet system model is the software package Delft3D by Deltares (2011a, 2011b). Brief (relevant) background information on Delft3D is provided in the next sections. Since the official Delft3D release currently does not support multiple sediment fractions that influence- and are linked to each other (using a cohesive and non-cohesive regime), an internal (Deltares) version is used. This internal version is in development within the 'Building with Nature' project (BwN-project) by Deltares, before and during the execution of this thesis.

---

[7] The reference to a stable bathymetry is made because the macro-scale bathymetry characteristics aren't significantly changing over many tidal periods. Intertidal (small scale) changes due to hydrodynamics hardly contribute to this macro-scale 'stable' behaviour.

[8] Note that the channel patterns and bathymetry differ from the actual observations in the Amelander tidal inlet system (figure 2.9). The elaboration of the research questions within this thesis does not require this exact behaviour to be reproduced, and a (more or less) stable bathymetry for the (boundary) conditions is preferred over an exact representation of reality, as the large-scale sand-mud segregation patterns due to forcing is looked into by comparing different model cases. The quality of representing the actual Amelander inlet system bathymetry has been assessed quantitatively within Dissanayake (2011) and could also be verified in a qualitative matter.

[9] Though, significant variation in results is found for various empirical erosion formulae, something further research should enlighten.

3.2 Model background

Delft3D is a computer software package, used for 3-dimensional computations/simulations (over time) in coastal-, river- and estuarine areas, which is developed by Deltares. The Delft3D software package is capable of simulating flows, waves, sediment transport, morphological development, water quality and ecology, and does so using various modules within Delft3D.

The main module within Delft3D is called Delft3D-FLOW (D-FLOW). This module is responsible for calculating hydrodynamic conditions, like velocities, water elevations, density, salinity, vertical eddy viscosity and vertical eddy diffusivity. Apart from the hydrodynamics, this module is also capable of regular sediment transport calculations and updates the bed level and composition accordingly. The hydrodynamic conditions can be used as input for all other modules within Delft3D[10]. This data is, for this reason, stored in a 'communication file', which communicates with all the other modules.

Another relevant module, linked to this thesis, is Delft3D-WAVE (D-WAVE, a short wave propagation module, which is a specific version of SWAN), which also builds upon the results from D-FLOW. Figure 3.3 shows the system architecture of the overall Delft3D software package with its various modules and connections, while indicating the relevance of the module to this thesis (using colours).
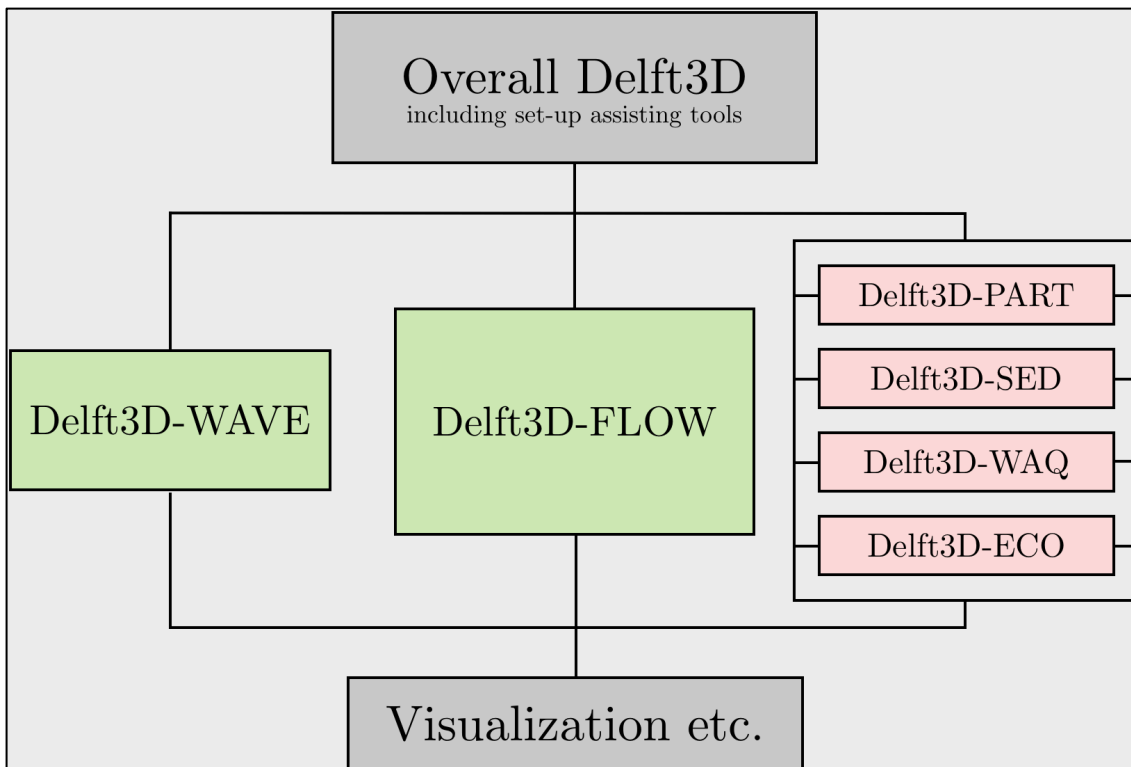
Figure 3.3: Architecture of the total Delft3D system with, in green, relevant modules and, in red, modules that are not used within this thesis.

In principle, if the D-FLOW module writes results (that are required by other modules) to the communication file, other modules start their individual calculations. If the results from these modules are required in other modules as well, these modules also start writing the required results to the communication file. This way, the different modules are linked and integrated with one-another (coupled).

---

[10] Hydrodynamic input conditions for the various modules within Delft3D are, logically, only used if this specific module is called upon in a certain model case.

A clear and relevant example of this connection between different modules is found within the D-WAVE module, which (for instance) updates the water level due to short wave setup. This updated water level influences the hydrodynamic conditions in the D-FLOW module and is thus written to the communication file with this purpose. This is called online wave coupling (the communication between D-FLOW and D-WAVE during a computation).

The Delft3D-SED module is responsible for cohesive and non-cohesive computations (where D-FLOW is responsible for non-cohesive computations only). Due to the implementation of principles from section 2.3.4 in D-FLOW, regarding cohesive and non-cohesive mixtures, this module will slowly become obsolete over time and functionality from D-SED will be found in D-FLOW.

Furthermore, within each module, specific results are saved in certain result files that are used for visualization and animation of results during post-processing.

The following sections globally describe the basics behind the modules that are used within this thesis.

3.2.1 Delft3D-FLOW module

The hydrodynamic Delft3D-FLOW module solves the unsteady shallow water equations (Navier Strokes equations for incompressible fluid, combined with the shallow water and Boussinesq assumptions) in two (depth average) or three dimensions. This set of equations is based on the continuity and momentum balance principles. The depth and density averaged continuity equation (neglecting precipitation and evaporation) is given in equation 3.1, while the depth and density averaged momentum equations (in x- and y-direction, respectively) are given in equations 3.2 and 3.3.

$$\frac{\partial \eta}{\partial t} + \frac{\partial (h_0 + \eta)u}{\partial x} + \frac{\partial (h_0 + \eta)v}{\partial y} = 0 \tag{3.1}$$

$$\underbrace{\frac{\partial u}{\partial t}}_{1} + \underbrace{u\frac{\partial u}{\partial x}}_{2} + \underbrace{v\frac{\partial u}{\partial y}}_{3} + \underbrace{g\frac{\partial \eta}{\partial x}}_{4} - \underbrace{fv}_{5} + \underbrace{\frac{guU}{C^2(h_0 + \eta)}}_{6} - \underbrace{\frac{F_x}{\rho_w(h_0 + \eta)}}_{7} - \underbrace{v\left(\frac{\partial^2 u}{\partial x^2} + \frac{\partial^2 u}{\partial y^2}\right)}_{8} = 0 \tag{3.2}$$

$$\underbrace{\frac{\partial v}{\partial t}}_{1} + \underbrace{u\frac{\partial v}{\partial x}}_{2} + \underbrace{v\frac{\partial v}{\partial y}}_{3} + \underbrace{g\frac{\partial \eta}{\partial y}}_{4} + \underbrace{fu}_{5} + \underbrace{\frac{gvU}{C^2(h_0 + \eta)}}_{6} - \underbrace{\frac{F_y}{\rho_w(h_0 + \eta)}}_{7} - \underbrace{v\left(\frac{\partial^2 v}{\partial x^2} + \frac{\partial^2 v}{\partial y^2}\right)}_{8} = 0 \tag{3.3}$$

In which (valid for both x- and y-direction):

1	Velocity gradient
2 & 3	Advection terms
4	Pressure gradient
5	Coriolis 'force'
6	Friction term
7	External forcing (e.g. waves and wind)
8	Viscosity term
f	Coriolis force
C	Chézy coefficient
F_x	External forcing in x-direction
F_y	External forcing in y-direction

Sediment transport

As indicated in section 2.3.1, sediment transport is assumed to take place in both suspended- and bed load transport. The bed load transport is described empirically, section 2.3.2 introduced one of these empirical

relationships in equation 2.17 (Van Rijn, 1993) and, corrected for non-cohesive sand-mud mixtures, in equation 2.31 (Van Ledden, 2003).

For calculations regarding suspended transport, the concentrations of suspended matter are needed (e.g. in equations 2.16 and 2.27). Since sand and mud can both be transported in suspension, but behave differently herein; two expressions (one for the sand- and one for the mud concentration) are needed. The advection-diffusion equations for suspended sand and mud transport (Van Rijn, 1993) behave independent as long as the mud concentrations stay below the so-called 'gel-point' concentration (Torfs *et al.*, 1996 and Winterwerp, 1999). According to Van Ledden (2003), this condition is valid within practical applications (like the Wadden Sea) and the equations for sand and mud transport reduce to the uncoupled advection diffusion equations, given for sand and mud in equation 3.4 and 3.5, respectively, where deposition and erosion fluxes are found in the vertical velocity w.

$$\frac{\partial c_s}{\partial t} + u\frac{\partial c_s}{\partial x} + v\frac{\partial c_s}{\partial y} + (w - w_s)\frac{\partial c_s}{\partial z} = \varepsilon_{s,x}\frac{\partial^2 c_s}{\partial x^2} + \varepsilon_{s,y}\frac{\partial^2 c_s}{\partial y^2} + \frac{\partial}{\partial z}\left(\varepsilon_{s,z}\frac{\partial c_s}{\partial z}\right) \tag{3.4}$$

$$\frac{\partial c_m}{\partial t} + u\frac{\partial c_m}{\partial x} + v\frac{\partial c_m}{\partial y} + (w - w_m)\frac{\partial c_m}{\partial z} = \varepsilon_{m,x}\frac{\partial^2 c_m}{\partial x^2} + \varepsilon_{m,y}\frac{\partial^2 c_m}{\partial y^2} + \frac{\partial}{\partial z}\left(\varepsilon_{m,z}\frac{\partial c_m}{\partial z}\right) \tag{3.5}$$

Bed level changes

Changes in bed levels occur due to exchange of sediments at the bed surface and consolidation ('packing') of sediment mixtures. Within this thesis, only the exchange of sediment is considered, as the knowledge on consolidation effects are limited and model implementation is fairly complex in a large process based model (Van Ledden, 2003). Furthermore, the bed density is assumed to be constant in both space and time.

Considering the above, the changes in bed levels occur due to gradients in bed load transport (of sand) and erosion and deposition fluxes (of both sand and mud). This can be expressed with equation 3.6 (see also equations 2.31, 2.32 and 2.33).

$$\underbrace{(1 - \varepsilon_p)}_{\substack{Porosity\\correction}} \quad \underbrace{\frac{\partial z_b}{\partial t}}_{\substack{Bed\,level\,change\\over\,time}} \quad = \quad \underbrace{-\frac{\partial q_b}{\partial x} - \frac{\partial q_b}{\partial y}}_{\substack{Gradients\,in\\bed\,load\,transport}} \quad + \quad \underbrace{D_s - E_s}_{\substack{Vertical\\sand\,fluxes}} \quad + \quad \underbrace{D_m - E_m}_{\substack{Vertical\\mud\,fluxes}} \tag{3.6}$$

Expressions for bed load transport (q_b) and erosion fluxes (E_s and E_m), which can be substituted within this equation, are found in section 2.3 (with the previously mentioned equations). Within Delft3D, the deposition fluxes (D_s and D_m) are based on the product of the instantaneous concentrations (c_s and c_m) and the associated settling velocities (w_s and w_m), rather than using a critical shear stress for deposition (as proposed by Van Ledden (2003)).

Implementation of wind driven flow

Wind driven currents are also implemented in D-FLOW. This method is based on the shear stresses due to wind, imposed at the surface boundary conditions. The momentum equations are given by equations 3.7 and 3.8 (for the x- and y-direction respectively).

$$\frac{v_V}{h}\frac{\partial u}{\partial \sigma}\bigg|_{\sigma=0} = \frac{1}{\rho_0}|\vec{\tau}_s|\cos(\theta) \tag{3.7}$$

$$\frac{v_V}{h}\frac{\partial v}{\partial \sigma}\bigg|_{\sigma=0} = \frac{1}{\rho_0}|\vec{\tau}_s|\sin(\theta) \tag{3.8}$$

In which:

$$|\vec{\tau}_s| = \rho_a C_d U_{10}^2 \tag{3.9}$$

Where:

ν_V	Vertical eddy viscosity
σ	Scaled vertical coordinate (surface is $\sigma = 0$, bed level is $\sigma = -1$)
θ	Angle between wind (stress) vector and local direction of grid
$\lvert\vec{\tau}_s\rvert$	Magnitude of the wind shear stress vector and local direction of grid line
ρ_a	Density of air
C_d	Wind drag coefficient
U_{10}	Wind speed, 10 meter above the free surface

3.2.2 Delft3D-WAVE module

The D-WAVE module is responsible for wave computations within the Delft3D model. It is a specific version of the SWAN module, which relies on the action balance principle (using the action density spectrum N). Wave-current interactions are effectively taken into account using the action balance principle, as it is conserved in presence of currents (as opposed to using the energy balance principle, which uses the energy density spectrum E, see equations 2.4 and 2.5 in section 2.2.2). This is essential for a successful coupling with D-FLOW computations. The relation between the energy density spectrum and the action density spectrum is found in equation 3.10. Both spectra are dependent on the relative frequency (σ) and the wave direction (θ). The relative frequency can be related to the absolute frequency (ω), this relation is found in equation 3.11.

$$N(\sigma, \theta) = \frac{E(\sigma, \theta)}{\sigma} \tag{3.10}$$

$$\omega = \sigma + k U_n \tag{3.11}$$

The action balance equation is found in equation 3.12. Note that multiplying equation 3.12 with the relative frequency σ results in the energy balance equation.

$$\underbrace{\frac{\partial N}{\partial t}}_{\substack{Local\ rate\ of\ change \\ of\ action\ over\ time}} + \underbrace{\frac{\partial c_x N}{\partial x}}_{\substack{Propagation\ of\ action \\ in\ x-direction\ with\ c_x}} + \underbrace{\frac{\partial c_y N}{\partial y}}_{\substack{Propagation\ of\ action \\ n\ x-direction\ with\ c_y}} + \underbrace{\frac{\partial c_\sigma N}{\partial \sigma}}_{\substack{Relative\ frequency \\ shifting}} + \underbrace{\frac{\partial c_\theta N}{\partial \theta}}_{\substack{Refraction \\ term}} = \underbrace{\frac{S}{\sigma}}_{\substack{Source \\ term}} \tag{3.12}$$

The Source term S in the balance equations (energy or action) is used to represent physical processes like generation, dissipation and nonlinear wave-wave interactions. Within SWAN, wind is responsible for generation of waves, while white capping, bottom friction and depth-induced breaking are responsible for dissipation. Furthermore, triads and quadruplets (Holthuijsen, 2007) are responsible for nonlinear wave-wave interactions. Expressions for the implementation of these source terms are found in Holthuijsen (2007) and Deltares (2011b).

D-WAVE communicates the results with D-FLOW through a communication file (section 3.2).

3.3 Numerical aspects of the sand-mud model

Within the BwN-project, the sand-mud interaction, the different sediment layers (and associated mixing) and fluff layer concepts have been implemented in Delft3D. These concepts are shortly enumerated and explained below, apart from the sand-mud interaction, as it was introduced in previous research (Van Ledden, 2003). This description can be found in section 2.3.4.

3.3.1 Fluff layer

The fluff layer is a thin horizontal layer, directly situated between the bed layer(s) and the water column and is used as a tool for the representation of mud-related calculations in short timescales. While the fluff layer is assumed to be above the bed level, it does not contribute to it. Therefore, it also does not decrease the water depth. Furthermore, it is assumed that the fluff layer only contains mud (the sand fluxes only occur between the bed layer(s) and water column) and has a lower critical shear stress compared to the bed layer(s). From a physical point of view, the fluff layer is used to describe the slow consolidation of mud particles into the bed. In reality, after settling towards the bed, mud particles do not tend to consolidate immediately, as it remains above the bed (in a state comparable to a fluid mud mixture), before consolidating into the bed. The critical shear stress for erosion is much lower in the fluff layer (compared to the consolidated bed layers underneath).

While the bed layer(s) respond slowly to hydrodynamic changes, the fluff layer responds quickly. This way, the concentration can vary significantly during, for instance, the tide. Roughly speaking, sediment is in suspension in the water column during higher hydrodynamic activity and in the fluff layer during lower hydrodynamic activity, a phase lag between these two cases is, of course, present. This fluff layer timescale is significantly shorter than that for the bed layer(s) underneath; the fluff layer is therefore treated separately.

The mud content in the fluff layer is dependent on erosion- and deposition fluxes, both from and to the water column above- and the bed layer(s) below it. Expressions for these fluxes are given below.

Erosion

The expression for the erosion from the fluff layer into the water column is given with equation 3.14, while the erosion from the bed layer(s) into the water column is described with equation 3.15.

$$E_f = p_{m,f} M_f (\tau_b - \tau_{f,cr}) \tag{3.14}$$

$$E_b = p_m M_b \left(\frac{\tau_b}{\tau_{b,cr}} - 1 \right) \tag{3.15}$$

Deposition

Deposition of mud from the water column into the fluff layer is described by equation 3.16, where the deposition of mud from the water column into the bed layer(s) is given in equation 3.17

$$D_f = e_d (1 - \alpha) w_m c_m \tag{3.16}$$

$$D_b = e_d \alpha w_m c_m \tag{3.17}$$

Where:

α	Deposition fractions to the bed layer(s) $(0 \leq \alpha \leq 1)$
e_d	Deposition efficiency

When $\alpha = 0$, no deposition from the water column into the bed layer occurs. In this case $(\alpha = 0)$, the deposition is described with a burial term. This burial term describes the deposition of mud from the fluff layer into the bed layer(s) and is expressed by equation 3.18.

$$B_f = p_{m,f}\min(mB_1, B_0) \tag{3.18}$$

Where:

B_0, B_1 Burial coefficients ()

m Total mass of the fluff layer per unit area

The introduction of this burial term (when $\alpha = 0$) results in two distinct approaches. Now, $\alpha = 0$ means that mud can only deposit into the fluff layer before it deposits to the bed layer(s) or re-suspends into the water column, whereas $0 < \alpha \le 1$ results in deposition to both the fluff layer and bed layer(s)[11]. Erosional behaviour is the same in both of these approaches.

These two approaches are both implemented in the BwN version of Delft3D and are graphically introduced in figure 3.4, where the dotted boxes indicate the differences with $\alpha = 0$ and $0 < \alpha \le 1$, respectively.

The conceptual description of fluid mud by Kessel (1997) can be considered as a first introduction into the fluff layer (though it has both similarities and differences), while Orvain *et al.* (2003), Kessel *et al.* (2011a; 2011b) mention, describe and apply the fluff layer (in a practical application).
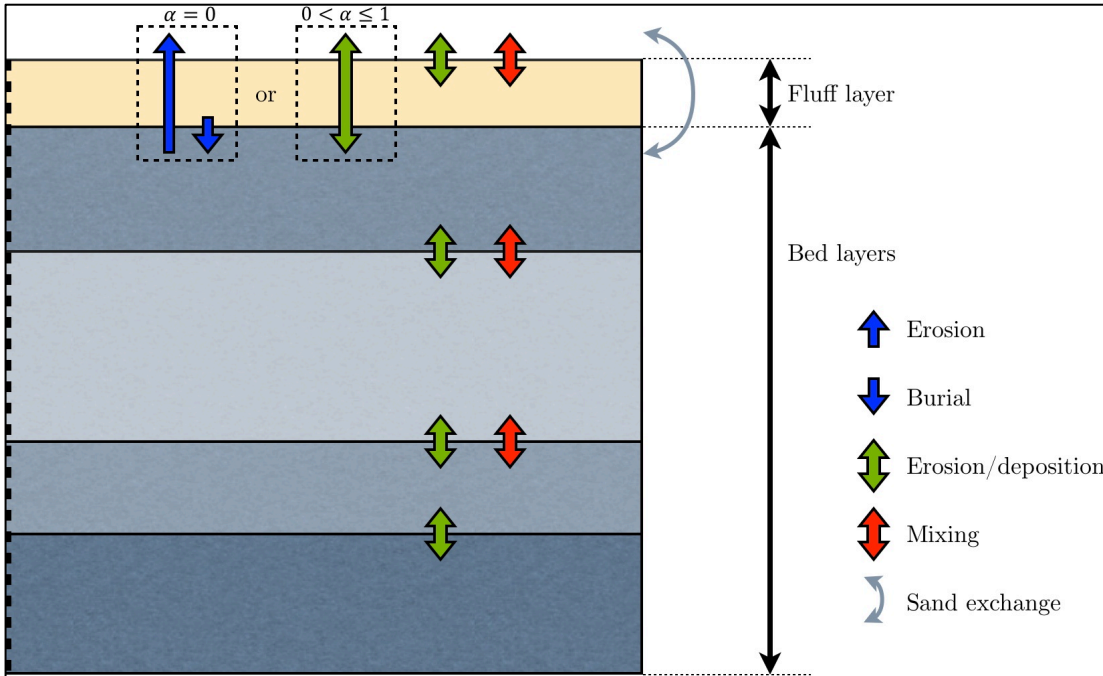
Figure 3.4: Fluff layer concept and indication of the two available methods in Delft3D

3.3.2 Mixing of layers

As indicated in figure 3.4, deposition, erosion and mixing between different layers can occur in a layered stratigraphy, where mixing can occur due to biological and/or physical processes, both non-diffusive and diffusive. Currently, diffusive processes have been implemented in the BwN version of Delft3D (apart from the erosion and deposition terms, which were introduced in the previous section). The diffusion is implemented using a vertical scheme, which is used for each grid cell. This scheme is given with equations 3.19 to 3.22 for a stratigraphy with k layers and l sediment fractions, the calculations are run with morphological time steps of Δt at time level n. Furthermore, note that this scheme is based on central differences and diffusion only occurs in non-active layers (so underneath the active top layer).

$$m_{k,l}^{n+1} = m_{k,l}^n + F_{k+\frac{1}{2},l}\Delta t - F_{k-\frac{1}{2},l}\Delta t \tag{3.19}$$

---

[11] Note that $\alpha = 1$ results in no fluff layer usage

$$F_{k+\frac{1}{2},l} = \rho_l \phi^n_{k+\frac{1}{2}} K_{k+\frac{1}{2}} \frac{p^n_{k+1,l} - p^n_{k,l}}{\Delta z^n} \tag{3.20}$$

$$\phi^n_{k+\frac{1}{2}} = \frac{\phi^n_k + \phi^n_{k+1}}{2} \tag{3.21}$$

$$\Delta z^n = \frac{\Delta^n_k + \Delta^n_{k+1}}{2} \tag{3.22}$$

Where:

$m^n_{k,l}$	Mass of sediment fraction l in layer k at time level n
$F_{k+\frac{1}{2},l}$	Diffusive flux of sediment fraction l between layer k and $k+1$
ρ_l	Density of sediment fraction l
ϕ^n_k	Solid volume fraction of layer k at time level n
$K_{k+\frac{1}{2}}$	Diffusion coefficient at the interface between layer k and $k+1$
$p^n_{k,l}$	Mass (or volume) fraction of sediment fraction l in layer k at time level n
Δz^n	Vertical distance between centre of layer k and $k+1$
Δ^n_k	Thickness of layer k at time level n

3.4 Case specific assumptions

While most of the above sections (in particular section 2.3, 3.2 and 3.3) are related to the 'foundations' of the sand-mud version of Delft3D, some important case specific assumptions must be made, while using this sand-mud mixture version of Delft3D along with the schematized Amelander tidal inlet system model. These assumptions are automatically related to certain model case properties, in which this model operates.

3.4.1 Morphological updating

Changes in bathymetry (morphology), over time, occur due to gradients in sediment transport, which are dependent on hydrodynamic conditions. Significant changes in bathymetry occur over certain morphological time periods, rather than hydrodynamic conditions[12]. Within this thesis, the aim is on sand-mud segregation patterns, rather than the influences on morphology. Furthermore, the timescale for obtaining these sand-mud segregation patterns appear much smaller than the timescales for morphological stability. Clear observations of sand-mud segregation patterns in the Amelander inlet system model occur after a, hydrodynamic- and morphodynamic ($Morfac = N = 1$), timescale of approximately 3 months, while morphological stability[13] is expected anywhere between 20 and 50 years (see section 3.1 and figure 3.2).

Applying morphological updating, while applying the 3-month timescale of sand-mud segregation patterns, implies non-significant changes in morphology within the different model scenarios. As each scenario has a different morphological response to the different hydrodynamic forcing, the comparison of different scenarios becomes harder (as the hypsometry, which is used within the analysis, will change for each scenario), while the conclusions from large-scale sand-mud segregation patterns don't (or hardly) change. Due to these observations, it is chosen to use a fixed morphology (as shown in figure 3.2 and 3.5), in which layers with different mud content can still develop.

In this approach with no morphological updating, the deposition of a new sediment layer 'pushes' the underlayers downwards in the model (as the level of the top layer is fixed), instead of building the layers up from below (as would occur on a even much larger (history) timescale than described above, 100's of years, say). Furthermore, the erosion of a top layer results in underlayers to move upwards, to meet the fixed position of the top layer.

3.4.2 Model artefacts

As indicated with figure 3.2, the applied morphology has not changed trough the entire spatial domain of the tidal lagoon. Roughly the South-western and South-eastern part still feature a continuous initial depth of 3 meter. Initial computations show unrealistic accumulation of mud in these areas that are not under influence of morphodynamic evolution, called model artefacts. Therefore, the model domain (grid) in the tidal lagoon has been changed accordingly, which is indicated in figure 3.5, as this prevents the model artefacts from occurring and influencing the results.

---

[12] It is because of this reason that the morphological factor is implemented in Delft3D, while an accurate hydrodynamic computation is quickly stable (short spin-up times), changes in morphology occur on a much larger timescale.

[13] While the model is in morphological equilibrium for a 'sand-only' simulation, the addition of mud changes this state. The adaptation time of 20-50 years is based on the time the 'sand-only' model needed to get morphologically stable.
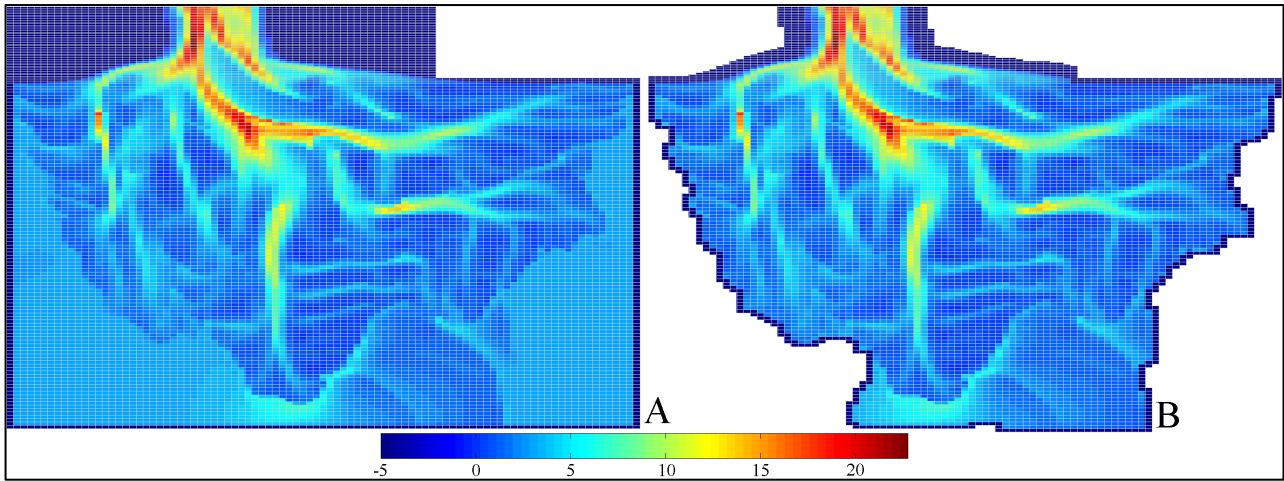
Figure 3.5: Changes in the tidal lagoon spatial domain due to the occurrence of model artefacts, with (A) the original and (B) the final tidal lagoon spatial (grid) domain

3.4.3 Parameter specification

Various parameters, as described in previous sections, are visualized in figure 3.6 below, where values are also specified. These parameters are used for the reference scenario, which is introduced in chapter 4.
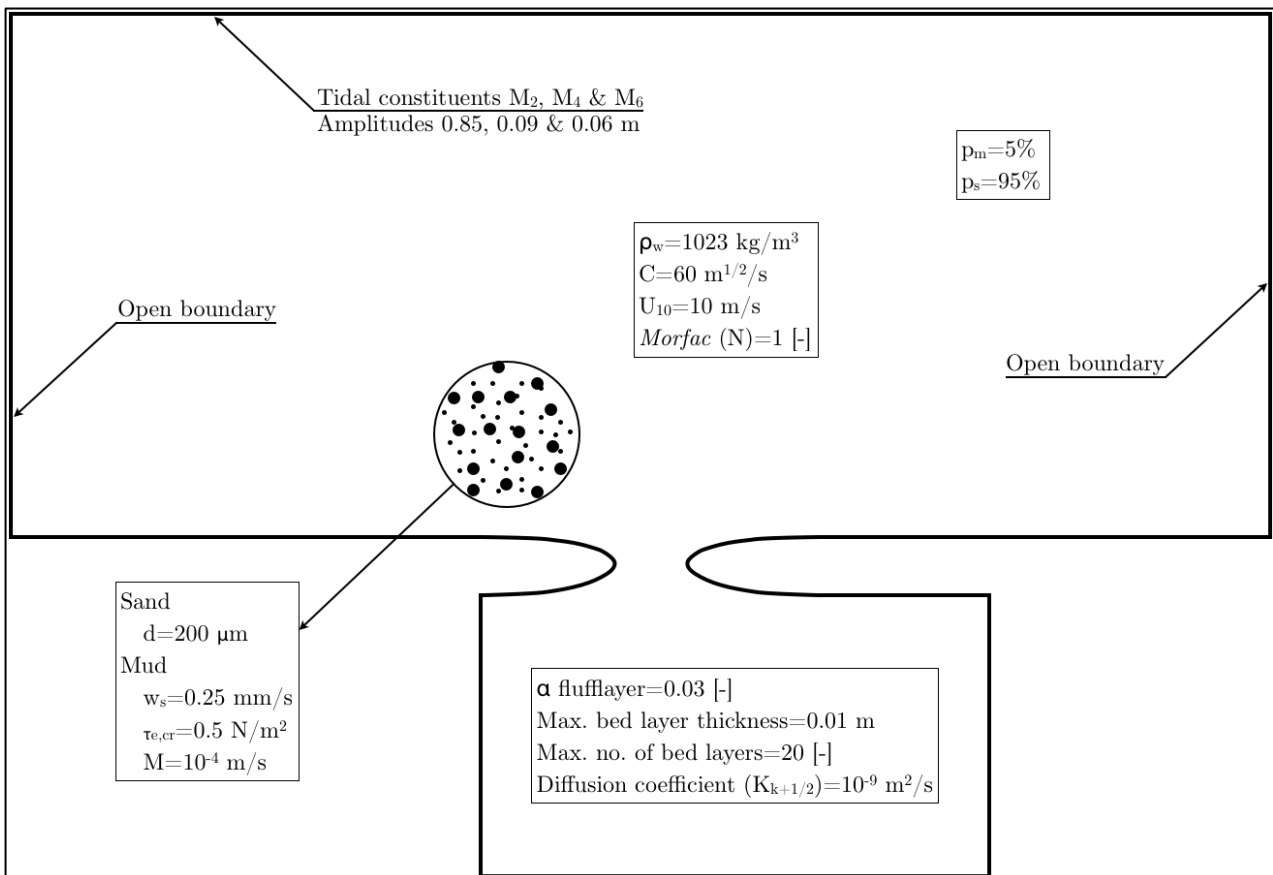
Figure 3.6: Visualization and values of parameters for the reference scenario

3.5 Model and parameter verification using 1D model

Before applying the layered bed Delft3D sand-mud model on the schematized Amelander tidal inlet system model, a verification of the Delft3D sand-mud model is preferred, as it is in a state of development. To compare and verify results, a previously elaborated (highly simplified) model is used from Van Ledden *et al.* (2004b), which is based on chapter 5.4 from Van Ledden (2003). This 1D model can also be used to quickly verify changes in model parameters (before being implemented in the Amelander inlet system model).

3.5.1 Introduction to 1D short tidal basin model

The 1D tidal basin model, introduced by Van Ledden (2003) and Van Ledden *et al.* (2004b), considers a short tidal basin with a length L of 20 km, an initial water depth h_0 of 5 meter and a tidal (M_2) forcing at the model boundary (which also supplies mud into the system with a concentration $c_{m,0}$ of 50 g/m^3). A cross section of this model is given in figure 3.7.
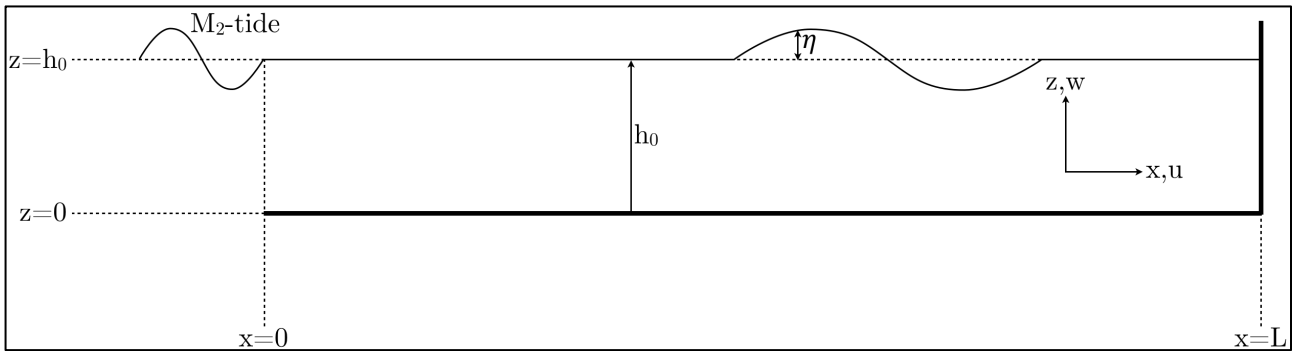
Figure 3.7: Cross section and frame of reference for the 1D short tidal basin model

To relate the results from this model to the results by Van Ledden (2003) and Van Ledden *et al.* (2004b), all physical parameters are assumed to be equal to the ones from these studies. These values are given in table 3.1 below.

Physical parameters for short 1D tidal basin model			
Description	Symbol	Value	Unit
Sand grain size	d_{50}	150	μm
Settling velocity of sand	w_s	0.016	m/s
Settling velocity of mud	w_m	0.5	mm/s
Chézy-coefficient	C	50	m$^{1/2}$/s
Critical mud content	$p_{m,cr}$	0.3	-
Horizontal fluid mixing	v_x, v_y	10	m^2/s
Critical erosion shear stress	$\tau_{e,nc}, \tau_{e,c}$	0.25	N/m^2
Erosion coefficient	M_{nc}, M_c	10^{-6}	m/s

Table 3.1: Overview of physical parameters in 1D short tidal basin model, based on Van Ledden *et al.* (2004b)

Since the current Delf3D sand-mud model approach is (moderately) different from Van Ledden (2003) and Van Ledden *et al.* (2004b), not all parameters stated in these studies are used, but also new parameters are introduced in the current approach. Obviously, the introduction of the fluff layer (section 3.3.1) requires new parameters, while describing deposition terms with w_m and c_m means omitting τ_d (critical deposition shear stress) from the list of parameters, where this was used in Van Ledden (2003) and Van Ledden *et al.* (2004b).

Due to the different approaches within the models, exact reproduction is not expected. Though, a physical relation between both models should be found. Since this is already the case with the work by Van Ledden (2003) and Van Ledden *et al.* (2004b), the model is expected to result in similar behaviour.

3.5.2 Short tidal basin model with bound flat bed

To simulate the initial flat bed over a longer period, a model case with a bound bed is used. This case can be explained in great detail using physical reasoning, as no changes in morphology imply a nearly constant bed shear stress over time. Where, in the case of a flat bed, the tidal forcing results in a linear decreasing discharge (towards the end of the model), the bed shear stress decreases quadratic towards the end of the model (figure 3.8). When the occurring bed shear stress drops below the critical erosion shear stress of a specific sand-mud mixture, it will no longer erode from that location. This behaviour is seen in figure 3.8 and shows the exact same behaviour observed by Van Ledden (2003) and Van Ledden *et al.* (2004b).
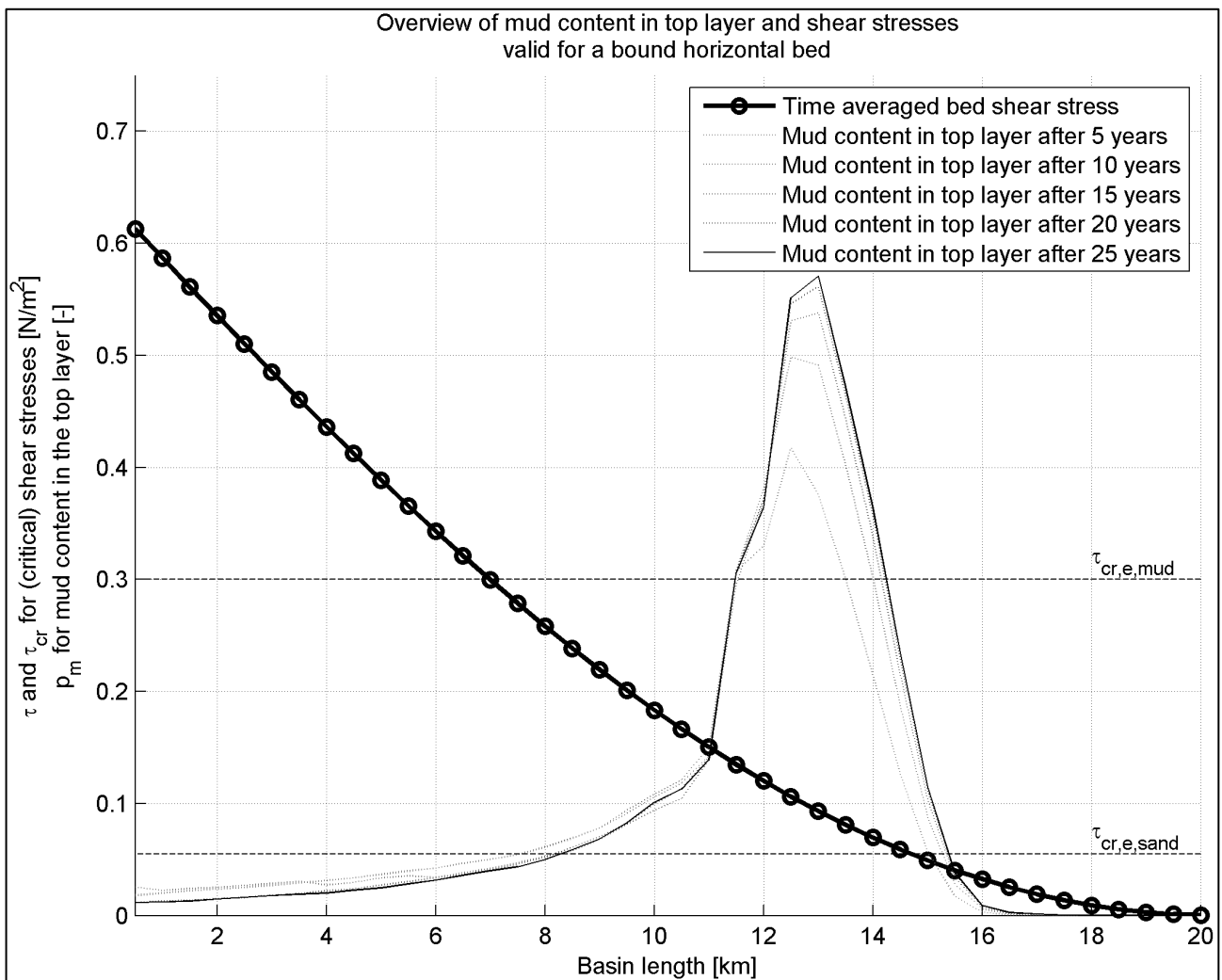
Figure 3.8: Instantaneous mud content in the top layer versus occurring (time averaged) bed shear stress

3.5.3 Short tidal basin model with initial flat bed

When morphodynamic development of a (initially flat) bed is simulated, the development of a stable (more or less linear increasing) morphology is eventually observed. Figure 3.9 shows the development of this equilibrium on the timescale used by Van Ledden (2003) and Van Ledden *et al.* (2004b), as they also observed this behaviour.
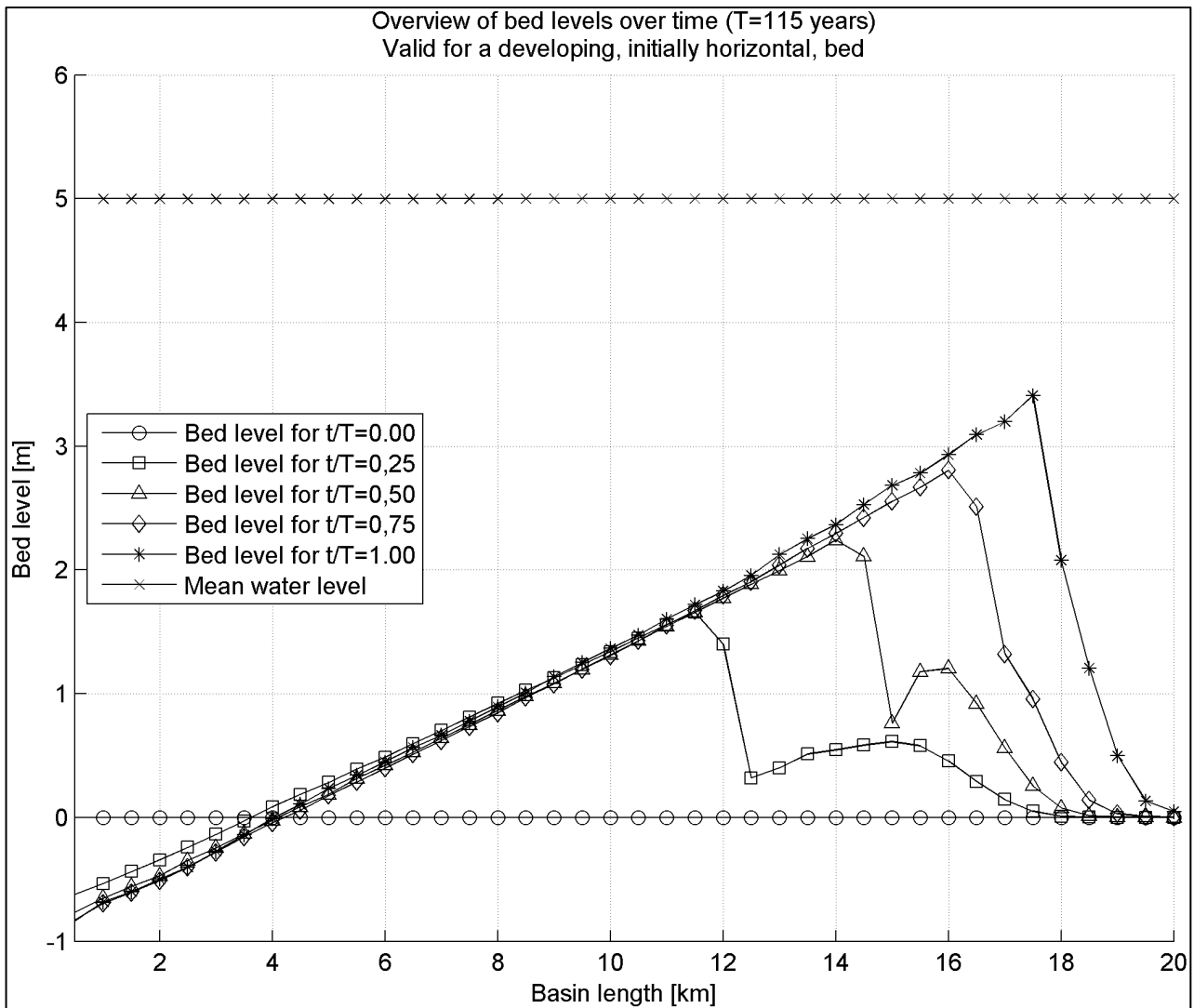
Figure 3.9: Overview of bed levels over morphological time (T_m), using parameter values from Van Ledden (2003) and Van Ledden *et al.* (2004b)

Van Ledden (2003) and Van Ledden *et al.* (2004b) also observed mud waves traveling through the spatial domain, as already seen in figure 2.19. These observations are again observed using the Delft3D sand-mud model, as seen in figure 3.10 and 3.11 (where figure 3.10 represents the results with parameters from Van Ledden (2003) and Van Ledden *et al.* (2004b), while figure 3.11 represents observations with parameters and boundary conditions which are used in the final 2DH Amelander tidal inlet system model (described in section 3.4.3, figure 3.6)). The differences between figure 2.19 and figure 3.10 can be attributed to the different parameters, the different model approach and by using figure 3.9. This figure shows a process towards an equilibrium state (which is not reached yet), while Van Ledden (2003) and Van Ledden *et al.* (2004b) already observe an equilibrium state after 120 years of morphological development.
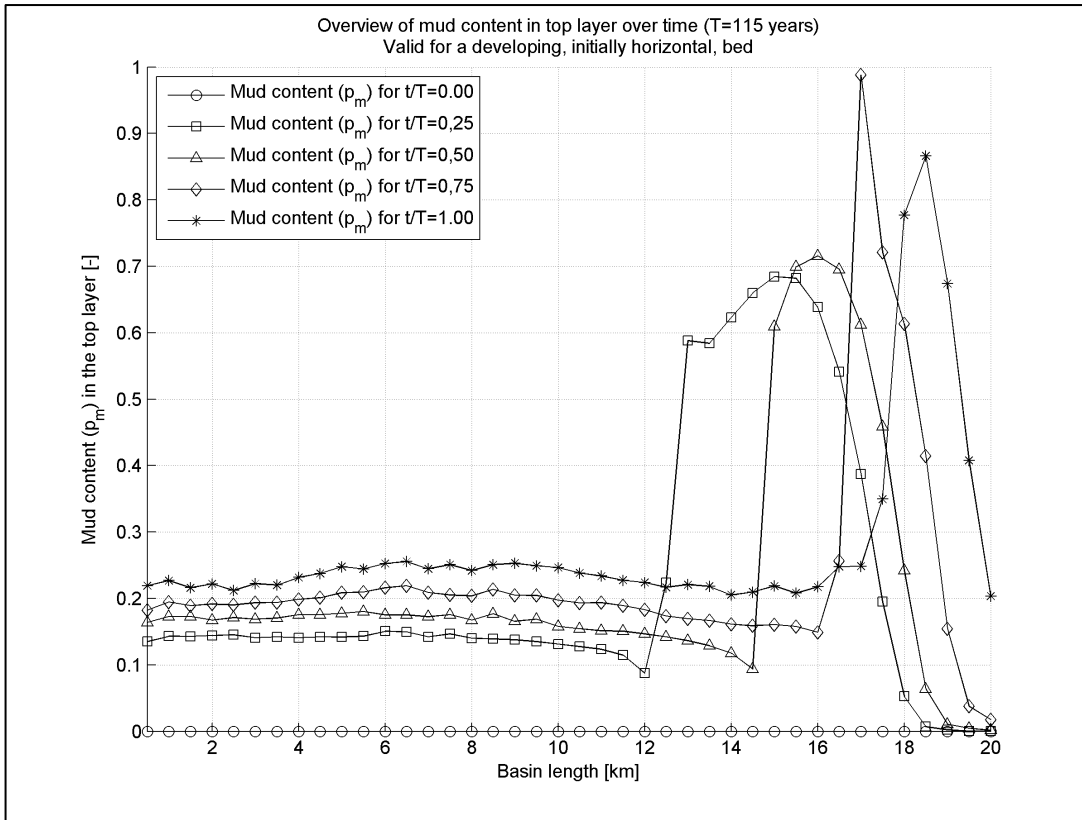
Figure 3.10: Instantaneous mud content in the top layer over morphological time (T_m), showing travelling mud waves, using parameter values from Van Ledden (2003) and Van Ledden *et al.* (2004b)
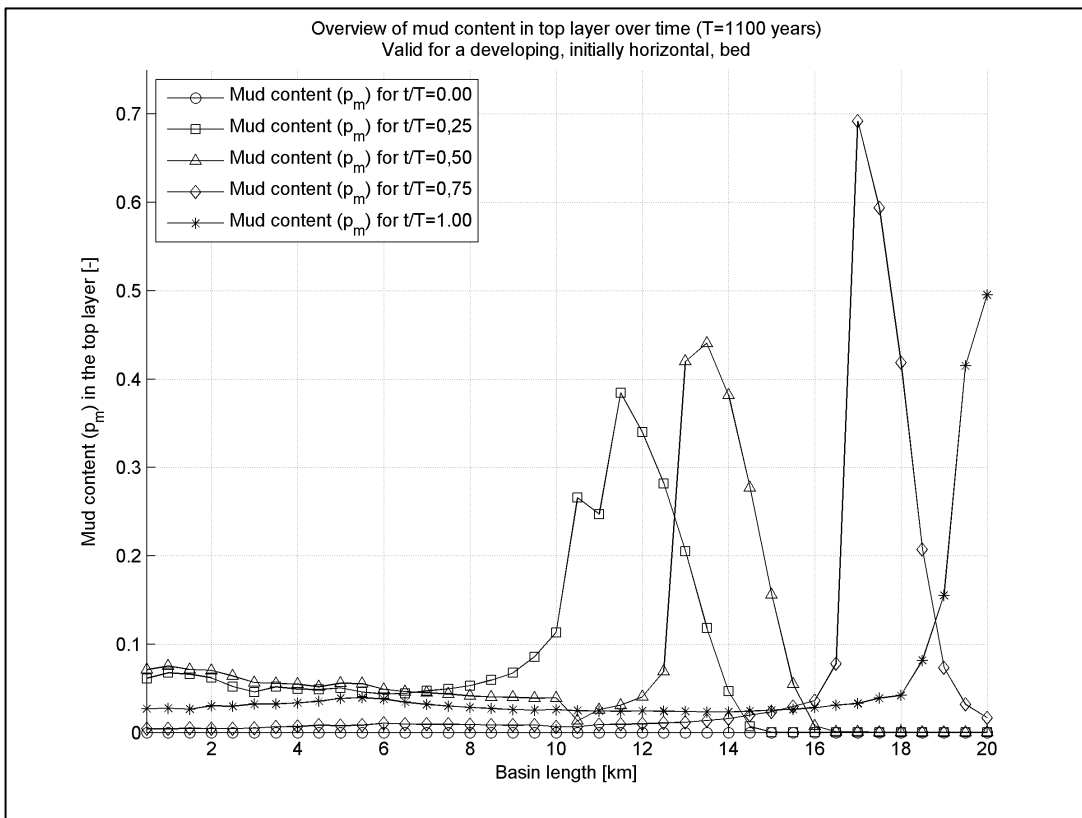
Figure 3.11: Instantaneous mud content in the top layer over morphological time (T_m), showing travelling mud waves, using parameter values from final simulations

Chapter 4

Model Results, Observations & Analysis

With the introduction of the Amelander tidal inlet system model (in the previous chapter) it is now possible to execute the model. Looking at the objectives and classification hypothesis (section 2.4), some scenarios are needed. The first scenario is the reference, which is used to analyse large-scale sand-mud segregation patterns in general and assess the ability of the schematized approach to represent sand-mud segregation as observed in the field (based on observations). This scenario features normal tidal conditions and average wind conditions (responsible for wind driven flow). Furthermore, in line with the assessment of relative contributions by wind and tide and the associated classification hypothesis, three additional scenarios are considered. These scenarios show variations in tide (larger or smaller) and additional short wave forcing (based on extreme wind conditions), when compared to the reference scenario. For easier and straightforward comparison, all scenarios are run with identical settings and parameters (as described in section 3.4.3 and as assessed in section 3.5).

The different scenarios are found in table 4.1 below.

Scenario name	Properties
A) Reference	Reproduction of the 'real life' situation. Realistic tide and average wind conditions
B) Large tide	A copy of the reference situation, though, the tidal amplitudes are doubled
C) Small tide	A copy of the reference situation, though, the tidal amplitudes are halved
D) Short wave	A copy of the reference situation, though, with implementation of waves ($U_{10} = 20$ m/s)

Table 4.1: List of different model scenarios and their associated specific properties

Notice the relation between these scenarios and the classification hypothesis from section 2.4, related to Nichols & Boon (1994). The reference, large- and small tide scenarios can be used to verify/reproduce the observations made in figure 2.28-C (Arcachon Bay), related to relative tidal-dominance (according to the classification hypothesis), while the wave scenario can be used to verify/reproduce the observations made in figure 2.28-A (Mobile Bay), related to relative wave-dominance (according to the classification hypothesis). So, in line with the classification hypothesis, only the forcing conditions are changed.

To compare the different scenarios, the mud content in the top layer is mainly used. Due to the different forcing conditions the time aspect of the model becomes important, since equilibrium spatial distribution of mud content in the top layer is needed for meaningful comparison. Therefore, section 4.1 will analyse this time aspect of the model, before the results for the different scenarios are provided in section 4.2-4.4. The chapter is ended with a proposition for a general classification and a discussion.

4.1 Model time aspect analysis

As stated in section 3.4.1, the considered model is not using morphological updating. This assumption allows for different curves (like the upcoming figures 4.7, 4.11 and 4.15) to be fully compared, without the bed level distribution (vertical-axis) to be distorted. Therefore, instead of using morphological updating, the bed composition (mainly depending on mud content (p_m) within this model) is given time to develop (given the hydrodynamic conditions) towards a distribution of mud content throughout the spatial domain that is (more or less) in equilibrium.

Due to this model assumption, an equilibrium situation is not found in transport patterns or equilibrium morphology, but rather in a stable distribution of mud content within the bed. Within this equilibrium, transport of sand and mud from one location to another (for instance import into the system through the tidal inlet) is still possible, though, as long as it is in balance with the sediment that is gained in the underlayers. Therefore, an equilibrium state will be indicated by continuous transports, which are in balance with sediment transport towards the underlayers. Therefore, the mud content within the top layer remains (more or less) constant.

To compare all different scenarios (as will be done in the following sections), it is of paramount importance to verify that the model results are indeed in line with this equilibrium. To verify this, two options are selected[14]. First, an indication of changes in mud content in the top layer is given by computing the differences in mud content (p_m) for some successive computational time steps. Figure 4.1 is used for this first approach, it indicates the differences in mud content in the top layer between (A) day 31 and 36 (at approximately 40% of the entire simulation) and between (B) day 85 and day 90 (at the end, as day 90 marks the end of the simulation).
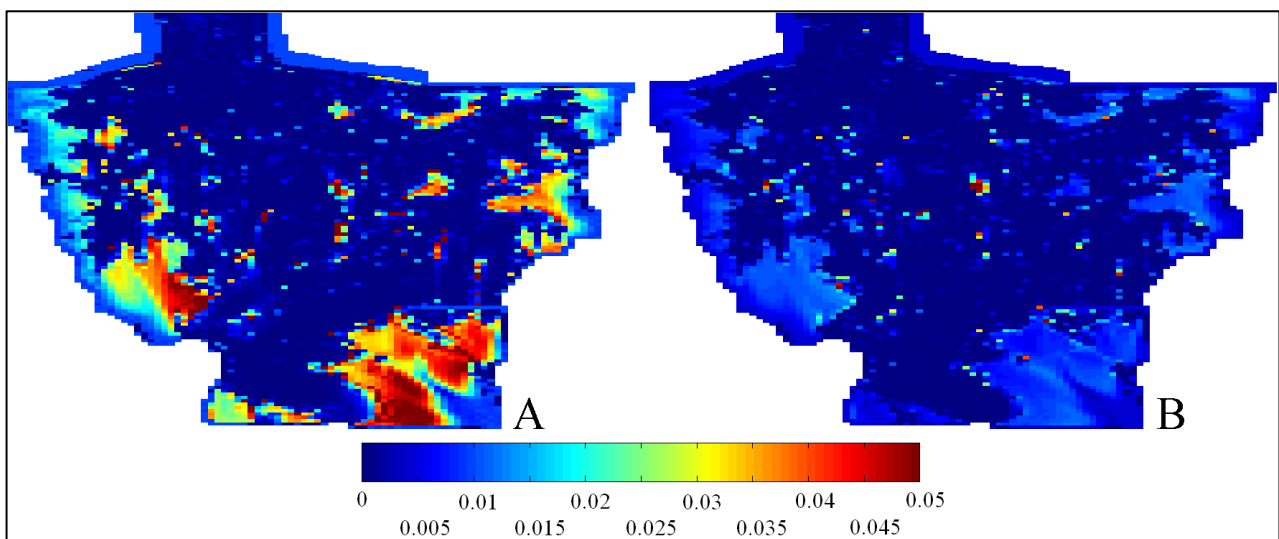
Figure 4.1: Absolute difference in mud content in the top layer over a period of 5 days, between (A) day 31 and 36 and (B) day 85 and 90, for the reference scenario.

Figure 4.1 clearly indicates how the changes in bed composition slowly develop towards an equilibrium situation. Looking at the changes of mud content in the top layer after 3 months of hydrodynamic forcing (4.1-B), which is the total computational time, the changes in mud content (even over a period of 5 days) are far from significant.

The second approach for visualizing the equilibrium situation of mud content in the top layer is by adding up all values of mud content in the top layer throughout the tidal lagoon for each time step, while looking at

---

[14] The first approach will be used for the reference scenario (but is valid for all), while the second approach is used for all scenarios

the differences in the values (for this sum) between each time step[15] (called ξ within this thesis). By doing so, a dynamic equilibrium state for the distribution of mud content in the top layer is achieved when the value of ξ approaches to- and is near zero. From this description, ξ can mathematically be defined as:

$$\xi = p_{m,sum}^{t+\Delta t} - p_{m,sum}^{t} = \sum_{i=1}^{N} \sum_{j=1}^{M} p_m^{t+\Delta t}(i,j) - \sum_{i=1}^{N} \sum_{j=1}^{M} p_m^{t}(i,j) \tag{4.1}$$

Where:

$p_{m,sum}^{t}$	Sum of all p_m values in the tidal lagoon for time step t
$p_m^{t}(i,j)$	Value of p_m for time step t at grid cell (i,j)
N	Number of grid cells in the tidal lagoon in x-direction
M	Number of grid cells in the tidal lagoon in y-direction

Figure 4.2 shows the evolution of ξ over the total computational period (T) for all scenarios.
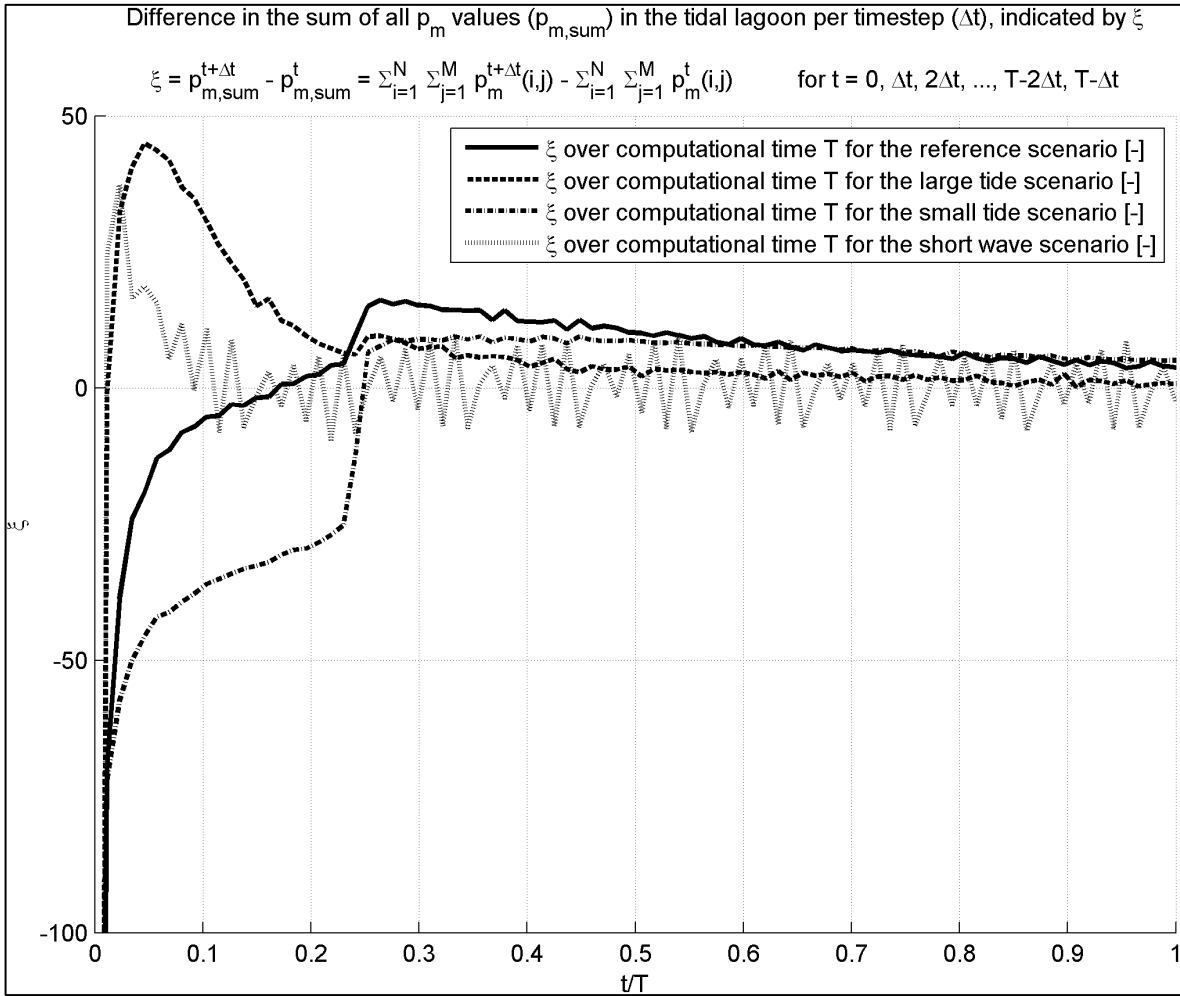
Figure 4.2: Evolution of ξ (equation 4.1) over the total computational time (T)

From the above description, it appears that the spatial distribution (through the tidal lagoon) of mud content in the top layer is indeed showing equilibrium behaviour for all tidal scenarios. The variations, observed for the short wave scenario, can be addressed by the influence of short waves in different areas, due to the different water levels (due to the tide). Therefore, the chosen 3-month period of hydrodynamic activity appears to be a practical value, from both an equilibrium- and computational time perspective.

---

[15] This approach is quite pragmatic, since mud content could decrease at one location, and increase at another, thus cancelling each other out. Though, these sudden changes are not observed within the model (figure 4.1), given this, the approach becomes quite robust.

4.2 Reference scenario

To assess the large-scale sand-mud segregation patterns in the reference scenario, observations of variables (like the spatial distribution of mud content or mud concentrations) can be used to quickly give insight in the results. But apart from these observations, further analysis (using multiple variables) can give great insight in the results, because relations between these variables get visualized. Therefore, this section is split up in both observations and further analysis of the results. Finally, the section is closed with a discussion. This discussion is used to elaborate on the classification hypothesis and the relation with the associated observations and analysis (based on the reference scenario).

4.2.1 Observations

Over a period of 3 months, the forcing conditions in the reference scenario are redistributing mud through the spatial model domain (normal tidal- and average wind conditions (responsible for wind driven flow), as introduced in table 4.1). Due to this, the initial mud content of 5% ($p_m = 0.05$) in the bed (as stated in figure 3.6) is changing for each location (dependent on the local hydrodynamic forcing conditions). The inflow of mud through the tidal inlet (due to tidal asymmetry) could also be responsible for additional mud content in the system (and eventually in the bed).

Since the bed consists of various sediment layers (consisting of diverse sand-mud mixtures), one can look at the top layer for a birds-eye view of the mud content. This is referred to as mud content in the top layer. The mud content in the top layer, after 3 months of hydrodynamic forcing in the reference scenario, is found in figure 4.3.
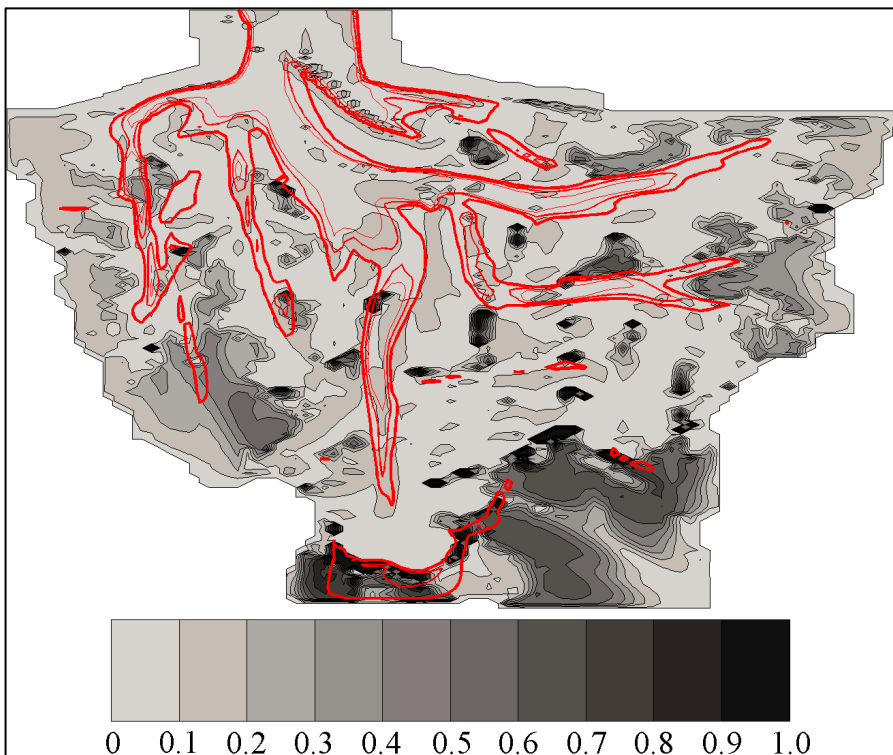
Figure 4.3: Mud content in the top layer (after 3 months) for the reference scenario, along with red contour lines for 8, 6 and 4 meters depth w.r.t. MSL (respectively from thin to thick lines)

When looking at figure 4.3, some initial observations can be made. First, it appears that mud is mainly abundant on the tidal flats and near the southern land boundaries, the relatively shallow areas, far from the tidal inlet itself. Furthermore, small mud contents are found near the inlet and the inner model areas, these locations are commonly deeper.

Mud concentrations are responsible for changes in mud content in the bed (like the observed changes in figure 4.3, compared to the initial values from figure 3.6), as mud deposition is dependent on fall velocity (w_m) and instantaneous mud concentration (c_m) in the water column. The distribution of suspended mud is therefore an important indicator for sediment (mud) supply/availability. Figure 4.4 shows the instantaneous mud concentrations (during slack water) after a period of 3 months. When looking at this figure, an increase in mud concentrations towards the inner side of the tidal lagoon is observed. Just like higher mud contents are observed towards the inner side of the tidal lagoon, see figure 4.3. Furthermore, the higher concentrations mostly appear in the south-eastern areas of the tidal lagoon, supporting the transport patterns (channels) in figure 2.10 and 2.11.

Finally, note the zero valued concentrations near the model boundaries. These values indicate dry areas (and thus no concentrations in the water column). It is very common for areas in the Dutch Wadden Sea to fall dry during low water levels (see for instance table 2.1).
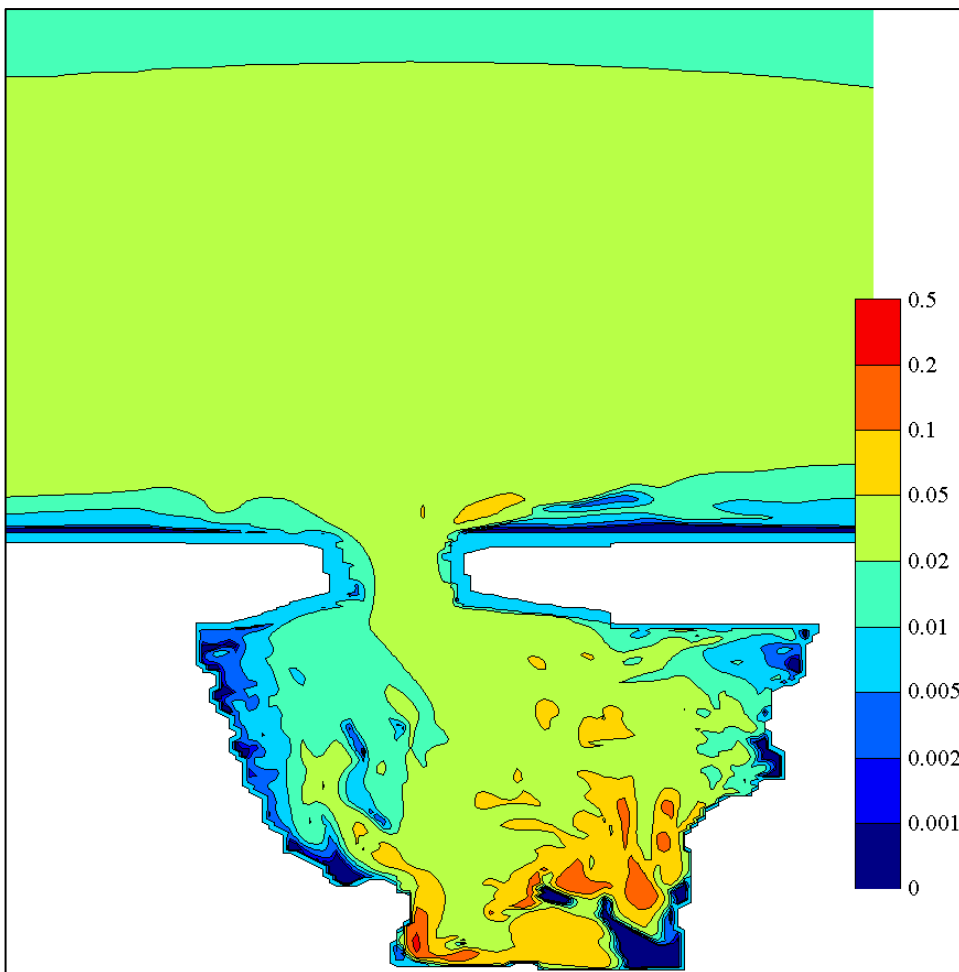
Figure 4.4: Instantaneous mud concentrations (after 3 months) during slack water for the reference scenario [g/l = kg/m^3]

In the area of the North Sea, which is covered in the model domain, observations in the field show common mud concentrations in the order of 10 (at sea) up to 30 g/m^3 (near the Frisian Islands). Within the tidal lagoons, mud concentrations increase from these common North Sea values up to a maximum of 100-200 g/m^3 (see e.g. Postma, 1981). Figure 4.4 appears in line with these typical values/observations, although some locations show slightly larger concentrations.

4.2.2 Analysis

Sand-mud segregation occurs because of differences in occurring bed shear stress. When mud is absent in certain areas, the occurring bed shear stress does not allow mud to settle. This also holds for areas with mud abundance, here the bed shear stress does allow mud to settle. These occurring bed shear stresses can be related to different areas, like tidal flats and channels. To further analyse this relation, the different areas must be described by some parameter. The bed level seems to meet this requirement, as this parameter (or depth) describes the features like tidal channels and tidal flats. Therefore, figure 4.5 is set up. This figure indicates the median shear stress that occurred in one tidal cycle for each grid cell within the tidal lagoon, and relates it to the bed level (for each associated cell).

When observing figure 4.5, a relation between bed shear stress and bed level can be identified. It appears that the smallest values for the bed shear stress occur in shallow areas, while the larger bed shear stresses mainly occur in deeper areas. Furthermore, the relation appears like a smooth transition between these 'extremes'.
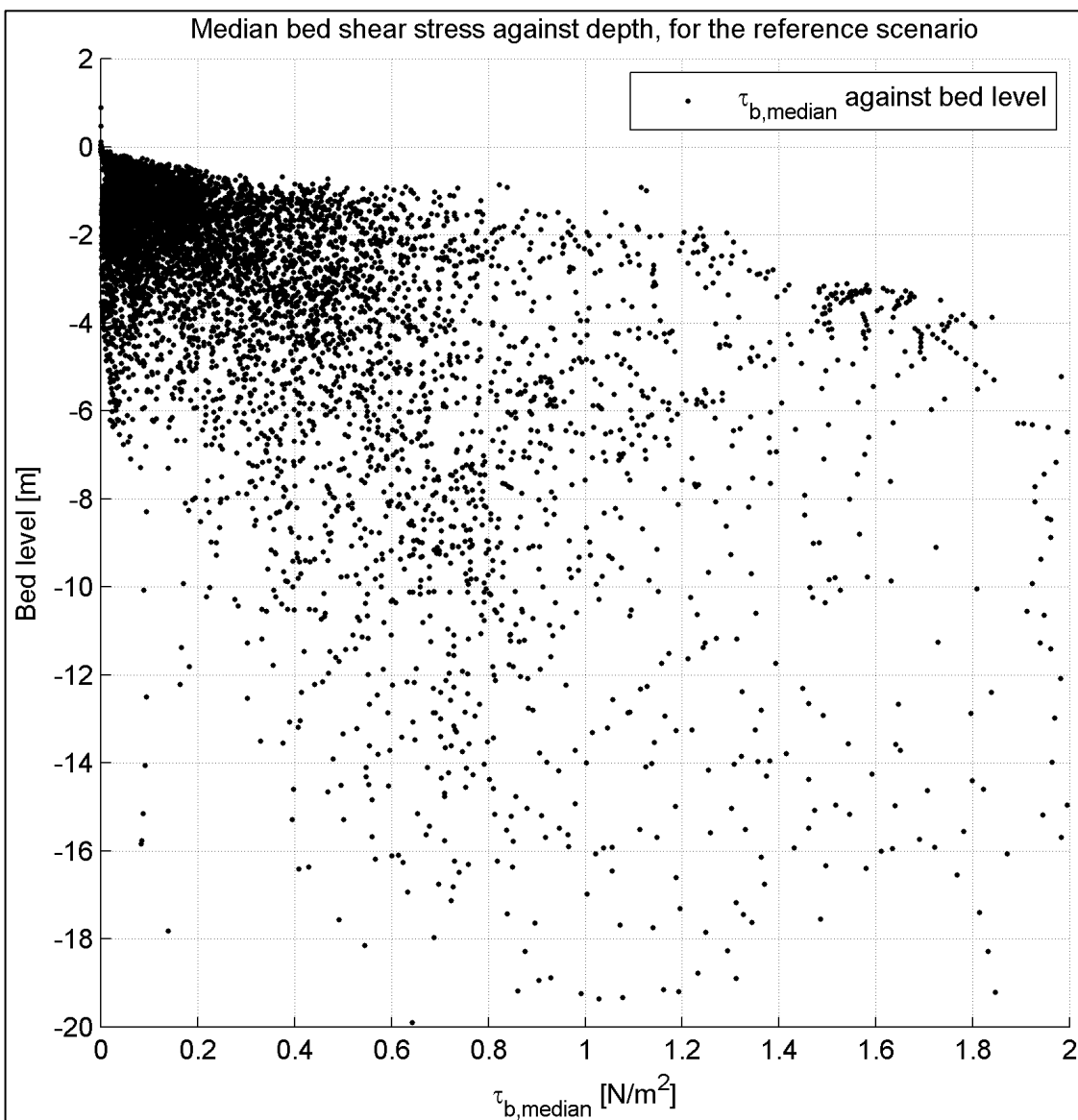
Figure 4.5: Median bed shear stress (over one tidal cycle) for each grid cell related to the bed level, for the reference scenario

Figure 4.5 indicated a rough relation between depth and bed shear stress (valid for the tidal lagoon). Since smaller shear stresses are observed in shallow areas, like tidal flats, and vice versa. When relating bed shear stress to mud content in the bed, one expects higher mud content when smaller bed shear stresses occur (in line with the theory for erosion of mud, from sections 2.4.3 and 2.4.4).

To visualise a relation between bed shear stress and mud content within the model of the tidal lagoon, these variables can be plotted against each other. Figure 4.6 is used for this purpose. This figure indicates the mud content in the top layer against an instantaneous occurring bed shear stress, which is normalized by the maximal critical bed shear stress (for mixtures with $p_m = 1$).

When looking at figure 4.6, two important observations can be made. First, it appears that high values of mud content in the top layer (above $p_{m,cr}$, so the mixture is thought to be in the cohesive regime) mainly occur when the bed shear stress is below its critical value. Since this figure is instantaneous, some cohesive mixtures are also found for higher shear stresses. But according to the definition, mud is eroding at these locations (and mud content will therefore eventually decrease). The second observation is valid for high occurring shear stresses. It appears that mud content in the top layer is commonly small for larger shear stresses.
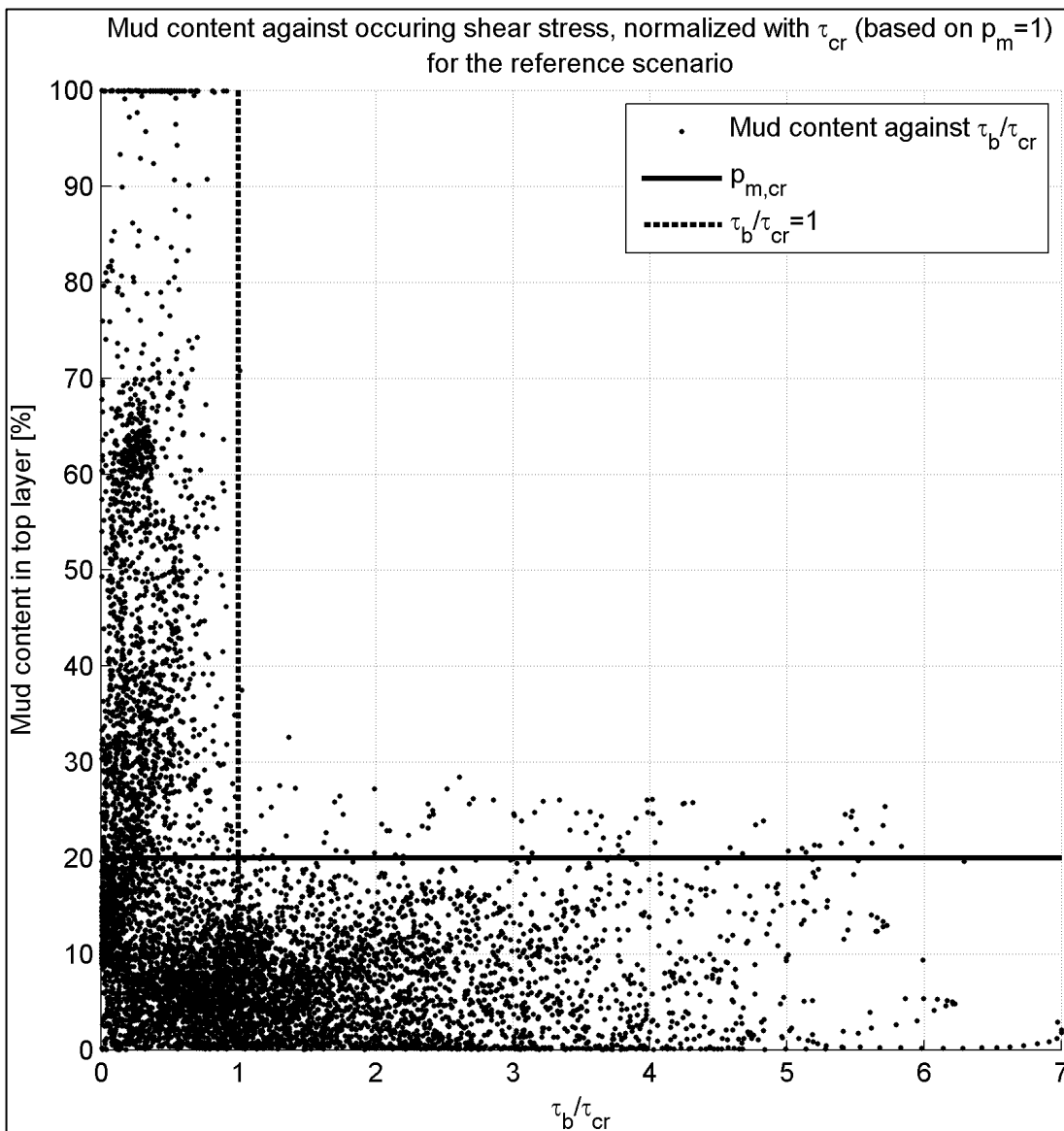
Figure 4.6: Normalized bed shear stress against mud content for each grid cell related to the bed level, for the reference scenario

Figure 4.5 suggests a relation between bed shear stress and bed level, while figure 4.6 suggests a relation between bed shear stress and mud content (in the top layer). By combining these relations, a suggestion can be made for a relation between mud content and bed level. Roughly speaking, figure 4.5 and 4.6 would suggest a relation where mud content is higher in shallow areas and smaller for deeper areas.

To assess this suggestion, the relation between bed level and mud content should be visualized. By introducing hypsolaspy[16] curves, the relation between these variables is made visible, while indicating a range in the data is suggested (as a single, average line is just part of the story).

Figure 4.7 introduces this hypsolaspy curve for the reference scenario, along with a data range for all the occurring mud content values (25 to 75% for each meter of bed levels).

By observing figure 4.7, an overall relation between bed level and mud content (in the top layer) can be produced. It appears that mud content is increasing for the shallow areas, while it is decreasing for the deeper areas. Furthermore, mud, which is located near mean sea level, appears to get transported to slightly deeper (though shallow) areas. Though, this observation hardly contributes to the overall tendency for mud to be transported to- and settle in shallow areas.

The above observations appear in line with the previous observations from figures 4.5 and 4.6. The suggested relation is indeed found in the hypsolaspy curve for the reference scenario (figure 4.7).
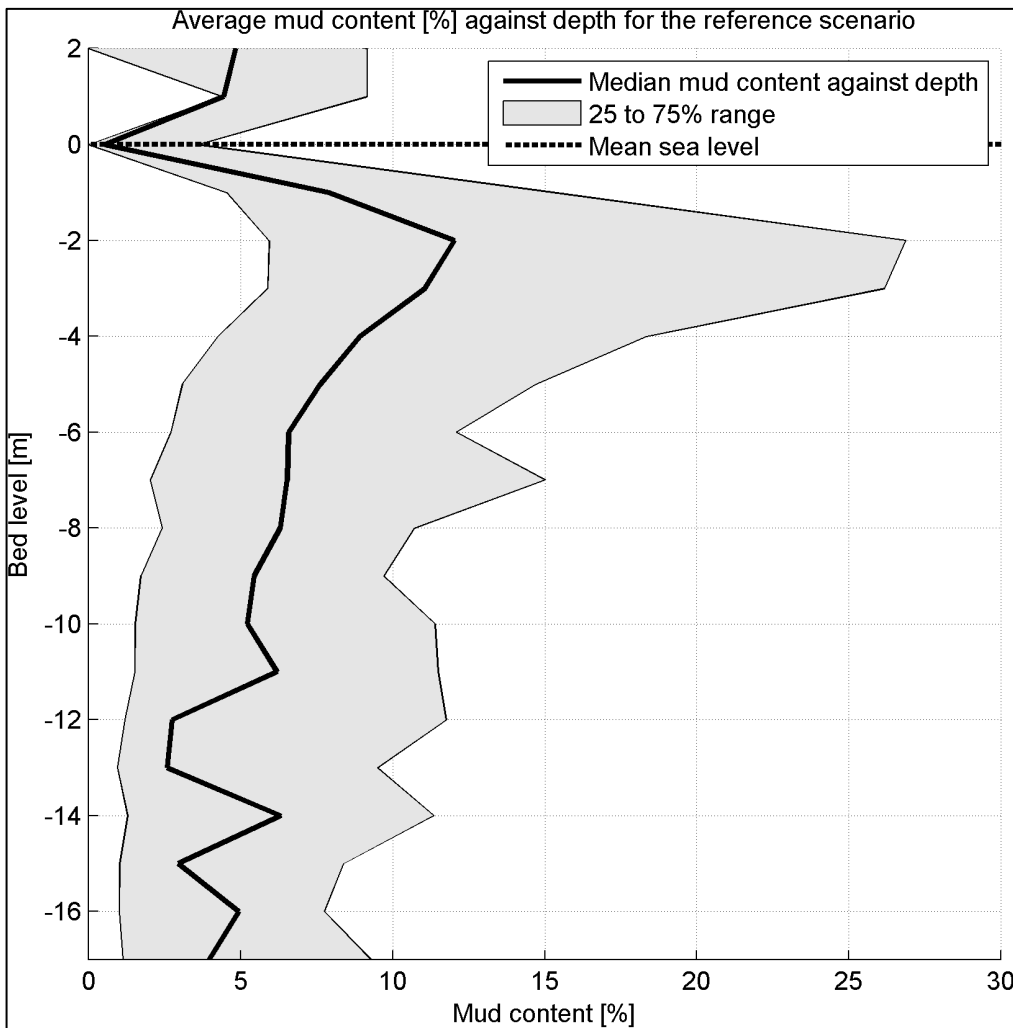
Figure 4.7: Hypsolaspy curve for the reference scenario (after 3 months)

---

[16] Inspired by hypsometry curves (e.g. Yu *et al.* (2011)), hypsolaspy curves relate height (from Greek: ὕψος, hupsos) and mud (from Greek: λάσπη, láspi) in a single curve, indicating the relation between the spatial distribution of mud and depth ('height').

With the above relations between bed level, bed shear stress and mud content (in the top layer) one important aspect of mud transport is missing: mud availability. According to Liu *et al.* (2011), mud concentrations are an important indicator for mud availability. This statement is also supported by the combination of figure 4.3 and 4.4, where high mud contents within the bed occur at locations where high mud concentrations are found as well. By combining this with the previous analysis, a relation between mud concentration (availability) and bed level is suggested.

Therefore, figure 4.8 is visually indicating the relation between instantaneous mud concentrations and the associated bed levels, from which some clear observations can be made. High concentrations are only found in shallow areas, while deeper areas are only governed by small concentrations. Relating this to mud availability, it appears that the available mud in shallow areas is (potentially) larger than that in deeper areas, while deeper areas never experience a large availability of mud.
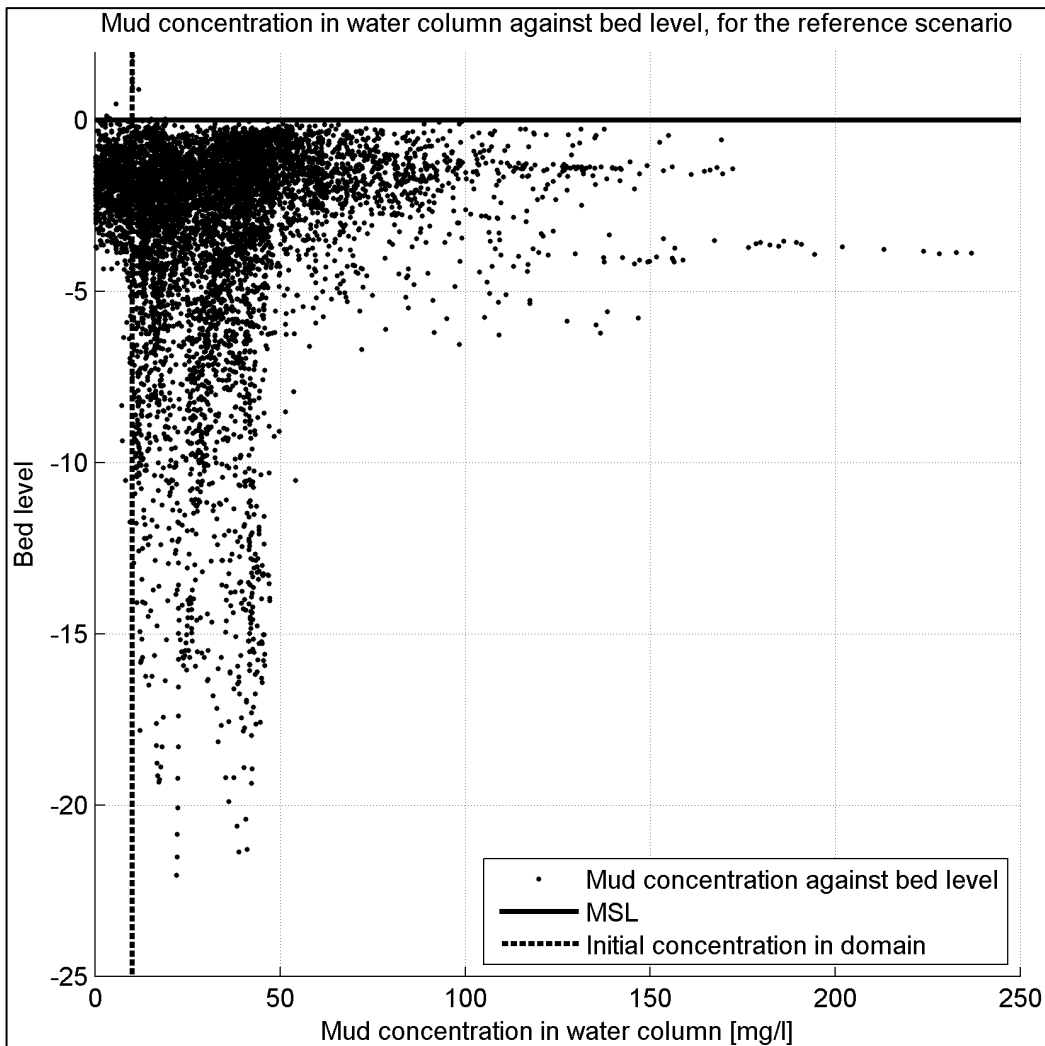
Figure 4.8: Instantaneous mud concentrations (after 3 months) during slack water for the reference

Although larger shear stresses were observed in deeper areas (suggesting erosion of available mud in deeper areas), mud is found in shallow areas according to figure 4.8. Two processes can be responsible for this. First, non-linear tidal effects (section 2.2.1 and 2.3.1) are responsible for transporting suspended sediment (mud) further into the basin (and thus towards shallower areas). Furthermore, the large eroding shear stresses in the deeper areas (along with the transporting current) result in small mud contents within the bed, decreasing mud availability in the bed and thus in associated concentrations (availability of mud in the water column).

4.2.3 Discussion

With the observations and analysis for the reference scenario given in the previous two sections, a comparison with the observations, theory and classification hypothesis from chapter 2 is now possible. By doing so, bare in mind the relative dominance for the reference scenario, which is by tidal currents.

Starting with the observations from the reference scenario (section 4.2.1), it appears that the mud content within the bed is in line with large-scale sand-mud segregation patterns, as introduced in section 2.1.4. The theory (e.g. shear stress due to hydrodynamic activity and tidal asymmetry) also suggests the observed large-scale patterns. Looking at the mud concentrations in the water column, the relation with the mud content in the bed (or top layer) is evident, as it indeed indicates the mud availability (as suggested by Liu *et al.* (2011)). Apart from the qualitative results, the model appears capable of delivering quantitative information as well. The mud concentrations are in line with field measurements (e.g. Postma, 1981) and the values for mud content in the bed (or top layer) are in line with figure 2.14. Though slight overestimations are found.

With these observations, both qualitative and quantitative, the schematized model has proven to deliver, not only realistic sand-mud segregation patterns, but also realistic values for important variables that represent these patterns. The reference scenario is therefore considered capable of representing large-scale sand-mud segregation patterns, one of the main goals within this thesis (section 1.3).

The analysis for the reference scenario, given in section 4.2.2, shows some important relations between variables that are related to large-scale spatial sand-mud segregation patterns, valid for a tidally dominated system.

First, the relation between shear stress and bed level, valid for this system, is given. Mainly because of the increase in system width, further into the system, smaller shear stresses are found. These are also the locations where shallow areas are abundant. More hydrodynamic activity is found near the tidal inlet, which is, along with the tidal channels present here, much deeper. When relating this to theory, mud settling is expected in areas with less hydrodynamic activity. These areas are found further into the system (far away from the tidal inlet). For this system, it is very common that these areas are relatively shallow.

The second relation is found between the bed shear stress and mud content within the bed. From this, it appears that high mud contents (mixtures that are considered as cohesive) can only occur in areas with small hydrodynamic activity (smaller than the critical shear stress). This observation is in line with the theory for erosion (section 2.3.4) but also indicates capturing of mud at locations that are considered cohesive. Combined with the relation between bed shear stress and bed level an important and insightful relation between mud content and bed level is suggested as well.

This relation (between bed level and mud content in the top layer) shows increasing mud content for shallow areas and vice versa. Within this figure, the overall trend and relations between bed shear stress, bottom depth and mud content is shown. Changes in this figure for different scenarios will therefore be used to assess the relative contribution of different forcing (representing dominance of short waves and tidal currents). Furthermore, the analysis verifies that mud availability is indeed related to mud concentrations (figure 4.8).

The reference scenario can be considered as tidally dominated, according to figure 2.29. Furthermore, when looking at figure 2.28, the reference scenario can be related to Arcachon Bay (figure 2.28-C). The classification hypothesis, which is stated in the associated section (2.4), appears in line with all of the above observations and analysis for the reference scenario (taking the tidal dominance into account). The tidal currents increase hydrodynamic activity in deeper areas (compared to the shallows), while higher mud content is found in shallow areas. Tidal asymmetry and bed shear stress distribution (related to erosion formulations) are important initiators for these large-scale sand-mud segregation patterns.

From this, it appears that all the results are in line with the combination of observations in the field (for comparable cases, like figure 2.28-C), the associated theory and classification hypothesis.

4.3 Results for changes in forcing conditions

The hypothesis, that relates the classification in figure 2.28 (Nichols & Boon, 1994) to relative forcing dominance (like tides and waves), which can be classified using figure 2.29 (Davis & Hayes, 1984), resulted in the short wave-, high tide- and low tide scenario (as introduced in the beginning of this chapter). This section will elaborate on the results from these scenarios using observations and analysis (comparable to section 4.2), divided in tidal influence and short wave influence. Using these results, the classification hypothesis can be discussed. This is addressed at the end of each sub-section (on tidal influence and short wave influence, respectively).

4.3.1 Influence by tide

Observations

The changes in tidal amplitudes can be observed in both water levels and associated tidal currents. To verify the proposed scenarios (table 4.1), figure 4.9 is used. This figure shows the water levels in the North Sea during two tidal cycles for the reference- and the different tidal scenarios. By observing the tidal amplitudes, it appears that the different scenarios are successfully executed (halved and doubled amplitudes).
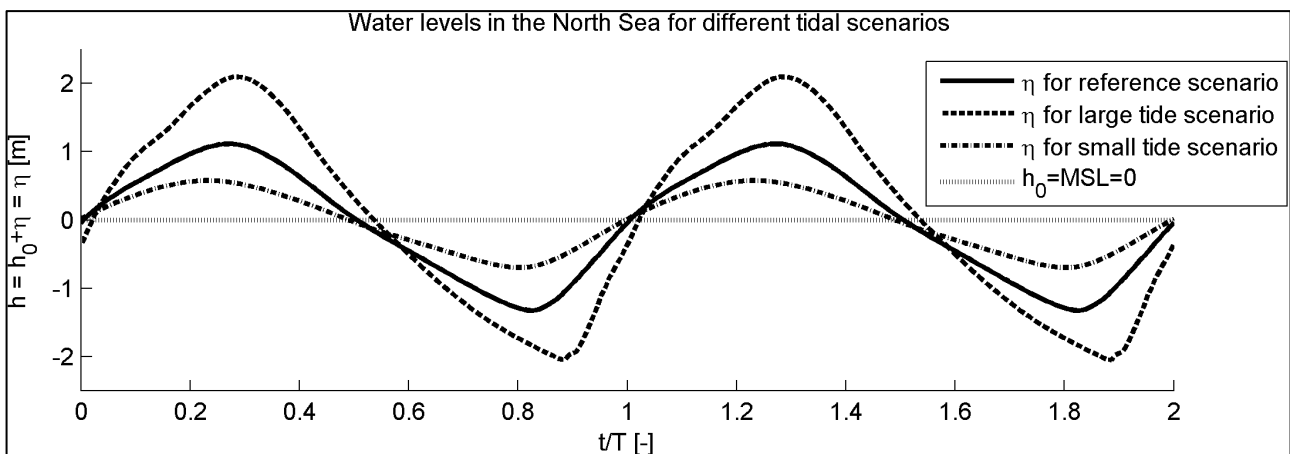
Figure 4.9: Water levels in the North Sea during two tidal cycles, for the reference- and tidal scenarios

Notice how the M_4 and M_6 tidal components result in shorter flood- and longer ebb periods, which implies import of fine sediment (mud) towards the land boundaries in the tidal lagoon. This is addressed in section 2.2.1 (indicated by tidal asymmetry) and 2.3.1 (indicated by horizontal transport) as an important mechanism for transporting fine sediment (mud) into a system (and for this system, towards shallow areas).

The reference scenario clearly indicated the occurrence of sand-mud segregation under normal conditions. Higher mud concentrations are observed in shallow/less active areas (tidal flats and basin boundaries) whereas sand is mainly found in hydrodynamically active areas (channels and tidal inlet). Figure 4.10 shows the mud content in the top layer under the influence of large- and small tidal amplitudes (and thus tidal prism Ω), respectively the left and right image. This image can be related to figure 4.3 (for the reference scenario), which is plotted on an identical scale.

Again, note that the time aspect of the model is very important. Within this analysis, it is assumed that the spatial distribution of mud content in the top layer is (more or less) in an equilibrium state. This assumption has been verified in section 4.1.

The large tide scenario features twice the original tide, when compared to the reference situation (as indicated in table 4.1). When looking at the mud content in the top layer (left image in figure 4.10), it appears that mud content increased near the model boundaries (shallow areas), while smaller mud contents

are observed within the tidal lagoon. Furthermore, the size of the area in which higher mud contents are found appears to be smaller, when compared to the reference situation.

The small tide scenario is a copy of the reference scenario, though it features tidal components with halved tidal amplitudes (as indicated in table 4.1). Figure 4.10 (right hand image) no longer shows distinct mud abundance at the tidal flats within the lagoon, but on the other hand, deeper areas also hardly indicate patches with higher mud content. It appears that the mud content distribution is more evenly spread throughout the tidal lagoon.
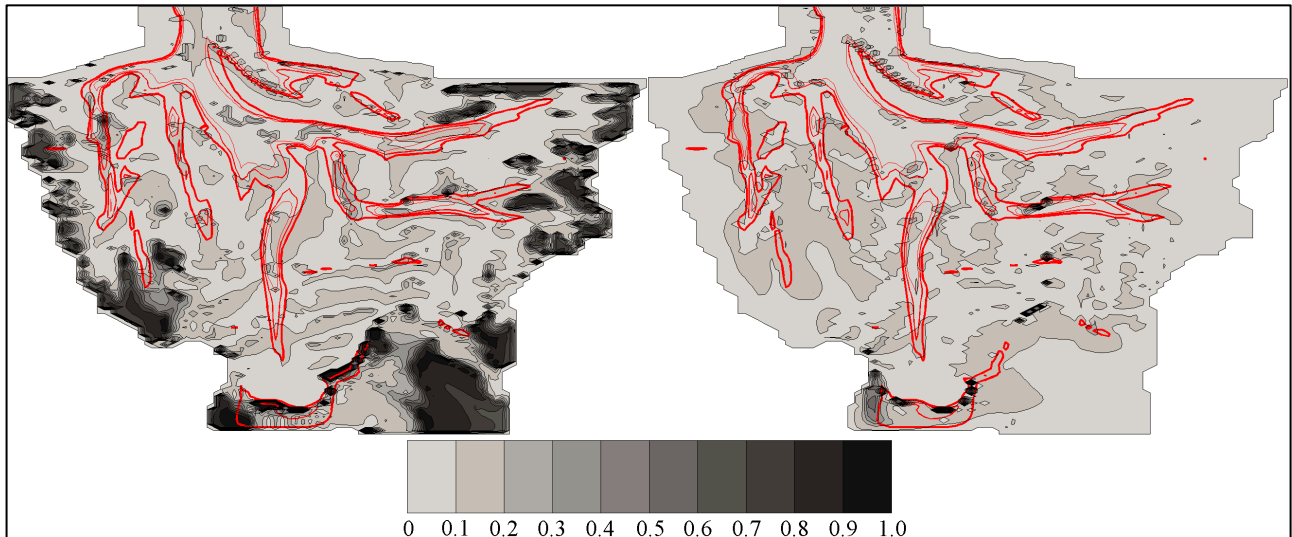
Figure 4.10: Mud content in the top layer (after 3 months) for respectively the large- and small tide scenario (left and right), along with red contour lines for 8, 6 and 4 meters depth w.r.t. MSL (respectively from thin to thick lines)

Analysis

To further (quantitatively) support the above (qualitative) observations, an analysis is used. Therefore, hypsolaspy curves can be used again. Figure 4.11 shows these curves for, respectively, the large- and small tide scenario. By relating figure 4.11 to the hypsolaspy curve for the reference scenario (figure 4.7), some conclusions, related to the differences between these tidally dominated scenarios, can be drawn.

First, the large tide scenario shows slightly larger differences between shallow and deeper areas (figure 4.11, left image), these differences appear to occur because of the decrease in mud content in deeper areas. The increase in shear stress (due to the larger tidal prism Ω) within the tidal channels is most likely responsible for the decrease in mud content (as nothing else is changed in the model, compared to the reference scenario). It appears that the characteristics of the reference scenario (which were related to tidal dominance in the classification hypothesis) are slightly enhanced by the increase in tidal dominance.

The small tide scenario shows a decrease in the differences of mud content (related to depth, see figure 4.11, the image on the right hand side), when compared to the above observations. It appears that mud is still transported to the shallow areas (as mud content increased from the initial 5% (figure 3.6) to a median value of 10%), though, these differences are smaller than the reference- or large tide scenario[17]. Therefore, the spatial distribution of mud content trough the tidal lagoon appears to be more evenly spread out.

---

[17] Again, note the importance of the time aspect in this scenario, the assumption of an equilibrium state for the mud content in the top layer (which is used here) is essential and has been verified in section 4.1
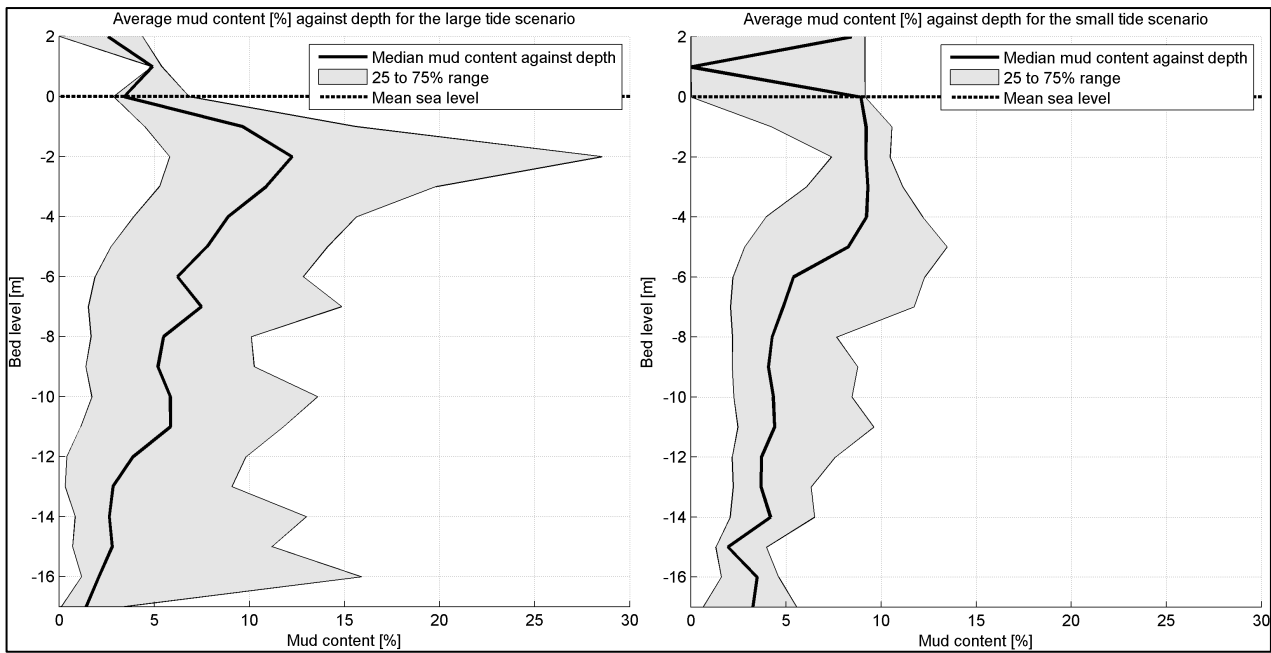
Figure 4.11: Hypsolaspy curves for large- and small tide scenarios (after 3 months), note that tidal ranges also increase and decrease (see figure 4.9)

Discussion

As indicated above, due to the increase/decrease in tidal prism (Ω) the model scenarios will respond with different timescales. For successful comparison, it is important that the spatial distribution of mud content is in an (more or less) equilibrium state. This has been addressed and verified in section 4.1.

When looking at the observations and analysis for the large tide scenario, while linking this to the classification hypothesis (section 2.4), an enhancement of large-scale sand-mud segregation pattern characteristics (as found in the reference scenario) is expected. This expectation is found within the relative dominance of the tide, which is larger for the large tide scenario. It appears that the observations indeed indicate an increase in these characteristics (as found in for instance figure 2.28-C). This statement is based on the differences between figure 4.3 & 4.10, but also the differences between figure 4.7 & 4.11. It appears that more mud is found near the margins, whereas the mud content in the deeper areas (channels) has diminished. Furthermore, the area in which higher mud contents are found appears to be smaller, this can be addressed by the increase of the area where mud erosion is found.

The small tide scenario shows a decrease in distinct sand-mud segregation, in line with the classification hypothesis, since the tidal dominance has decreased. This statement is also based on the differences between figure 4.3 & 4.10, and the differences between figure 4.7 & 4.11. When relating this to the classification by Nichols & Boon (1994), it appears that the two extreme cases (figure 2.28-A and 2.28-C) are mixed (with the dominance of the tide still having a small upper hand in the spatial sand-mud distribution).

These statements all appear in line with the classification hypothesis (section 2.4), mainly related to the properties found in for instance figure 2.14 and 2.28-C.

4.3.2 Influence by short waves

The short wave scenario is based on the reference scenario, though it features a strong (extreme) wind speed ($U_{10} = 20$ m/s), which is responsible for short wave generation. Wave penetration through the tidal inlet is neglected, as concluded/advised by Nieuwenhuis (2001) and explained in section 2.2.2.

Observations

Due to the model boundaries in the tidal lagoon (based on higher bathymetry ($+5$ meter w.r.t. MSL)) wave characteristics and wind fetch are not implemented on the model boundaries, as this would require significant changes in the model (an additional grid, grid coupling and changes in bathymetry). These changes would be (1) not in line with the uniform and schematized approach and (2) would result in comparing models with different approaches, which is meaningless. Nieuwenhuis (2001) also describes this problem for the boundary near the western tidal divide.

Due to this, an increase in significant wave height is observed in the direction of the wind (from west to east). Common values run from 0 up to 1 meter in this direction (from west to east), as fetch increases (see figure 4.12, in which this increase is clearly visible during high tide). Furthermore, it appears that tidal channels are subject to even higher waves, as depth increases and hardly remains a limiting factor for wave build-up.
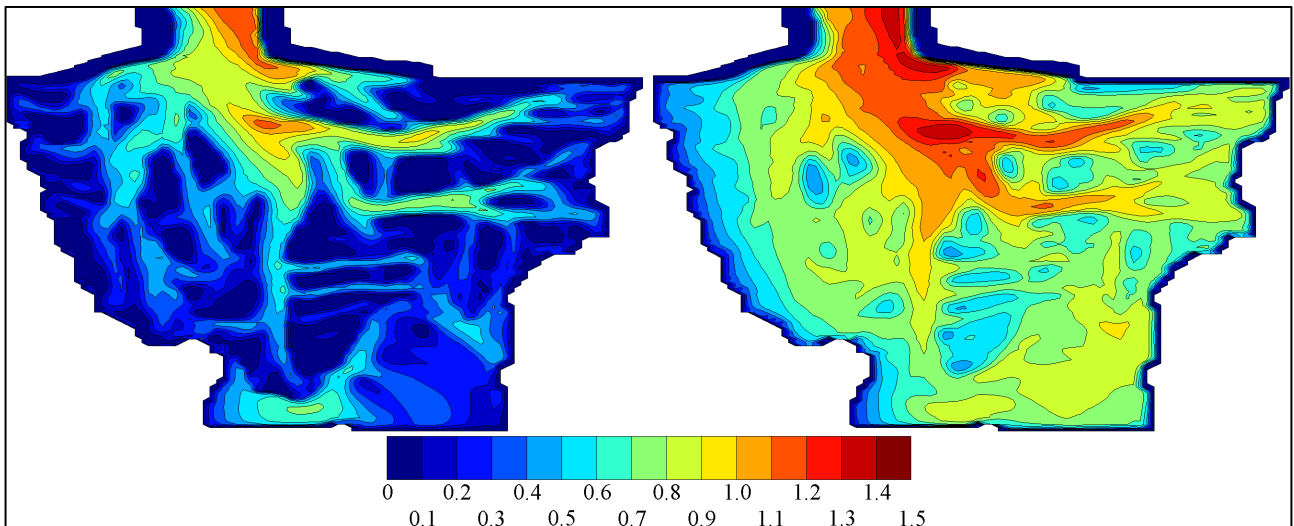
Figure 4.12: Instantaneous significant wave height during low- and high tide (respectively the image on the left and right hand side)

The combination of these short waves and the bottom depth determines the magnitude of the orbital velocities near the bed. Given identical wave heights, these velocities decrease for deeper areas, while shallow areas are subject to larger orbital velocities near the bed (as observed in figure 2.23). An increase in orbital velocities near the bed is responsible for an increase in local bed shear stress (and vice versa) and is therefore an important indicator for energy dissipation near the bed.

Combining the bed level with the above wave heights during high tide (right hand side image in figure 4.12) results in the instantaneous orbital velocities as found in figure 4.13, indicating the hydrodynamic activity near the bed (or energy dissipation) due to short waves only. It appears that hydrodynamic activity due to short waves is indeed found in shallow areas, while tidal channels are hardly subject to energy dissipation due to the short waves. Figure 4.13 also indicates the increase in orbital velocities from west to east, again indicating the observations from figure 4.12 (because of inducing no fetch at the western side of the tidal lagoon).
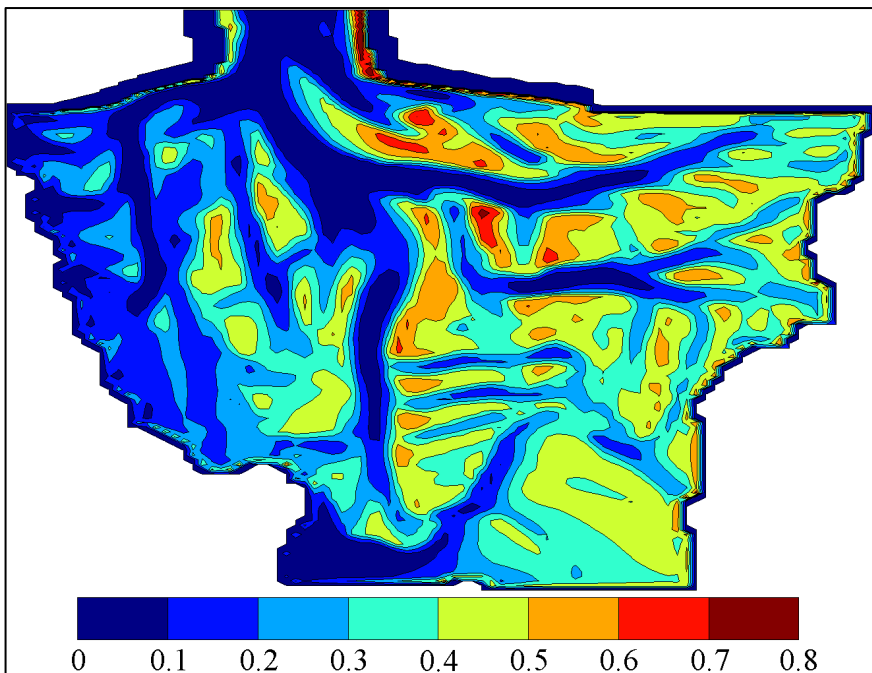
Figure 4.13: Instantaneous orbital velocities near the bed during high tide (after 3 months)

Due to the addition of short waves, the spatial distribution of mud content (in the top layer) changed significantly[18], as observed in figure 4.14. Although patches of 10-20% of mud content are observed, clear conclusions cannot be drawn from this figure and a further analysis (for instance using hypsolaspy curves) is, again, indispensible.
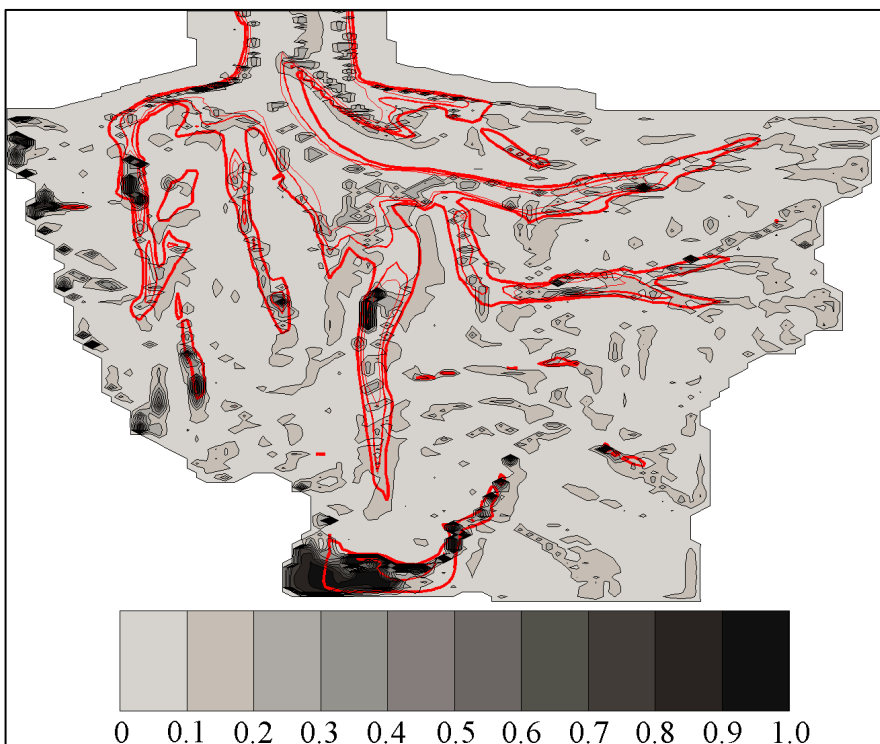
Figure 4.14: Mud content in the top layer (after 3 months) for the short wave scenario, along with red contour lines for 8, 6 and 4 meters depth w.r.t. MSL (respectively from thin to thick lines)

---

[18] Note the relation between the small orbital velocities in the shallow eastern areas (figure 4.13) and the patches of high mud content in the same area (figure 4.14). It appears that short waves significantly influence the mud content in the bed for shallow areas, as observed from the differences between the eastern and western part of the tidal lagoon.

Analysis

By again constructing a hypsolaspy curve, the relation between mud content (in the top layer) and bed level is made visible for the short wave scenario. This relation is shown in figure 4.15.

Within figure 4.15, higher mud patches (10-20% and higher) are mainly observed in areas deeper than 3 to 4 meters, say. This is a new observation, when compared to the previous hypsolaspy curves (figures 4.7 and 4.11), indicating the influence from short waves into the model (even given the fact that the eastern part of the tidal lagoon underestimates the short wave influence). Furthermore, the median mud content in shallow areas is smaller than that in areas with intermediate depth. This is also a new observation.
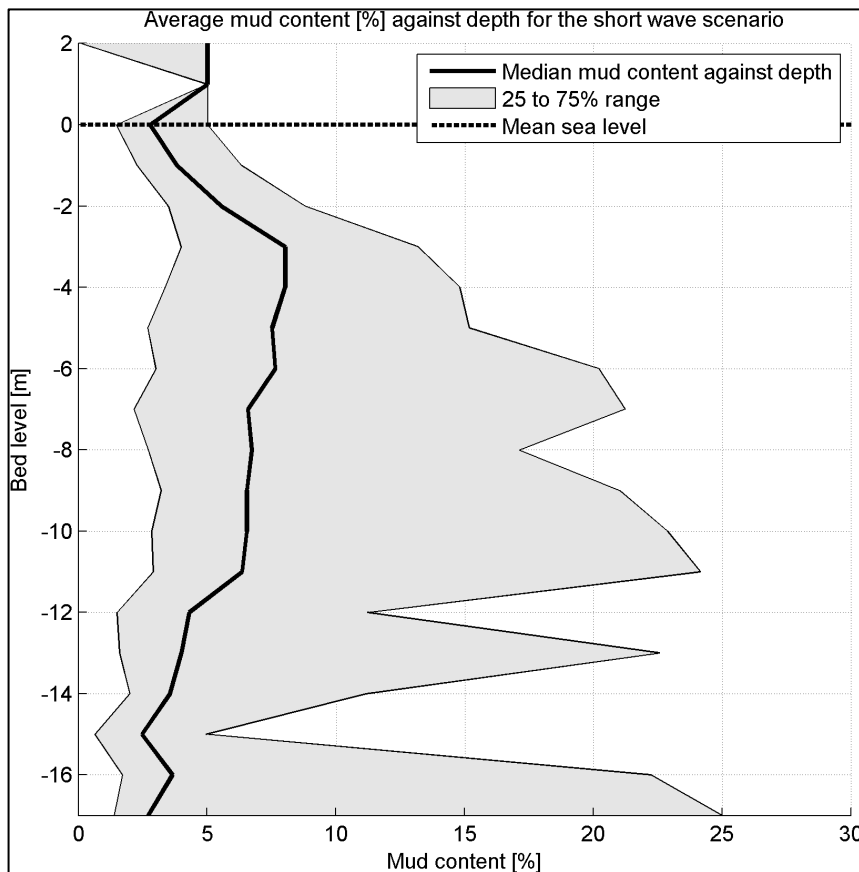
Figure 4.15: Hypsolaspy curve for the short wave scenario (after 3 months)

Discussion

According to the classification hypothesis, a wave-dominated system is expected to behave like Mobile Bay (figure 2.28-A), with mud absent from the basin margins due to (dominating) wave action (energy dissipation) in these regions. The short wave scenario introduces short waves into the model, moving it from a tide-dominated system to a mixed energy system, with a small upper hand for wave-dominance (figure 2.29). Therefore, according to the classification hypothesis, more mud is expected in deeper areas, while smaller areas lose mud (due to wave energy dissipation).

The observations of mud content indeed indicate how less mud is found in shallow areas (like tidal flats), as explained above. Furthermore, higher mud contents are observed in deeper areas. Therefore, the short wave scenario is in line with the classification hypothesis, relating relative forcing dominance to large-scale spatial sand-mud segregation patterns (section 2.4).

4.4 Tidal influence on mud transport within the tidal lagoon

The observations and analysis, made in sections 4.2 and 4.3, are based on the spatial mud (and sand) content in the top layer, which indicates the spatial distribution of sand and mud that can be observed, as it is comparable to a birds-eye view of the mud content (only the visible top layer). Since the underlayers also contributed to the total mud transport over time (along with the top layer), a sediment (mud) transport balance is set up, to quantify the total mud transports trough the tidal lagoon.

By introducing different cross-sections within the tidal lagoon, the accumulation of mud (using the total in- and output) in the sections between these cross-sections can be tracked over time, using the principles of an Euler Balance[19]. While an increase/decrease of tidal amplitude is mostly expected to have an effect in the North-Southern direction, the West-Eastern direction is also considered, as channels are mainly found in the centre of all these sections. Figure 4.16 graphically introduces the different sections in the tidal lagoon.
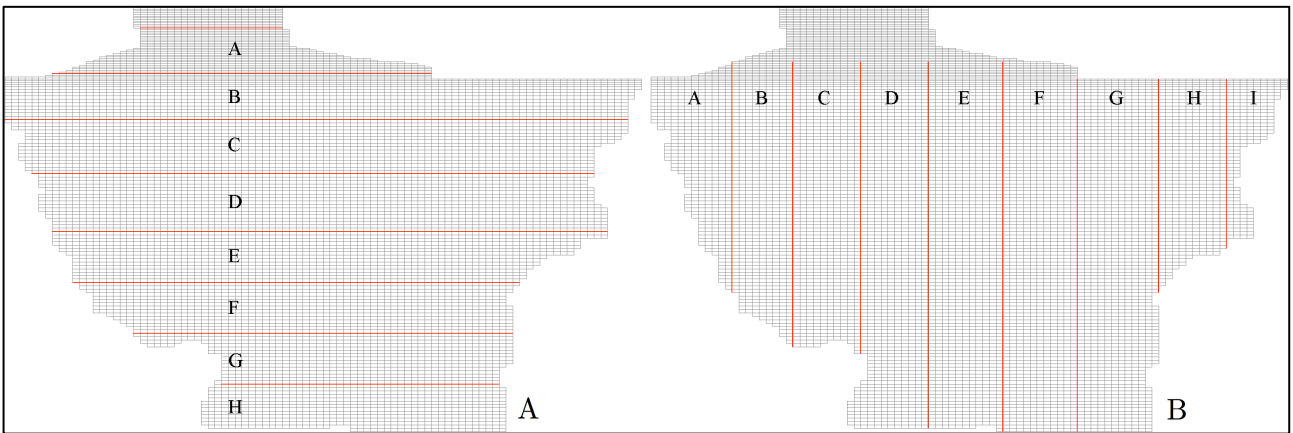
Figure 4.16: Sections, used for analysing mud transport trough the tidal lagoon using the principle of Euler balances, with (A) North to South sections A-H and (B) West to East sections A-I

Net mud imports, for the above sections (figure 4.16), are shown in figure 4.17, where figure 4.17-A indicates the North to South sections and figure 4.17-B the West to East sections. By dividing the net mud imports by the total section area, the average amount of mud import per unit area (m^2), for each section, is given. This step is essential for comparison, as each section is different is areal size (figure 4.16). In figure 4.17, the average amount of net mud import per section is given in kg/m^2. Qualitative observations (from section 4.2 and 4.3) can be further supported by this quantitative analysis.

First of all, looking at the reference scenario, mud is eroded from the northern area (mainly deep channels and hydrodynamically active areas), and deposited in the southern area (mainly tidal flats). Looking from west to east, the accumulation of fines is found near the western and eastern side of the basin (mainly tidal flats), while mud erosion is observed in the centre of the tidal lagoon (mainly channels and hydrodynamically active areas). These observations are also in line with the large-scale sand-mud segregation patters, described in section 2.1.4 and throughout this thesis, they also support results from the analysis of the reference scenario (section 4.2.2).

---

[19] An Euler balance is based on a static spatial reference frame in combination with mass balance within this reference frame, the mass balance for section i is based on the equation $Input^i - Output^i = Accumulation^i$, or in this mud-related case, the following equation: $m^i_{m,input} - m^i_{m,output} = \Delta m^i_m$ can be used, with m^i_m the total mud mass (gained), related to section i.
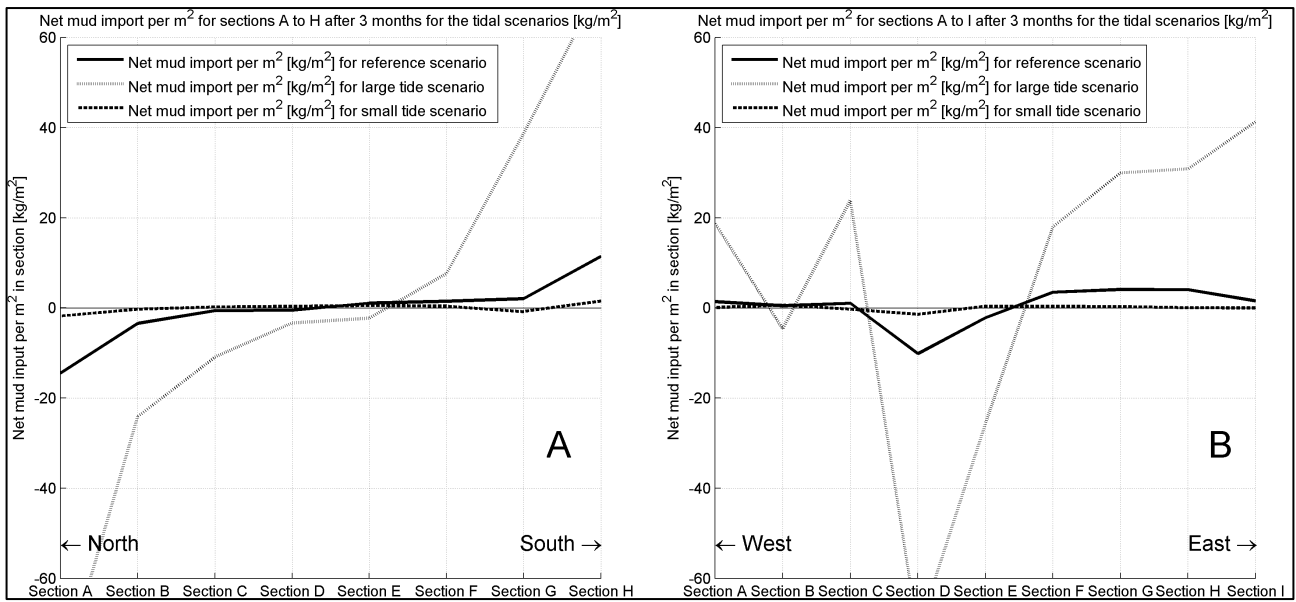
Figure 4.17: Average net mud import [kg/m^2] in tidal lagoon sections (as indicated in figure 4.15), with (A) indicating the North to South sections and (B) indicating the West to East sections for the different scenarios related to tide (reference, large- and small tide).

The high tide scenario behaves comparable to the reference situation in both directions, though, the transported values are almost an order larger. The same is valid for the small tide scenario, where values are almost an order smaller. It appears as if mud transport has a logarithmic relation with the tidal amplitude. Apart from just the relation, these results are also in line with observations made in section 4.3.1.

An interesting observation that could also be made from figure 4.17-A is the location of the transition between net import and -export of mud. This location (the intersection with the horizontal axis) is moving further into the tidal lagoon for higher tidal amplitudes and suggests smaller areas of higher mud content in the case of larger tidal dominance, as the area where mud gets eroded increases. This observation makes an important statement, as it shows how sharp transitions in mud content (as observed in previous research, e.g. Van Ledden *et al.* (2004b) and in sections 3.5.2, 4.2 and 4.3) could increase/decrease because of higher/smaller tidal dominance. The moving intersection in figure 4.17-A is (logically) related to the hydrodynamic activity, which reaches further into the tidal lagoon for higher tidal amplitudes[20].

---

[20] This statement could also be made inversely for waves, as an increase in hydrodynamic activity due to waves 'reaches out' (from the shallows) towards greater depths. The results from figure 4.15 also support this conclusion.

4.5 General classification of sand-mud segregation

Using the results from previous sections, the classification hypothesis from section 2.4 can be verified. This classification is based on mud availability and hydrodynamic activity in certain (deep or shallow) areas, in relation to different forcing conditions. To classify this, table 4.2 is constructed. In this table, the 'near bed hydrodynamic activity' is relating to bed shear stress, while the 'mud availability' is relating to mud concentrations and –content in the bed. This is (roughly) related to the overall depth where mud is found and to the forcing conditions (tide- or wave only).

	Tide only		Waves only	
	Near bed hydrodynamic activity	Mud availability	Near bed hydrodynamic activity	Mud availability
Shallow areas	−	+	+	−
Deep areas	+	−	−	+

Table 4.2: The area where mud is generally found, as a response to different forcing conditions, valid for typical tidal lagoon morphology

By using various conclusions from the previous sections, this classification can be expanded for all possible relative dominances of short waves and tidal currents (also mixed cases). Furthermore, typical hypsolaspy curves can be added to this classification as well. Table 4.3 introduces this classification with typical hypsolaspy curves and -properties, related to large-scale sand-mud segregation patterns, according to the conditions.
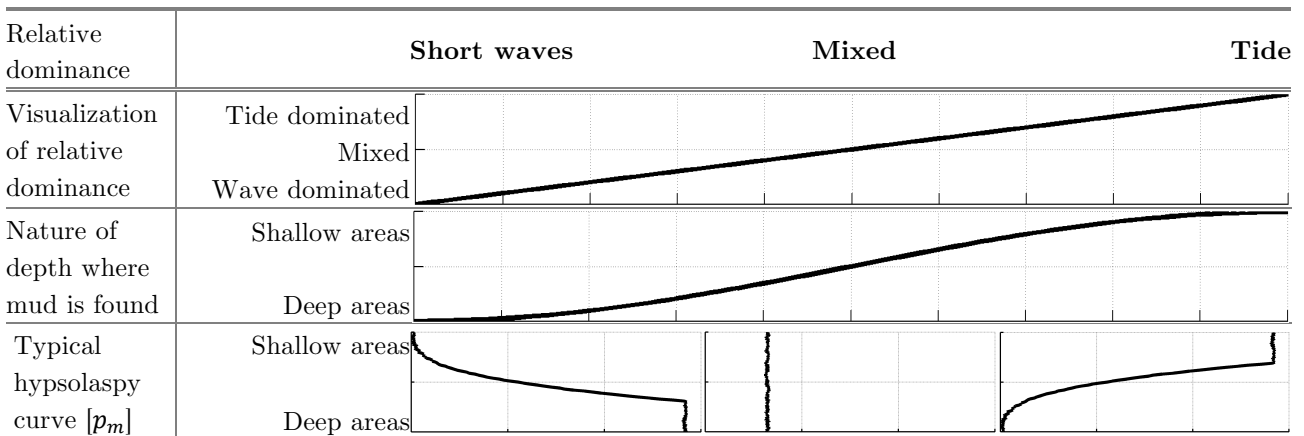
Table 4.3: Classification diagram, indicating highly schematized conclusions related to relative tidal- and short wave dominance

Considering table 4.3 and the classification by Davis & Hayes (1984) from figure 2.29, a suggestion for a general classification is made. Table 4.3 is mainly based on the relative contribution from short waves or tidal currents, where the classification from figure 2.29 is based on this as well. By consistently adding the conclusions from the above tables (4.2 and 4.3) to figure 2.29, figure 4.18 is constructed. This figure can be considered as a general classification for large-scale sand-mud segregation, given the relative forcing dominance. Therefore, this figure can be regarded as an answer to the final (5th) sub-question.
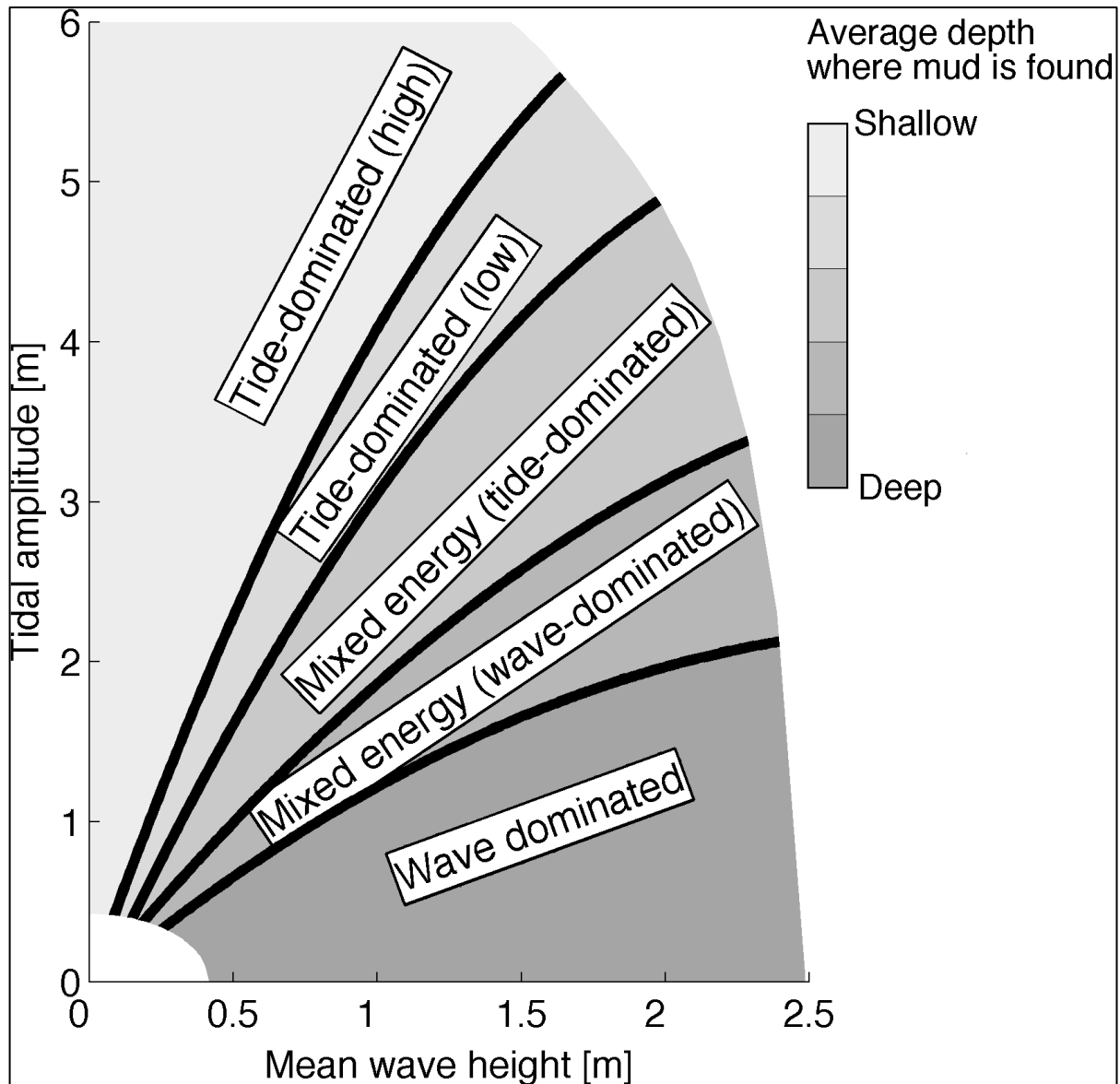
Figure 4.18: Sand-mud segregation classification, based on the relation between classification (based on relative dominance of tide or waves) and the average depth where mud is found (image inspired after the classification by Davis & Hayes (1984), modified from Hayes (1975; 1979))

This figure represents a few important conclusions, as previously stated throughout this chapter. The relative contribution of forcing is important, not the absolute value, as the results come from an interaction between the different forcing conditions. This is in line with the original classification from Davis & Hayes (1984). Furthermore, waves are responsible for transporting mud to deeper areas, while tidal currents commonly transport it towards the shallows.

4.6 Discussion

Assessing the large-scale sand-mud segregation patterns has appeared to be possible, as results from the reference scenario (section 4.2) are in line with the general sand-mud segregation description (section 2.1.4). Changing the forcing conditions to assess the hypothesis relating relative tide- or short wave dominance to sand-mud segregation was mainly aimed at changes in tide, since the original case study (Amelander tidal inlet system) is tidally dominated. While a short wave scenario is considered (which is wave dominated according to figure 2.29), which also supports the classification hypothesis (section 2.4), the case study does not perfectly reflect a wave-dominated system. Morphological features like tidal channels and tidal flats will not be found in wave-dominated systems like Mobile Bay (figure 2.28-A), while other typical ('wave-build') features could be found. One of these differences could be river runoff, when discharging into the basin; it can have mayor effects on the mud content. In total 6 rivers discharge in the Mobile Bay area[21]. This system difference can explain the higher mud contents that are observed in Mobile Bay by Nichols & Boon (1994). As mud import from tidal input is absent, it must come from somewhere else (like discharging rivers). Wind driven flow, turbulence and horizontal diffusion is then probably responsible for transporting stirred sediments (due to short wave energy dissipation) towards deeper areas.

Using the model by Dissanayake (2011), which is based on the morphological formation from a sand bed, this thesis research is initiated by adding mud to this morphology (which is based on sand simulations). According to Geleynse *et al.* (2011) mud has significant influence on the nature of the delta/channel formation. This would imply (apart from the differences in sand and sediment mixtures) another factor that is responsible for the system not being completely in equilibrium. This choice had to be made for computational reasons (section 3.4.1) and since the exact morphology is not needed to assess large-scale sand-mud segregation patterns, it can be justified (though further research could be aimed at this problem).

Section 3.4.1 describes how morphological updating would result in longer computational times and (most of all) harder comparison between the different scenarios. The hypsolaspy curves in section 4.2 and 4.3 are a good example of this statement. Knowing that morphological changes affect the depth distribution (hypsometry) in the system, these curves could not be related to each other for different scenarios (as it results in an inconsistent vertical axis). With that statement made, it becomes evident how important no morphological updating is within this research, as it makes comparison between the different scenarios possible and meaningful.

The classification from figure 4.18 is relevant for the overall (average) conditions in a system. Note that extreme conditions (most likely waves, as tides are quite 'static' in their properties) can significantly change these patterns, something to bear in mind when relating the classification to cases in the field.

While the final classification from figure 4.18 (as hypothesised in section 2.4) could have been constructed using theory (section 2.2 and 2.3) and observations (section 2.1.4 and figure 2.28), the verification, using a process-based morphodynamic model, is an addition in the verification of this classification.

---

[21] Mobile River is (by far) the most significant here, discharging an area of approximately 115.000 km², which includes almost the entire inner part of the state Alabama, US. It is famous for its mud supply, as the name of adjoining lakes, like 'Lake Negro', also suggest.

Chapter 5

Conclusions & Recommendations

By again highlighting the research questions, the objective of this thesis becomes clear. Therefore, the main research question and associated sub-questions are reprinted from section 1.3.

The main research question: *"What are the relative influences of tide and (short) waves on the large-scale sand-mud segregation patterns and spatial sand-mud distribution in a tidal inlet system?"* featured the following sub-questions:

- How can the large-scale sand-mud segregation patterns and spatial distribution in a tidal inlet system (like one in the Dutch Wadden Sea) generally be described?
- What are (presently) the governing equations regarding the erosional behaviour of sand-mud mixtures (which are used in the chosen model)?
- To what extend do the results from a schematized model (dis)agree with the general description of large-scale sand-mud segregation patterns and spatial distribution, as described with the assessment of sub-question one?
- How are sand-mud segregation patterns responding to different forcing, using different combinations of waves and currents in a number of model cases? Can these responses be explained qualitatively, using physical properties, -processes and –mechanisms?
- Is it possible to develop a general classification related to relative dominance of different forcing (like short waves or tide), regarding the results from sub-question four?

Considering these sub-questions, it becomes evident how the main research question is fully answered when all sub-questions are addressed. Therefore, the final conclusions (section 5.1) will be given for each sub-question. In total, this can be considered as a complete set of answers to both main- and sub-questions.

Section 5.2 will conclude this thesis with recommendations regarding related- and further research.

5.1 Conclusions

This section is dedicated to answering each sub-question, from which final conclusions can be drawn.

Sub-question 1:   How can the large-scale sand-mud segregation patterns and spatial distribution in a tidal inlet system (like one in the Dutch Wadden Sea) generally be described?

A description of the large-scale sand-mud segregation patterns and spatial distribution in a tidal inlet system (which is, by definition, tidally dominated) is based on both observations in the field and from a more theoretical and physical perspective. The latter is related to general formulations for (fine) sediment transport, overall tidal inlet system geometry and the tidal dominance (forcing). From both approaches, tidal basins reveal common large-scale patterns regarding sand-mud segregation and spatial distribution. Due to the tidal dominance and -asymmetry, mud is transported further into the system, where shallow areas are commonly found. Since hydrodynamic activity also decreases further into the system (due to the increase in system width), mud is able to settle in these areas. Furthermore, higher bed shear stresses are found in deeper areas (due to tidal currents), these result in sandy tidal channels and inlets. Although short waves are not dominating in tidal inlet systems, their influence is found in the shallows, as short wave energy dissipation is responsible for (re)suspension of fine sediment. Though, it appears that tidal dominance diminishes the relative effect of waves on the spatial sand-mud distribution in tidal inlet systems.

Sub-question 2:   What are (presently) the governing equations regarding the erosional behaviour of sand-mud mixtures (which are used in the chosen model)?

This sub-question is mainly aimed at understanding the model description of physical processes. The sand-mud mixture version of Delft3D (used within this thesis) is mainly based on erosion formulations and associated concept (using cohesive and non-cohesive mixtures, defined using $p_{m,cr}$) by Van Ledden (2003). These formulations describe how the bed shear stress for erosion is enhanced due to the mud content (p_m) in the bed, which is also used to determine whether a mixture is considered cohesive or non-cohesive. Furthermore, deposition is based on the instantaneous mud concentration (c_m) and settling velocity (w_m). Finally, concepts like the fluff layer and bed layer mixing are introduced in this model as well. These concepts represent various physical processes that are observed in the field. Although these formulations and concepts are well supported by various researches, the various parameters still indicate the pragmatic approach for the encountered problems. Combined with the initial problems regarding practical 3D applications/reproduction, further research and development for the sand-mud modelling concept is advised. Regarding the hydrodynamics, the sand-mud mixture version of Delft3D uses concepts and formulations from the regular Delft3D version.

Sub-question 3:   To what extend do the results from a schematized model (dis)agree with the general description of large-scale sand-mud segregation patterns and spatial distribution, as described with the assessment of sub-question one?

By considering the model results from the reference scenario, and comparing it to the description from sub-question 1, the relation between the model and observations can be assessed. The agreement between the model and the description of large-scale sand-mud segregation patterns (based on observations and physical theories) can be considered as good. Not only does the model reproduce the large-scale patterns, the values of various variables agree with values found in the field (like concentrations of dissolved fine sediment), although some slight overestimations are found. In this agreement, the analysis of the model results is of paramount importance, as relations between different variables get visualized. This analysis shows the relations between bed shear stress, bottom depth, mud content and concentrations, while the description of large-scale sand-mud segregation patterns is also based on such relations. In the case of a tidally dominated

system (like the reference scenario) high shear stresses are only found in deeper areas, whereas high mud concentrations (mud supply) are mainly found in shallow areas. Furthermore, (also because of the previous relations) higher mud contents are found in shallow areas as well, where less hydrodynamic activity is found. These observed relations agree well with theory, as described for sub-question 1. Some observed model problems are related to 'mud-capturing', it appears that areas entering the cohesive regime capture mud and continue to do so as long as mud is available (and hydrodynamic activity allows net deposition). This results in patches with mud contents near 1 (or 100%), while in reality this value is probably limited. The continuous boundary conditions are probably responsible for this problem (as accumulating areas keep accumulating over time). Using morphological updating could also resolve this problem, though, this is yet to be investigated.

Sub-question 4:   How are sand-mud segregation patterns responding to different forcing, using different combinations of waves and currents in a number of model cases? Can these responses be explained qualitatively, using physical properties, -processes and –mechanisms?

The response of the model to different forcing is as expected from the large-scale sand-mud segregation pattern description and associated classification hypothesis. According to this hypothesis, the influence of dominance from tidal currents and short waves is of paramount importance to the spatial distribution of sand and mud. According to it, tidal currents transport mud to shallow areas, far from hydrodynamic activity, while short waves 'transport' mud to deeper areas, where short wave energy dissipation is practically absent. The results from the tidally dominated model show deposition of mud in shallow areas (tidal flats), while an increase/decrease in tidal dominance results in increasing/decreasing mud deposition in these shallow areas. Furthermore, an increase in tidal dominance results in mud deposition in smaller areas (near the margins) as the deposition area for mud decreases. Finally, tidal currents (and tidal asymmetry) are also responsible for horizontal transport towards hydrodynamically less active areas (commonly shallow in tidal inlet systems), due to both lag effects and tidal asymmetry itself (enhancing lag effects). Unfortunately, these horizontal transport processes are hard to analyse, but support model observations. On the other hand, short wave dominance is responsible for mud deposition in deeper areas (like channels), according to the model. This statements can also be verified by analysing the (short wave scenario) model results. When relating these results to physics, the interaction between bed shear stress (hydrodynamic activity), (relative) forcing and mud availability is important. The hydrodynamic activity is depending on morphology as well, which is based on the case of a tidal lagoon within this thesis.

Sub-question 5:   Is it possible to develop a general classification related to relative dominance of different forcing (like short waves or tide), regarding the results from sub-question four?

Looking at the description of large-scale sand-mud segregation (sub-question 1) and model results (sub-question 4), a classification can indeed be set up. For which a hypothesis was supplied within this thesis. This classification can be based on relative dominance of short waves and the tide. The classification describes how tide/wave dominated systems are governed with mud in shallow/deep areas, respectively. An important aspect for this classification is the availability of mud, because these characteristics cannot develop if mud particles are absent.

5.2 Recommendations

Within this thesis, the relative dominance of (short) waves and tide is used to classify and qualitatively assess the large-scale sand-mud segregation patterns and spatial distribution, using a case study. Since the case study considers a tide-dominated system (in reality), the scenario in which the forcing is changed to represent wave dominance can be considered as 'artificial'. To further elaborate on the (short) wave-dominated system it is recommended to consider a system that is dominated by waves in reality. This advice is related to the morphological characteristics, which are found in a wave-dominated system (as these are different from a tide-dominated system (this is not taken into account in this thesis for the sake of brevity and consistency)).

The presence of mud is an important variable in the development of morphological features in a morphodynamic system (Geleynse *et al.*, 2011). It is advised to assess the sand-mud segregation patterns on a morphological timescale; the focus of this research should also be on the practical aspects while using the morphological factor (N) and the influence on the results (related to sand-mud modelling).

Within the formulations for sediment transport (erosion) of sand-mud mixtures, various parameters are used. It is recommended to further develop these formulations. This development is found within a further understanding of the various parameters and what they represent, but also minimizing the usage of parameters is (always) advised, as the link to physical processes is often hard to identify. Therefore, further development of the concepts that are used is also recommended.

The fluff layer is an interesting addition to the sand-mud mixture version of Delft3D, as it is a proposition to describe physical processes like consolidation lag. It is recommended to further assess the occurrence of a fluff layer (in the field) and its relations, for instance using measurements/experiments. Possibly, relations between physical conditions and fluff layer parameters can be found (for instance the percentage of consolidating mud over time, given a shear stress and/or various mixture properties).

During the execution of the model scenarios, mud ripples and chessboard patterns in mud content are observed on the grid for the outer (ebb-tidal) delta. Although this area is out of the area of interest for this thesis (we mainly consider the tidal lagoon itself and use the North Sea for consistent hydrodynamics), it could pose problems during applications of the sand-mud mixture version of Delft3D in the future. These patterns probably indicate numerical issues/instabilities, possibly in relation to hydrodynamic activities. It is recommended to further investigate and assess these observations to find a solution or to state criteria in which these problems could appear.

Although some scenarios were considered within this thesis, some interesting additional scenarios can be thought of. First, the influence of different tidal asymmetry could be considered, as it is very important for the overall mud transport (in theory). Furthermore, the influence of (relative) sea level rise could be an interesting addition for this research, but also variations in tidal lagoon geometry could be considered.

In the beginning of this thesis, some environmental aspects regarding the sand-mud distribution (e.g. potential pollution and flora & fauna) were given (in section 1.1). To assess these topics, cooperation with ecologists is indispensible. With this cooperation, the consequences for these environmental topics can be defined and quantified, according to the results from (amongst others) this thesis.

References

Ahmad, M.F., Dong, P., Mamat, M., Wan Nik, W.B., & Mohd, M.H. (2011). "The Critical Shear Stresses for Sand and Mud Mixture." Springer, *Applied Mathematical Sciences, Vol. 5, no. 2.*, pp. 53-71.

Airy, G.B. (1845). "Tides and Waves." London Scientific department, *Encyclopaedia Metropolitana, Mixed Sciences, Vol. 3.*, pp. 241-396.

Bake, D. de, (2000). *Zand-slibsegregatie in de Westerschelde* (in Dutch). Repository Delft University of Technology, 116 pp.

Bosboom, J. & Stive, M.J.F. (2011). *Coastal Dynamics I - Lecture notes CT4305.* Version 0.2, VSSD Delft, 567 pp.

Carter, R.W.G. (1988). *Coastal environments: An introduction of physical, ecological and cultural systems of coastlines.* Academic Press, 619 pp.

Chesher, T.J., & Ockenden, M.C. (1997). "Numerical modelling of mud and sand mixtures." John Wiley & Sons Ltd. *Cohesive sediments, Proceedings of the 4th Nearshore and Estuarine Cohesive Sediment Transport Conference.* pp. 367-381.

Cleveringa, J., Israël, C.G. & Dunsbergen, D.W. (2005). *De westkust van Ameland. Resultaten van 10 jaar morfologisch onderzoek in het kader van de Rijkswaterstaat programma's KUST2000 en KUST2005.* RIKZ, rapport RIKZ/2005.029, 74 pp.

Cleveringa, J., & Oost, A.P. (1999). "The fractal geometry of tidal-channel systems in the Dutch Wadden Sea." Kluwer Academic Publishers, *Geologie en Mijnbouw 78.* pp. 21-30.

Dalrymple, D.W. (1992). "Tidal depositional systems." Geological Association of Canada, *Facies Models Response to Sea Level Changes*, pp. 195-218.

Dastgheib, A., Roelvink, J.A., & Wang, Z.B. (2008). "Long-term process based morphological modelling of the Marsdiep Tidal Basin." Elsevier, *Marine Geology 256*, pp. 90-100.

Davis, R.A., & Hayes, M.O. (1984). "What is a wave-dominated coast?" Elsevier, *Marine Geology, Vol. 60*, pp. 313-329.

Deltares. (2011a). *Delft3D-FLOW, Simulation of multi-dimensional hydrodynamic flows and transport phenomena, including sediments, User Manual.* Version 3.15, 674 pp.

Deltares. (2011b). *Delft3D-WAVE, Simulation of short-crested waves with SWAN, User Manual.* Version 3.04, 204 pp.

Dissanayake, D.M.P.K., Ranasinghe, R., & Roelvink, J.A. (2009a). "Effect of Sea Level Rise in tidal inlet evolution: a numerical modelling approach." CERF, *Journal of Coastal Research, Sprecial Issue 56.*

Dissanayake, D.M.P.K., Roelvink, J.A., & Wegen, M. van der, (2009b). "Modelled channel patterns in a schematized tidal inlet." Elsevier, *Coastal Engineering 56*, pp. 1069-1083.

Dissanayake, D.M.P.K. (2011). *Modelling Morphological Response of Large Tidal Inlet Systems to Sea Level Rise.* CRC Press/Balkema, Leiden, 178 pp.

Dongeren, A.R. van, de Vriend, H.J. (1994). "A model on morphological behaviour of tidal basins." Elsevier, *Coastal Engineering 22.* pp. 287-310.

Duren, L. van, Winterwerp, J.C., Van Prooijen, B.C., Ridderinkhof, H., Oost, A. (2011). *Clear as Mud: Understanding fine sediment dynamics in the Wadden Sea – Action Plan (Draft Version)*, 55 pp

Elias, E. (2006). *Morphodynamics of Texel Inlet.* PhD thesis, IOS Press, Delft University Press, Repository Delft University of Technology. 280 pp.

Elias, E., Koningsveld, M. van, Tonnon, P.K., & Wang, Z.B. (2007). *Sediment budget analysis and testing hypotheses for the Dutch coastal system.* Deltares Public, VOP II-1.2 Long term coastal management & DC05.20 North Sea and Coast, 145 pp.

Escoffier, F.F. (1940). "The Stability of Tidal Inlets", ASBPA, *Shore and Beach, Vol. 8, No. 4,* pp. 114-115.

Eysink, W.D. (1993). *Impact of sea level rise on the morphology of the Wadden Sea in the scope of its ecological function. General considerations on hydraulic conditions, sediment transports, sand balance, bed composition and impact of sea level rise on tidal flats.* Delft Hydraulics. 35 pp.

Flemming, B.W., & Bartholomä, A. (1997). "Response of the Wadden Sea to a Rising Sea Level: a Predictive Empirical Model." Springer, *Ocean Dynamics, Vol. 49, no. 2-3*, pp. 343-353.

Flemming, B.W., & Ziegler, K. (1995). "High resolution grain size distribution patterns and textual trends in the backbarrier environment of Spiekeroog Island (Southern North Sea)." *Seckenbergianna Maritima, 26*, pp. 1-24.

Fockert, A. de, (2008). *Impact of relative sea level rise on the Amelander inlet morphology.* Repository Delft University of Technology, 203 pp.

Förstner, U., & Wittman, G.T.W. (1979). "Metal Pollution in the Aquatic Environment." Springer Verslag. 486 pp.

Geleynse, N., Storms, J.E.A., Walstra, D.J.R., Jagers, H.R.A., Wang, Z.B., & Stive, M.J.F. (2011). "Controls on river delta formation; insights from numerical modelling." Elsevier, *Earth and Planetary Science Letters 302.* pp. 217-226.

George, D.A., Hill, P.S., & Milligan, T.G. (2007). "Flocculation, heavy metals (Cu, Pb, Zn) and the sand-mud transition on the Adriatic continental shelf, Italy." Elsevier, *Continental Shelf Research 27,* pp. 275-488.

Glopper, R. de, (1967). Over de bodemgesteldheid van het Waddengebied (in Dutch). Tjeenk Willink, *Van Zee tot Land, no. 43.*

Groen, P. (1967). "On the residual transport of suspended matter by an alternating tidal current", *Netherlands Journal of Sea Research 3, 4.* pp. 564-574.

Hayes, M.O. (1975). "Morphology of sand accumulation in estuaries: an introduction to the symposium." Academic press, New York, *Estuarine research II.* pp. 3-22.

Hayes, M.O. (1979). "Barrier island morphology as a function of tidal and wave regime." Academic Press, New York, *Barrier Islands.* pp. 1-27.

Hayes, M.O. (1980). "General morphology and sediment patterns in tidal inlets." Elsevier, *Sedimentary Geology 26.* pp. 139-156.

Hibma, A. (2004). *Morphodynamic modelling of estuarine channel-shoal systems.* PhD thesis, Repository Delft University of Technology. 143 pp.

Holthuijsen, L.H. (2007). *Waves in Oceanic and Coastal Waters.* Cambridge University Press. 387 pp.

Interwad, (2008). *Waddenzee: Watlas.* [online] available at http://www.waddenzee.nl/ Watlas.27.0.html [accessed 3 October 2011].

Jacobs, W. (2011). *Sand-mud erosion from a soil mechanical perspective.* PhD thesis, Repository Delft University of Technology. 255 pp.

Jacobs, W., Le Hir, P., Kesteren, W. van, & Cann, P. (2011). "Erosion threshold of sand-mud mixtures." Elsevier, *Continetal Shelf Research 31*, pp. 14-25.

Kessel, T. van, (1997). *Generation and transport of subaqueous mud layers.* PhD thesis, Repository Delft University of Technology, 150 pp.

Kessel, T. van, Vanlede, J., & Kok, J. de. (2011). "Development of a mud transport model for the Scheldt estuary." Elsevier, *Continental Shelf Research 31.* pp. 165-181.

Kessel, T. van, Winterwerp, J.C., Van Prooijen, B.C., Van Ledden, M., & Borst, W. (2011). "Modelling of the seasonal dynamics of SPM with a simple algorithm for the buffering of fines in a sandy seabed." Elsevier, *Continental Shelf Research 31*, pp. 124-134.

Kvale, E.P. (2008). *Tidalites.* AccessScience, [online] available at http://accessscience.com/content/Tidalites/696800, [accessed 21 September 2011].

Le Hir, P., Cann, P., Waeles, B., Jestin, H., & Bassoullet, P. (2008). "Erodibility of natural sediments: experiments on sand/mud mixtures from laboratory and field erosion tests." Elservier, *Proceedings in Marine Science, Vol. 9*, pp. 137-153.

Le Hir, P., Cayocca, F., & Waeles, B. (2011). "Dynamics of sand and mud mixtures: A multiprocess-based modelling strategy." Elsevier, *Continental Shelf Research 31*, pp. 135-149.

Ledden, M. van, (1998). *Zand-slibsegregatie, modelleren van zand-slibstructuren in de Nieuwe Merwede* (in Dutch). Repository Delft University of Technology, 203 pp.

Ledden, M. van, (2003). *Sand-mud segregation in estuaries and tidal basins.* PhD thesis, Repository Delft University of Technology. Also: Communications on Hydraulic and Geotechnical Engineering, ISSN 0169-6548, No. 03-2, Faculty of Civil Engineering and Geosciences, Delft, The Netherlands. 248 pp.

Ledden, M. van, Kesteren, W.G.M. van, & Winterwerp, J.C. (2004a). "A conceptual framework for the erosion behaviour of sand-mud mixtures." Elsevier, *Continental Shelf Research 24*, pp. 1-11.

Ledden, M. van, Wang, Z.B., Winterwerp, J.C. & Vriend, H. de, (2004b). "Sand-mud morphodynamics in a short tidal basin." Springer, *Ocean Dynamics, Vol. 54*, pp. 385-391.

Ledden, M. van, Wang, Z.B., Winterwerp, H. & De Vriend, H. (2006). "Modelling sand-mud morphodynamics in the Friesche Zeegat." Springer, *Ocean Dynamics 56.* pp. 248-265.

Liu, X.J., Gao, S., & Wang, Y.P. (2011). "Modelling profile shape evolution for accreting tidal flats composed of mud and sand: A case study of the central Jiangsu coast, China." doi: 10.1016/j.csr.2011.08.002. Elsevier, *Continental Shelf Research.* 11 pp.

Louters, T., & Gerritsen, F. (1994). *The Riddle of the Sands. A Tidal System's Answer to a Rising Sea Level.* Rijkswaterstaat RIKZ, Report RIKZ-94.040, 70 pp.

Marciano, R., Wang, Z.B., Hibma, A., Vriend, H. de, & Defina, A. (2005). "Modelling of channel patterns in short tidal basins." doi: 10.1029/2003JF000092. American Geophysical Union, *Journal of Geophysical Research, Vol. 110*, F01001. 13 pp.

Mitchener, H., & Torfs, H. (1996). "Erosion of mud/sand mixtures." Elsevier, *Coastal Engineering 29*, pp. 1-25.

Montserrat, F., Colen, C. van, Provoost, P., Milla, M., Ponti, M., Meersche, K. van den, Ysebaert, T., & Herman, P.M.J. (2009). "Sediment segregation by biodiffusing bivalves." Elsevier, *Estuarine, Coastal and Shelf Science 83*, pp. 379-391.

Nichols, M., & Boon, J.D. (1994). "Sediment Transport Processes in Coastal Lagoons". Elsevier, *Oceanography Series, Vol. 60*, pp. 157-219.

Nieuwenhuis, O. (2001). *Sand-mud distribution in the Amelander Inlet.* Repository Delft University of Technology, 147 pp.

Oost, A.P. (1995). *Dynamics and sedimentary development of the Dutch Wadden Sea with emphasis on the Frisian Inlet. A study of the barrier islands, ebb-tidal deltas, inlets and drainage basins.* PhD thesis, University of Utrecht, 455 pp.

Orvain, F., Le Hir, P., & Sauriau, P.G. (2003). "A model of fluff layer erosion and subsequent bed erosion in the presence of the bioturbator, Hydrobia ulvae." Yale University, *Journal of Marine Research 61.* pp 823-851.

Partheniades, E. (1965). Erosion and Deposition of Cohesive Soils. *ASCE, Journal of the Hydraulics Division, Vol. 91, no. HY 1*, pp. 105-139.

Postma, H. (1954). *Hydrography of the Dutch Wadden Sea.* PhD thesis, Archives Néerlandaises de Zoologie, Tome X, 4e Livraison, 1954. 106 pp.

Postma, H. (1961). "Transport and accumulation of suspended matter in the Dutch Wadden Sea." Netherlands Institute for Sea Research. *Netherlands Journal of Sea Research, 1/2.* pp. 148-190.

Postma, H. (1981). "Exchange of materials between the North Sea and the Wadden Sea." Elsevier Scientific Publishing Company, *Marine Geology 40.* pp. 199-213.

Prooijen, B.C., & Winterwerp, J.C. (2010). "A stochastic formulation for erosion of cohesive sediments." American Geophysical Union, *Journal of Geophysical Research, Vol. 115*, C01005. 15 pp.

Raudkivi, A.J. (1990). *Loose Boundary hydraulics.* Pergamon Oxford. 496 pp.

Reid, G.K., & Wood, R.D. (1976). *Ecology of inland water and estuaries.* Van Nostrand Company. 378 pp.

Rijkswaterstaat. (1997). *Project Strobodi, Meting Bornrif/Borndiep 1996.* Rijkswaterstaat, 89 pp.

Rijn, L.C. van, (1993). *Principles of sediment transport in rivers, estuaries and coastal seas.* Aqua Publications, 690 pp.

Rijn, L.C. van, (2000). *Not yet known.*

Rijn, L.C. van, (2001). *Not yet known.*

Rijn, L.C. van, Walstra, D., Grasmeijer, B., Sutherland, J., Pan, S., & Sierra, J. (2003). "The predictability of cross-shore bed evolution of sandy beaches at the time scale of storms and seasons using process-based profile models". Elsevier, *Coastal Engineering, Vol 47,* pp. 295-327.

RIKZ. (1998). *Sedimentatlas Waddenzee.* Rijksinstituut voor Kust en Zee, digital download.

Roudkivi, A.J. (1990). *Loose Boundary Hydraulics (3th edition).* Pergamon Press, 538 pp.

Sandford, L. (2008). "Modeling a dynamically varying mixed sediment bed with erosion, deposition, bioturbation, consolidation and armouring." *Computers and Geosciences 34.* pp. 1263-1283.

Shields, A. (1936). "Application of similarity principles and turbulence research to bed-load movement." *Mitteilungen der Preußischen Versuchsanstalt für Wasserbau und Schiffbau*, 45 pp.

Speelman, H., Oost, A., Verweij, H., & Wang, Z.B. (2009). *De ontwikkeling van het waddengebied in tijd en ruimte - position paper geowetenschap* (In dutch). Koningklijke Nederlanse Akademie van Wetenschappen, Waddenacademie, 104 pp.

Spek, A.J.F. van der, (1994). *Large-scale evolution of Holocene tidal basins in the Netherlands.* University Utrecht, 159 pp.

Steward, R.H. (2008). *Introduction To Physical Oceanography*. Texas A & M University, Department of Oceanography, 354 pp.

Straaten, L.M.J.U. van, & Kuenen, P.H. (1957). "Accumulation of fine grained sediments in the Dutch Wadden Sea." Lingua Terrae, *Geologie en Mijnbouw 19*, pp. 329-354.

Torfs, H. (1995). *Erosion of mud/sand mixtures*. PhD thesis, Catholic University of Leuven, 223 pp.

Torfs, H., Mitchener, H., Huysentruyt, H., Toorman, E. (1996). "Settling and consolidation of mud/sand mixtures." Elsevier, *Coastal Engineering 29*, pp. 27-45.

Veen, J. van, (1950). "Eb en vloedschaar systemen in de Nederlandse getijwateren." (in Dutch). KNAG, *Journal of the Royal Dutch Geographical Society, Vol. 67*, pp. 303-325.

Venema, L.B., Groen, P., De Meijer, R.J., Van Os, B., Gieske, J.M.J., & Van Wijngaarden, M.J. (1999). *Radiometric Survey of 'Hollandsch Diep' Part II: Mud-sand mapping*. (Prepared for: National Institute for Inland Water Management and Waste Water Treatment RIZA-30284/WST No. Z-78). Groningen: Nuclear Geophysics Division.

Vriend, H.J. de, Bakker, W.T., Bilse, D.P. (1994). "A morphological behaviour model for the outer delta of mixed-energy tidal inlets." Elservier, *Coastal Engineering 23*. pp. 205-327.

Vroom, J. (2011). *Tidal divides, a study on a simplified case and the Dutch Wadden Sea*. M.Sc. thesis, Repository Delft University of Technology. 127 pp.

Waeles, B., Le Hir, P., Lesueur, P., & Delsinne, N. (2007). "Modelling sand/mud transport and morphodynamics in the Seine river mouth (France): an attempt using a process-based approach." Springer, *Hydrobiologia, Vol. 588, no. 1*, pp. 69-82.

Waeles, B., Le Hir, P., & Lesueur, P. (2008). "A 3D morphodynamic process-based modelling of a mixed sand/mud coastal environment: the Seine estuary, France." Elsevier, *Marine Science 9*. pp. 477-498.

Wang, Z.B., Jeuken, C., de Vriend, H.J., Crosato, A., & Stive, M.J.F. (1999). *Tidal asymmetry and residual sediment transport in estuaries*. Delft Hydraulics Report, Z2749 66 pp.

Whitehouse, R., Soulsby, R., Roberts, W., & Mitchener, H. (2000). *Dynamics of estuarine muds*. Thomas Telford, London. 210 pp.

Winterwerp, J.C. (1999). *On the dynamics of high-concentrated mud suspensions*. PhD thesis, Repository Delft University of Technology. 204 p.

WL|Delft Hydraulics. (2008). *A tool for mud flat classification*. WL|Delft Hydraulics. (Prepared for: European Commission, MAST3 Programme No. Z2037.50).

Yu, Q., Wang, Y., Flemming, B.W., & Gao, S. (2011). "Modelling the equilibrium hypsometry of back-barrier tidal flats in the German Wadden Sea (southern North Sea)." doi: 10.1016/j.csr.2011.05.011. Elsevier, *Continental Shelf Research*. 10 pp.

Zwarts, L., Dubbeldam, W., Heuvel, H. Van Den, Laar, E. Van De, Menke, U., Hazelhoff, L., & Smit, C.J. (2004). *Bodemgesteldheid en machanische kokkelvisserij in de Waddenzee* (in Dutch). RIZA, Rapport RIZA/2004.028. 129 pp.

Publications

Scheel, F., van Ledden, M., van Prooijen, B.C., & Stive, M.J.F. (2012). "Simulating the large-scale spatial sand-mud distribution in a schematized process-based tidal inlet system model". doi: 10.3990/2.196. University of Twente, *NCK-days 2012: Crossing borders in coastal research*. pp. 191-195.

List of Figures

List of Tables

List of Symbols

SI-unit Symbols

l	Length	[m^1]
m	Mass	[kg^1]
t	Time	[s^1]

Roman Symbols

A	Cross sectional area	[m^2]
A_s	Cross sectional area associated with the tide	[m^2]
a	Reference height	[m^1]
B_0	Burial coefficient 1 in equation 3.18	[kg^{1}m^{-2}s^{-1}]
B_1	Burial coefficient 2 in equation 3.18	[s^{-1}]
b	Width	[m^1]
b_s	Width associated with the tide	[m^1]
C	Chézy-coefficient ($C = \sqrt{g/c_f}$)	[m$^{1/2}$s^{-1}]
C	Current related concentration of sand	[kg^{1}m^{-3}]
C_d	Wind drag coefficient	[-]
C_s	Shields 'constant'	[-]
c	Concentration of sediment	[kg^{1}m^{-3}]
$\tilde{c}$	Wave related concentration of sand	[kg^{1}m^{-3}]
c_0	Wave phase speed/celerity	[m^{1}s^{-1}]
c_a	Reference concentration for sand	[kg^{1}m^{-3}]
c_f	Friction coefficient ($c_f = g/C^2 = u_*^2/u^2$)	[-]
c_m	Mud concentration	[kg^{1}m^{-3}]
$c_{m,0}$	Initial mud concentration	[kg^{1}m^{-3}]
c_s	Sand concentration	[kg^{1}m^{-3}]
c_x	Wave propagation velocity in x-space	[m^{1}s^{-1}]
c_y	Wave propagation velocity in y-space	[m^{1}s^{-1}]
c_θ	Wave propagation velocity in θ-space	[m^{1}s^{-1}]
c_σ	Wave propagation velocity in σ-space	[m^{1}s^{-1}]
D_b	Deposition flux of mud into the bed layer(s)	[kg^{1}m^{-2}s^{-1}]
D_f	Deposition flux of mud into the fluff layer	[kg^{1}m^{-2}s^{-1}]
D_m	Deposition flux of mud	[m^{1}s^{-1}]
D_s	Deposition flux of sand	[m^{1}s^{-1}]
d_*	Dimensionless grain size; $d_* = d_{50}\{(s-1)g/v^2\}^{1/3}$	[-]
d	Grain size	[m^1]
d_{50}	Median grain size	[m^1]
d_n	Grain size of which n % is smaller ($0 \leq n \leq 100$, generally used with $n \in \mathbb{N}$)	[m^1]
E	Energy density spectrum (unit in 1D)	[kg^{1}s^{-1}]
E_b	Erosion flux of mud from the bed layer(s) into the water column	[kg^{1}m^{-2}s^{-1}]
E_f	Erosion flux of mud from the fluff layer into the water column	[kg^{1}m^{-2}s^{-1}]

E_m	Erosion flux of mud	[m^{1}s^{-1}]
E_s	Erosion flux of sand	[m^{1}s^{-1}]
E_t	Total erosion flux	[m^{1}s^{-1}]
e_d	Deposition efficiency	[-]
F	Force [Newton]	[kg^{1}m^{1}s^{-2}]
F_D	Drag force	[kg^{1}m^{1}s^{-2}]
F_G	Gravitational force	[kg^{1}m^{1}s^{-2}]
$F_{k+\frac{1}{2},l}$	Diffusive flux of sediment fraction l between layer k and $k+1$	[kg^{1}s^{-1}]
F_m	Net mud flux from the bed in the water column	[m^{1}s^{-1}]
F_s	Net sand flux from the bed in the water column	[m^{1}s^{-1}]
F_x	External force in x-direction	[kg^{1}m^{1}s^{-2}]
F_y	External force in y-direction	[kg^{1}m^{1}s^{-2}]
f	Coriolis parameter	[s^{-1}]
f	Frequency	[s^{-1}]
f_{SUSW}	User defined tuning parameter	[-]
g	Gravitational acceleration on earth ($g \approx 9{,}81$ m/s^2)	[m^{1}s^{-2}]
H	Wave height	[m^1]
H	Energy/total head in Bernoulli's law	[m^1]
H	Heaviside function ($H(f(x)) = 1$ if $f(x) \geq 0$, otherwise $H(f(x)) = 0$) in eq. 2.25	[-]
H_s	Significant wave height ($H_s = H_{1/3} = \frac{1}{N/3}\sum_{j=1}^{N/3} H_j \approx 4\sqrt{m_0}$)	[m^1]
h	Instantaneous (total) water depth ($h = h_0 + \eta$)	[m^1]
h	Piezometric/hydraulic head	[m^1]
h_0	Average and/or initial water depth (depending on the situation considered)	[m^1]
$K_{k+\frac{1}{2}}$	Diffusion coefficient at the interface between layer k and $k+1$	[m^{2}s^{-1}]
k	Wave number	[m^{-1}]
k	Layer number in stratigraphy in numerical calculations	[-]
L	System length; Wave length	[m^1]
L_T	Suspended sediment load ($L_T = 0{,}007\rho_s d_{50} M_e$)	[kg^{1}m^{-2}]
l	Sediment fraction number in numerical calculations	[-]
M	Dimensionless sediment mobility number due to waves and currents	[-]
M	Erosion parameter	[m^{1}s^{-1}]
M_b	Erosion coefficient in bed layers for equation 3.15	[kg^{1}s^{-1}m^{-2}]
M_c	Erosion parameter for cohesive beds	[m^{1}s^{-1}]
M_e	Dimensionless excess sediment mobility number	[-]
M_f	Erosion parameter for fluff layer	[m^{1}s^{-1}]
M_m	Erosion parameter for mud beds	[m^{1}s^{-1}]
M_{nc}	Erosion parameter for non-cohesive beds	[m^{1}s^{-1}]
m	Total mass of the fluff layer per unit area	[kg^{1}m^{-2}]
$m_{k,l}^n$	Mass of sediment fraction l in layer k at time level n	[kg^1]
m_m	Total mass of mud	[kg^1]
m_s	Total mass of sand	[kg^1]
m_{tot}	Total mass sediment	[kg^1]
m_0	Zeroth-order moment of a wave spectrum (e.g. of E, 1D)	[kg^{1}s^{-2}]
N	Action density spectrum (unit in 1D)	[kg^1]
N	Morphological factor	[-]
n	Time level in numerical calculations	[s^1]
p	Pressure	[kg^{1}m^{-1}s^{-2}]
$p_{k,l}^n$	Mass (or volume) fraction of sediment fraction l in layer k at time level n	[-]
p_m	Mud content (by dry weight) ($p_m = m_m/m_{tot}$)	[-]
$p_m^t(i,j)$	Mud content at grid cell (i,j) at time step t	[-]

$p_{m,cr}$	Critical mud content for non-cohesive of cohesive sand-mud mixtures	[-]
$p_{m,f}$	Mud content in fluff layer	[-]
$p_{m,sum}^t$	Sum of all mud content values in the tidal lagoon at time step t	[-]
p_s	Sand content (by dry weight) ($p_s = m_s/m_{tot}$)	[-]
Q	Discharge	[m^{3}s^{-1}]
q	Discharge per unit width	[m^{2}s^{-1}]
q_b	Total bed load transport rate (sand only) per unit width	[m^{2}s^{-1}]
q_s	Total suspended transport rate (both mud and sand) per unit width	[m^{2}s^{-1}]
q_t	Total transport rate ($q_t = q_b + q_s$) per unit width	[m^{2}s^{-1}]
R	Bend radius	[m^1]
Re_*	Grain Reynolds number ($Re_* = u_* d/v$)	[-]
r	$r = c_f|u|$ in equation 2.4	[m^{1}s^{-1}]
r	Radius	[m^1]
S	Salinity [ppt or PSU]	[kg^{1}kg^{-1}]
S	Source term	[kg^{1}s^{-2}]
S_b	Total bed load transport ($S_b = S_{b,c} + S_{b,w}$)	[kg^{1}s^{-1}m^{-1}]
$S_{b,c}$	Bed load transport (sand only) due to currents	[kg^{1}s^{-1}m^{-1}]
$S_{b,w}$	Bed load transport (sand only) due to waves	[kg^{1}s^{-1}m^{-1}]
S_{max}	Maximum salinity at which $w_{m,max}$ is specified	[kg^{1}kg^{-1}]
S_s	Total suspended transport ($S_s = S_{s,s} + S_{s,m}$)	[kg^{1}s^{-1}m^{-1}]
$S_{s,m}$	Suspended mud transport	[kg^{1}s^{-1}m^{-1}]
$S_{s,s}$	Total suspended sand transport ($S_{s,s} = S_{s,s,c} + S_{s,s,w}$)	[kg^{1}s^{-1}m^{-1}]
$S_{s,s,c}$	Suspended sand transport due to currents	[kg^{1}s^{-1}m^{-1}]
$S_{s,s,w}$	Suspended sand transport due to waves	[kg^{1}s^{-1}m^{-1}]
s	Specific gravity ($s = \rho_s/\rho_w$)	[-]
T	Tidal period	[s^1]
T_a	Non-dimensional bed shear stress	[-]
T_m	Morphological time period	[s^1]
T_{nc}	Transport parameter for non-cohesive sand-mud mixtures	[-]
U	Depth average velocity (in x-direction)	[m^{1}s^{-1}]
U	Absolute magnitude of depth average velocity in equations 3.2 & 3.3	[m^{1}s^{-1}]
$\vec{U}$	Total horizontal velocity vector by combining velocity components u and v	[m^{1}s^{-1}]
U_{10}	The wind speed 10 meter above the free surface	[m^{1}s^{-1}]
U_A	Velocity asymmetry value (Van Rijn, 2001 and Deltares, 2011a)	[m^{1}s^{-1}]
U_n	Current component in wave direction	[m^{1}s^{-1}]
U_{on}	Near-bed peak orbital velocity (in wave direction)	[m^{1}s^{-1}]
u	Current velocity in x-direction	[m^{1}s^{-1}]
$\tilde{u}$	Wave related velocity (in x-direction)	[m^{1}s^{-1}]
u_s	Current velocity in x-direction associated with the tide	[m^{1}s^{-1}]
u_*	Shear velocity ($u_* = u\sqrt{c_f} = u\sqrt{g/C^2}$)	[m^{1}s^{-1}]
$u_{*,cr}$	Critical shear velocity	[m^{1}s^{-1}]
V	Depth average velocity (in y-direction)	[m^{1}s^{-1}]
v	Current velocity in y-direction	[m^{1}s^{-1}]
v_{cr}	Critical depth average velocity for initiation of motion	[m^{1}s^{-1}]
v_{eff}	$v_{eff} = \sqrt{v_R^2 + U_{on}^2}$ (Deltares, 2011a)	[m^{1}s^{-1}]
v_R	Magnitude of an equivalent depth average velocity in equation 2.22	[m^{1}s^{-1}]
w	Current velocity in z-direction	[m^{1}s^{-1}]
w_m	Settling velocity of mud	[m^{1}s^{-1}]
$w_{m,0}$	Settling velocity of mud, corrected for salinity S_{max}	[m^{1}s^{-1}]
$w_{m,f}$	Settling velocity of mud in fresh water	[m^{1}s^{-1}]
$w_{m,max}$	Settling velocity of mud for	[m^{1}s^{-1}]

w_s	Settling velocity of sand	[m^{1}s^{-1}]
x	Horizontal coordinate	[m^1]
y	Horizontal coordinate	[m^1]
z	Vertical coordinate	[m^1]
z_b	Bed level (vertical)	[m^1]

Greek Symbols

α	Deposition fraction to the bed layer(s)	[-]
α_{b1}, α_{b2}	Coefficients in equation 2.31 and 2.32	[-]
β	Empirical coefficient in equation 2.29 and 2.34	[-]
γ	Phase lag coefficient (=0,2)	[-]
Δ	Relative sediment density ($\Delta = (\rho_s - \rho_w)/\rho_w$)	[-]
Δ	Change of a variable quantity	[-]
Δ_k^n	Thickness of layer k at time step n	[m^1]
Δt	(Morphological) discrete time step in numerical calculations	[s^1]
Δx	Horizontal discretization distance in x-direction in numerical calculations	[m^1]
Δy	Horizontal discretization distance in y-direction in numerical calculations	[m^1]
Δz	Vertical discretization distance in z-direction in numerical calculations	[m^1]
Δz^n	Vertical distance between centre of layer k and $k+1$	[m^1]
$\varepsilon_{m,x}$	Eddy diffusivity in x-direction for mud	[m^{2}s^{-1}]
$\varepsilon_{m,y}$	Eddy diffusivity in y-direction for mud	[m^{2}s^{-1}]
$\varepsilon_{m,z}$	Eddy diffusivity in z-direction for mud	[m^{2}s^{-1}]
ε_p	Porosity of the bed	[-]
$\varepsilon_{s,x}$	Eddy diffusivity in x-direction for sand	[m^{2}s^{-1}]
$\varepsilon_{s,y}$	Eddy diffusivity in y-direction for sand	[m^{2}s^{-1}]
$\varepsilon_{s,z}$	Eddy diffusivity in z-direction for sand	[m^{2}s^{-1}]
η	Instantaneous water level relative to h_0 (or other reference level)	[m^1]
θ	Angle between wind (stress) vector and local direction of grid	[-]
θ	Angle between wave propagation direction and local direction of grid	[-]
θ	Angle used to define 2-dimensional wave spectra	[-]
θ_{cr}	Critical Shields parameter	[-]
μ	Dynamic viscosity coefficient	[kg^{1}m^{-1}s^{-1}]
ν	Kinematic viscosity coefficient ($\nu = \mu/\rho_w$)	[m^{2}s^{-1}]
ν_x	Fluid mixing coefficient in x-direction (eddy viscosity)	[m^{2}s^{-1}]
ν_y	Fluid mixing coefficient in y-direction (eddy viscosity)	[m^{2}s^{-1}]
ν_z	Fluid mixing coefficient in z-direction (eddy viscosity)	[m^{2}s^{-1}]
ξ	Practical value, used in equation 4.1	[-]
ρ_a	Density of air	[kg^{1}m^{-3}]
ρ_l	Density of sediment fraction l	[kg^{1}m^{-3}]
ρ_m	Mud density	[kg^{1}m^{-3}]
ρ_s	Sand density	[kg^{1}m^{-3}]
ρ_{tm}	Density of the instantaneous transported mixture	[kg^{1}m^{-3}]
ρ_w	Water density	[kg^{1}m^{-3}]
σ	Relative frequency	[s^{-1}]
σ	Scaled vertical coordinate (surface is $\sigma = 0$, bed level is $\sigma = -1$)	[-]
τ_b	Bed shear stress	[kg^{1}m^{-1}s^{-2}]
$\tau_{b,cr}$	Critical bed shear stress	[kg^{1}m^{-1}s^{-2}]
τ_{cr}	Critical bed shear stress for sand only	[kg^{1}m^{-1}s^{-2}]
τ_d	Critical deposition shear stress	[kg^{1}m^{-1}s^{-2}]

$\tau_{d,m}$	Critical deposition shear stress for mud	$[\text{kg}^1\text{m}^{-1}\text{s}^{-2}]$
τ_e	Critical erosion shear stress	$[\text{kg}^1\text{m}^{-1}\text{s}^{-2}]$
$\tau_{e,m}$	Critical erosion shear stress for mud beds	$[\text{kg}^1\text{m}^{-1}\text{s}^{-2}]$
$\tau_{e,c}$	Critical erosion shear stress for cohesive mixtures	$[\text{kg}^1\text{m}^{-1}\text{s}^{-2}]$
$\tau_{e,nc}$	Critical erosion shear stress for non-cohesive mixtures	$[\text{kg}^1\text{m}^{-1}\text{s}^{-2}]$
$\tau_{f,cr}$	Critical erosion shear stress for the fluff layer	$[\text{kg}^1\text{m}^{-1}\text{s}^{-2}]$
$|\vec{\tau}_s|$	Magnitude of the wind shear stress	$[\text{kg}^1\text{m}^{-1}\text{s}^{-2}]$
φ	Angle between wave and current direction	$[°]$
ϕ_k^n	Solid volume fraction of layer k at time level n	$[-]$
Ω	Tidal prism	$[\text{m}^3]$
ω	Absolute (radian) frequency	$[\text{s}^{-1}]$

Mathematical Symbols

$=$	Equality sign (equals)	
$<$	Inequality sign (is less than)	
$\leq$	Inequality sign (is smaller than or equal to)	
$>$	Inequality sign (is greater than)	
$\geq$	Inequality sign (is greater than or equal to)	
$\approx$	Approximate equal sign (is approximately equal to)	
π	Sign for Greek number pi (equals 3,14159...)	
∂	Partial differentiation sign (the partial differentiation of)	
$\int$	Integral sign (the integral of)	
∇	Nabla sign (vector differential of)	
$|_{x=X}$	Valid at $(x = X)$ sign	
$\lim\limits_{x\to 0} f(x)$	Limit of $x \to 0$ in the expression $f(x)$	
Σ	Summation sign (the summation of)	
∞	Lemniscate sign (indicating infinite)	
$°$	Degree sign (degree)	
$|\ |$	Absolute sign (the absolute value of)	
$\Leftrightarrow$	Logical equivalence symbol (is logically equivalent to)	
$\propto$	Proportionality (is proportional to)	

Prefix Symbols

Micro	Milli	Centi	Deci	-	Deca	Hecto	Kilo	Mega
μ	m	c	d	-	da	h	k	M
10^{-6}	10^{-3}	10^{-2}	10^{-1}	10^{0}	10^{1}	10^{2}	10^{3}	10^{6}

Stay hungry, stay foolish.

2012
Freek Scheel